NOAA Technical Memorandum OAR PSD-312

SCIENTIFIC BASIS AND DESIGN OF A GROUND-BASED REMOTE ICING DETECTION SYSTEM (GRIDS)

W.C. Campbell
J.S. Gibson
R.F. Reinking
T.L. Schneider

Earth System Research Laboratory
Physical Sciences Division
Boulder, Colorado
July 2008

noaa NATIONAL OCEANIC AND ATMOSPHERIC ADMINISTRATION / Office of Oceanic and Atmospheric Research

NOAA Technical Memorandum OAR PSD-312

SCIENTIFIC BASIS AND DESIGN OF A GROUND-BASED REMOTE ICING DETECTION SYSTEM (GRIDS)

W. Carroll Campbell
Janet S. Gibson
Roger F. Reinking
Timothy L. Schneider

Earth System Research Laboratory
Physical Sciences Division
Boulder, Colorado
July 2008

UNITED STATES DEPARTMENT OF COMMERCE

Carlos M. Gutierrez
Secretary

NATIONAL OCEANIC AND ATMOSPHERIC ADMINISTRATION

VADM Conrad C. Lautenbacher, Jr.
Under Secretary for Oceans and Atmosphere/Administrator

Office of Oceanic and Atmospheric Research

Dr. Richard Spinrad
Assistant Administrator

NOTICE:

Mention of a commercial company or product does not constitute an endorsement by NOAA/ESRL. Use of information from this publication concerning proprietary products or the tests of such products for publicity or advertising purposes is not authorized.

CONTENTS

1. BACKGROUND 1

1.1 INTRODUCTION 1
1.2 HISTORY OF ICING HAZARDS RESEARCH AT ETL 3

2. SCIENTIFIC BASIS 4

2.1 RADAR 5
2.2 DUAL-CHANNEL RADIOMETER 9
2.3 TEMPERATURE PROFILING 10
2.3.1 Radar Detection of the Bright Band 11
2.3.2 Temperature Profiles from Radiosondes 11
2.3.3 RUC Model 12
2.3.4 Radiometric Temperature Profiling 12
2.4 ICING HAZARD ALGORITHM 15
2.5 GRIDS OPERATIONAL EXPERIENCE 17
2.5.1 AIRS II—Essence of Case of 11 November 2003 18
2.5.2 WISP04—Essence of Case of 10-11 March 22

3. DESIGN OF GRIDS 28

3.1 SENSORS 29
3.1.1 Radar 30
3.1.2 Radiometers 34
3.1.3 Temperature profiles 34
3.1.4 Surface Meteorological Sensors 35
3.2 ON-SITE COMPUTER SYSTEMS 35
3.2.1 GRIDS Software Architecture 35
3.2.2 GRIDS Computer Architecture 36
3.2.3 Radar Data Acquisition and Processing 38
3.2.4 Radiometer Data Acquisition and Processing 39
3.2.5 RUC Model Data Processing 39
3.2.6 Surface Met Data Processing 39
3.2.7 Icing Algorithm Processing 39
3.2.8 XRADS User Interface 40
3.3 ICING HAZARD ALGORITHM IMPLEMENTATION 40
3.3.1 Core Algorithm Implementation 40
3.3.2 Algorithm Enhancements 42
3.3.3 Important GRIDS Byproducts 44
3.4 MONITORING AND CALIBRATION 44
3.5 COMMUNICATION 46
3.5.1 Internet 46
3.5.2 Local Area Network (LAN) 46
3.5.3 IEEE-488 Bus 47
3.6 CONTAINER 47
3.7 OFF-SITE COMPUTER SYSTEMS 49
3.7.1 Software Architecture 49
3.7.2 Computer Architecture 50

4. SUMMARY 50

5. ACKNOWLEDGMENTS 51

6. REFERENCES 52

FIGURES

FIGURE 1. GROUND-BASED REMOTE ICING DETECTION SYSTEM (GRIDS) NEAR AN AIR TRAFFIC CENTER. 4
FIGURE 2. RADAR MEASUREMENT OF DEPOLARIZATION RATIO (DR) VS. ELEVATION ANGLE 8
FIGURE 3. RATIOS τ_w (89 GHZ) / τ_w (30 GHZ) (BLUE) AND τ_w(30 GHZ)/ τ_w(89 GHZ) (RED) AS A FUNCTION OF TEMPERATURE. 14
FIGURE 4. ILLUSTRATIONS OF THE MEAN LIQUID WATER TEMPERATURE RETRIEVALS IN "WARM" AND "COLD" STRATUS DURING AIRSII (FROM SCHNEIDER ET AL. 2004). 15
FIGURE 5. THE DECISION POINTS FOR THE GRIDS CORE ICING HAZARD. 17
FIGURE 6. NASA TWIN OTTER 2DC-GREY PROBE IMAGERY OF ICE CRYSTALS OBSERVED AT 1635 UTC. 19
FIGURE 7. NASA TWIN OTTER 2DC-GREY PROBE IMAGERY OF FREEZING DRIZZLE (SLD) OBSERVED AT 2031 UTC.19
FIGURE 8. TIME-HEIGHT IMAGE OF THE GRIDS' ICING HAZARD. 20
FIGURE 9. SPECTRA OF VERTICAL VELOCITY AS A FUNCTION OF ALTITUDE 21
FIGURE 10. INTEGRATED VAPOR AND LIQUID VALUES MEASURED BY THE GRIDS RADIOMETER 23
FIGURE 11. LIQUID WATER CONTENT MEASURED DURING CLIMB OUT AT ~2230 UTC. 24
FIGURE 12. VERTICAL SLICE (RHI SCAN) OF THE DEPOLARIZATION RATIO (DR) AT 2002 UTC 25
FIGURE 13. TIME-HEIGHT (MSL) IMAGE OF THE GRIDS ICING PRODUCT 26
FIGURE 14. HORIZONTAL AND VERTICAL CROSS SECTIONS OF CIP ICING POTENTIAL FOR 2300 UTC 27
FIGURE 15. SIMPLIFIED BLOCK DIAGRAM OF GRIDS SHOWING MAJOR SUB-SYSTEMS. 29
FIGURE 16. DIAGRAM OF RADAR IN GRIDS. 31
FIGURE 17. SOFTWARE ARCHITECTURE DIAGRAM SHOWING INFORMATION FLOW 36
FIGURE 18. CORE ICING HAZARDS ALGORITHM 41
FIGURE 19. PLAN VIEW OF GRIDS CONTAINER SHOWING LOCATION OF KEY EQUIPMENT 48
FIGURE 20. SIDE VIEW OF CONTAINER SHOWING 3-M ANTENNA. 48
FIGURE 21. DATAREXX SERVER DIAGRAM SHOWING DATA SOURCES, SERVER, AND DATA CLIENTS. 49

TABLES

TABLE 1. COMPARISON OF PURPOSE AND FEATURES OF KA-BAND AND S-BAND POLARIZATION DIVERSITY RADARS 5
TABLE 2. RADAR CHARACTERISTICS OF GRIDS OPERATING AT 40° ELEVATION 32
TABLE 3. ICING ALGORITHM THRESHOLDS 41
TABLE 4. ANALOG SIGNALS MONITORED BY RADAR MONITOR PROCESS 45

APPENDICES

Appendix A: History of Icing Hazards Research at NOAA/ETL…….. A-1

Appendix B: Enhancements to Core Icing Algorithm for GRIDS……. B-1

Appendix C: GRIDS Requirements…….. C-1

Appendix D: GRIDS Block Diagram and Parts List……... D-1

Appendix E: GRIDS Features and Benefits……. E-1

Appendix F: Software Catalog…….. F-1

Appendix G: GRIDS Software Specifications…….. G-1

Appendix H: Implementation of the Digital Receiver……. H-1

Appendix I: GRIDS Covariance Algorithms…….. I-1

Scientific Basis and Design of a Ground-based Remote Icing Detection System (GRIDS)

ABSTRACT. In-flight icing of aircraft has been identified by the Federal Aviation Administration as a serious problem for both commercial and general aviation. NOAA's Environmental Technology Laboratory[1] in conjunction with the FAA has identified and developed a measurement system to detect icing conditions in clouds. This Ground-based Remote Icing Detection System (GRIDS) utilizes state-of-the-art, ground-based remote sensors and an operational National Weather Service numerical model. The system incorporates four elements: a dual-polarization K_a-band radar to measure reflectivity and depolarization ratio of cloud hydrometeors, a two-channel microwave radiometer to measure cloud liquid water and water vapor profiles, another radiometer channel to measure the atmospheric temperature profile, and a meteorological model of the temperature profile retrieved via the Internet. This information is combined in an algorithm to measure the icing threat as a function of altitude above the radar. This document establishes the scientific basis of the icing algorithm, and specifies both the hardware and the software design of GRIDS. GRIDS makes all the required measurements to implement the icing algorithm, display the results locally, and disseminate the results via the Internet, to warn in real time of in-flight icing hazards. GRIDS also measures as by-products several meteorological parameters in addition to those required for the icing algorithm that can effectively complement and enhance local-area meteorological observations and local and mesoscale forecasts.

1. BACKGROUND

1.1 Introduction

Air traffic is increasing, spatial separations are decreasing, and aircraft in-flight icing is a growing threat to aviation, not only in the U.S. but worldwide. According to reports prepared for the FAA, aircraft accidents due to icing in the U.S. alone claim 30 lives annually, injure 14 others, and result in $96M in lost property (Paull and Hagy 1999). Icing conditions also disrupt air traffic operations resulting in large financial consequences for both airlines and passengers. Recommendations from a 1996 Federal Aviation Administration (FAA) workshop strongly emphasized the need to develop new remote sensors to detect Super-cooled Large Droplets (SLD), i.e., droplets approaching and including drizzle sizes, which can be particularly hazardous (Riley and Horn 1996; summarized by Reinking and Kropfli 2000).

In-flight aircraft icing occurs when cloud droplets or raindrops that are supercooled as liquid to temperatures below 0°C freeze upon impact on the surfaces of an aircraft. Federal aviation regulations (Federal Aviation Regulation Part 25 Appendix C; FAR25-C; FAA, 1982) established two decades ago specify maximum tolerable icing conditions in terms of cloud liquid water content, cloud droplet size, and sub-zero temperatures (°C), but these guidelines consider only droplets less than 50 microns in diameter. Recent research has established that still larger droplets 50-500 microns in diameter can also present a severe hazard. These SLDs can penetrate

[1] NOAA/ETL was merged into the Physical Sciences Division of the Earth System Research Laboratory on 1 October 2005.

the slip stream and freeze as rough ice on aircraft surfaces aft of the leading edge of the wing (Sand et al. 1984; Ashendon and Marwitz 1987; Politovich 1989; Cober et al. 1995; Ashendon et al. 1996, Politovich 1996). Droplets both smaller and larger than SLDs tend to spread evenly on the airframe and therefore cause a less hazardous coat of ice than that typically made by SLDs.

However, all supercooled droplets that are large enough to penetrate the airstream to reach an airfoil present a potential icing threat. They are difficult to forecast and to detect. Currently-available operational weather surveillance systems are inadequate for use in detecting icing conditions, because of non-optimal wavelengths, polarizations (or lack thereof), and scanning priorities.

This document presents the design of a remote sensing system that overcomes such impediments with hardware and software that brings the focus directly to the icing hazard, and thus addresses the national need to help mitigate hazards caused by supercooled water in clouds. This design specifies a prototype Ground-based Remote Icing Detection System (GRIDS). This system is based on research sponsored by the Federal Aviation Administration (FAA) and conducted and supplemented by NOAA's Environmental Technology Laboratory (ETL) over the preceding decade. The research was carried out under the auspices of the FAA's series of Winter Icing and Storms Projects (WISP). During this development, GRIDS and its predecessors were extensively field tested and modified many times to establish a reliable basis for the design of this prototype, which is suitable to build for operational application on a trial basis. GRIDS makes all the required measurements and supporting data acquisitions to implement the icing algorithm, display the results locally, and disseminate the results via the Internet, to warn in real time of in-flight icing hazards.

Two prestigious awards attest to the significance and potential of GRIDS to help to prevent icing accidents: In 2001, the NOAA/ETL Radar Meteorology and Oceanography Division was awarded the U.S. Department of Commerce Gold Medal "for theoretical, experimental, and engineering advances that led to the development of a new technology—an autonomous, ground-based, remote-sensing system to detect dangerous in-flight icing conditions in clouds," and in 2002 NOAA/ETL was presented the FAA Administrator's Excellence in Aviation Award "for outstanding contributions to the FAA Aviation Weather Research Program." Both of these awards are the result of the development of GRIDS. Schematically depicted in Figure 1 is a GRIDS unit supporting flight operations near an air terminal.

The focus of GRIDS is detection of the icing hazard in a local flight operations area. This hazard detection can be used not only in local warnings but also as a measurement to verify and extrapolate to a larger area the icing forecasts from operational numerical models. In particular, GRIDS is synergistic with forecast models that provide a product focused specifically on aircraft icing. A new product under development, the Current Icing Potential (CIP) algorithm (Bernstein et al. 2004), is especially promising in the modeling arena and has been interactively tested with GRIDS (Bernstein and Schneider 2004).

To obtain the key icing parameters, GRIDS also routinely measures a number of cloud and atmospheric parameters as by-products that can be used to enhance local area observations and forecasts. Measures of ceiling and vertical cloud structure, in-cloud turbulence, total precipitable water, and the atmospheric water vapor profile are examples of the several valuable by-products available in the GRIDS data stream.

In this document we discuss the many options that were considered in designing GRIDS, the rationale for making specific choices, and the tested and selected design. This document serves as a resource and a reference for the GRIDS development team, the FAA, NOAA, and any other potential user of this technology.

1.2 History of Icing Hazards Research at ETL

Over the past two decades NOAA ETL has, in partnership with the FAA, investigated the use of both passive and active remote sensors to determine when icing conditions exist aloft. A short history of ETL's research is outlined in Appendix A.

ETL's researchers have used theoretical modeling, instrument system development, and experimental observations to determine and refine optimal means to detect icing hazards. Each successive year sharpened the focus on observational methods that more confidently identify regions of hazardous cloud, and distinguish them from benign regions. Some failures steered the research to optimal technologies. ETL tried but abandoned dual-frequency (9.3 and 35 GHz) observations to detect and map super-cooled water in clouds, for both practical and scientific reasons (as detailed in Appendix A). A continued effort that focused on new radar polarization technologies proved successful and is described in this document.

Note that on October 1, 2005, ETL was merged into NOAA's Earth System Research Laboratory (ESRL) as part of the Physical Sciences Division (PSD) and no longer exists under the name Environmental Technology Laboratory. Historical references in this report, including reference to GRIDS development will still refer to ETL, however.

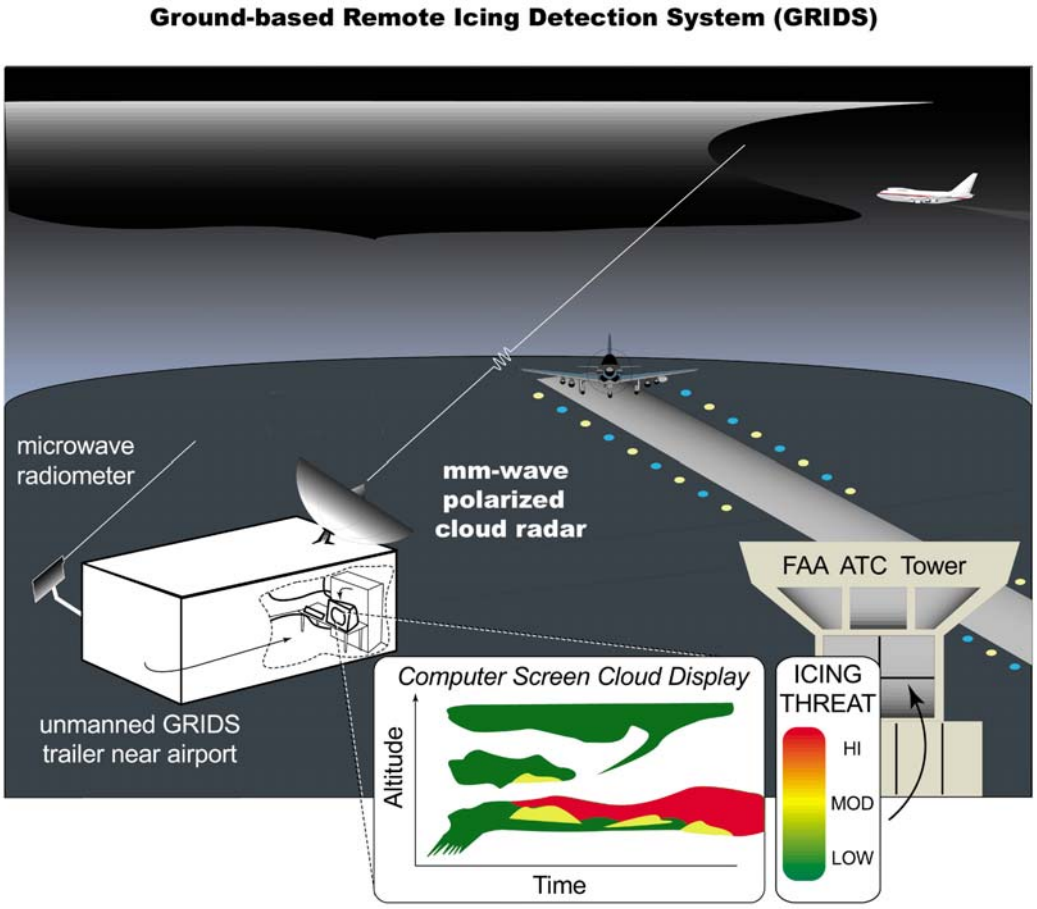

Figure 1. Ground-based Remote Icing Detection System (GRIDS) near an air traffic center. GRIDS will operate continuously and unattended, providing automated warning of icing hazards within clouds, as depicted in the overlay (from Reinking et al. 2001a).

2. SCIENTIFIC BASIS

Based on ETL's research, a system that consists of four primary elements has been developed to detect potentially hazardous icing conditions: a dual-polarization K_a-band radar to measure reflectivity and depolarization ratio of cloud hydrometeors, a two-channel microwave radiometer to measure cloud liquid water and water vapor profiles, another radiometer channel to measure the atmospheric temperature profile, and an operational meteorological model of the temperature profile retrieved via the Internet. This information is combined in an algorithm to measure the icing threat as a function of altitude above the radar. The following sections discuss these elements in greater detail.

2.1 Radar

The dual-polarization K_a-band cloud-sensing radar is the cornerstone of GRIDS. Its chosen operating frequency near 35 GHz (8.66 mm wavelength) is important because it is in an atmospheric "window" with little gaseous absorption to degrade signals. This frequency also allows the radar to easily detect the small cloud droplets (including SLDs) that pose a serious icing threat, a much more difficult task for lower-frequency radars such as the NEXRAD S-band (3-GHz/10-cm) radars that are used for weather surveillance. Another possible choice of frequency for GRIDS is near 90 GHz (W-band, ~3mm), the next higher "window." But at 90 GHz there remains significant (and time-varying) gaseous and liquid absorption, components are much more expensive, and transmitters are both less powerful and less reliable. At 35 GHz, the size of the antenna is more manageable for the same angular beamwidth, and sidelobes are reduced with respect to weather surveillance radars. Reduced sidelobes have the advantage of eliminating ground clutter that can overwhelm the desired atmospheric signals at short ranges. At 35 GHz, radar technology is relatively mature, meaning that while components are more costly than at lower frequencies, they are not exorbitant, and transmitter technology is robust and of sufficient power level. No single radar technology can be used for all weather sensing needs. Key features of 35 GHz technology that make it very suitable for detecting the in-flight icing hazard are noted in Table 1, where they are compared to features of the NEXRAD radars. The weather detection capabilities of these two types of radars are primarily complementary (compare Kropfli and Kelly 1996, to Zrnic and Ryzhkov 1999).

Table 1. Comparison of purpose and features of K_a-band and S-band polarization diversity radars

GRIDS K_a band	**NEXRAD S Band**
• Purpose: short-range cloud profiling	• Purpose: long-range surveillance
• High sensitivity to small hydrometeors	• Precipitation (large particle) sensing
• Polarization tailored to detecting in-flight icing hazard	• Polarization design focused on rain measurement and hail isolation
• Acceptable attenuation at short range, except in heavy rain	• No significant attenuation
• Minimal degradation from ground clutter	• Near-field ground clutter
• Fine spatial resolution	• Coarse spatial resolution
• Minimal Bragg (clear air) scattering	• Confused by Bragg scattering at SLD sizes
• Transportable and portable (1 seatainer)	• Not portable (some S-bands are transportable, in several seatainers)

In its simplest configuration, the GRIDS radar measures two parameters for input to the icing hazard algorithm: equivalent radar reflectivity factor (Z_e) and depolarization ratio (DR). Both are measured at a fixed-beam elevation angle of 40°, a carefully selected angle. DR is the primary measurement for GRIDS because it can be used to distinguish spherical from non-

spherical particles. Z_e is also important because it is determined by the size distribution of the cloud hydrometeors and thus relates to the mass of water substance per unit volume contained in the cloud being probed. To determine Z_e accurately, one must be assured of the radar calibration coefficients, which can drift and change. Hence it is important to routinely and automatically check the calibration of the GRIDS radar, which will measure clouds with reflectivities down to approximately -59 dBZ at a range of 10 km. At this level of sensitivity (-29 dBZ in strong channel, -59 dBZ in weak channel), the GRIDS radar can measure DR accurately in a 10-km-high cloud of mono-dispersed 20-micron droplets with a liquid water content as low as 0.06 g m^{-3}, or in a 400-micron droplet cloud with as little as 10^{-5} g m^{-3} liquid water content, both well below the level of any icing hazard. GRIDS is a Doppler radar, so estimates of the beam-radial velocity, V_e, of reflecting hydrometeors are also routinely measured. Enhancements to the icing algorithm could incorporate V_e.

As designed, the radar transmits purely polarized radiation and receive signals in two channels: one channel for the transmitted polarization (co-polar) and the other channel whose polarization is orthogonal to the transmitted polarization (cross-polar). Reflectivity factor Z_e is determined from signals in the stronger channel. DR, measured in dB, is defined as a logarithmic ratio of the radar reflectivity received in the weaker, cross-polar receiving channel to the reflectivity measured in the stronger, co-polar receiving channel. DR is determined by the dominant shape, settling orientation, and density of the population of cloud particles from which the transmitted radar pulses are scattered. For particles whose geometric cross section, as viewed by the radar, is nearly circular, very little depolarization occurs and DR is low. In theory, DR = $-\infty$ dB for truly circular targets or spherical particles. In practice, DR from such circular targets is determined as the radar's low-threshold value established primarily by the imperfect properties of the receiving antenna and transmitter (i.e., polarization cross-talk) and secondarily by the scattering particles. Typical radar cross-talk values for linear and circular polarized signals should be on the order of -30 dB for GRIDS.

Since ice particles typically have non-circular geometric cross sections as seen by the radar, they will produce depolarization ratios larger than the antenna cross-talk (except for some shapes like hexagonal plates, when viewed directly from below). Hence one can use DR and non-zenith view angles to distinguish non-hazardous ice particles from potentially hazardous spherical water droplets (which provide circular geometrical cross sections at any view angle).

Figure 2 shows DR of different hydrometeors as a function of the radar elevation angle, as actually measured by ETL's scanning 35-GHz polarimetric Doppler radar during the 1999 Mt. Washington Winter Icing Sensors Project (MWISP) campaign in New Hampshire (Ryerson et al. 2000). There is a clear distinction between patterns of DR vs. radar elevation angle for drizzle (i.e., SLD if super-cooled) and these regular types of ice crystals. Irregular ice crystals (e.g., conglomerates) produce somewhat lower depolarization ratios than regular types of ice crystals (Reinking et al. 2002), but their DR values are still well above those for supercooled droplets at non-zenith elevation angles.

The fixed 40° elevation chosen for GRIDS is within the 30°-45° elevation range established by Matrosov et al. (2001) as optimal for distinguishing cloud droplets from ice hydrometeors when using one fixed beam. As can be seen in Figure 2, when the radar is pointed to the zenith (90° elevation angle), planar-type crystals (e.g., hexagonal plates) produce DR values that are very close to that of water droplets (i.e., around -30 dB), because both types of particles have nearly circular geometrical cross sections. However, at elevation angles well removed from 90°,

there is a distinct separation between the DR values for spherical water droplets and any ice crystal for which the geometrical cross section is now non-spherical. Very low elevation angles will result in a significant increase of propagation path causing loss of sensitivity for upper cloud layers and will introduce possible propagation effects (e.g., attenuation and phase rotation).

Although it is not a primary function of GRIDS to categorize cloud ice, note that ice particle type (most basically, columnar vs. planar, but also graupel, aggregates, etc.) and the evolution of the ice type is better established by measuring DR at two fixed elevation angles (e.g., 90° and 40°). This configuration will provide an abbreviated and economical equivalent of the continuous range-height (RHI) scanning that so definitively identified hydrometeors in the WISP experiments (e.g., Figure 2 and Reinking et al. 2002). The introduction of ice into a cloud volume will influence the depletion of the liquid droplets that cause aircraft icing, and the ice type influences and reflects the rate of that depletion. Thus, the basic GRIDS algorithm may be enhanced by an automated accounting of ice presence, type and evolution. Significant updrafts and turbulence can produce cloud liquid and influence droplet growth, so Doppler velocity and velocity variance measurements at vertical incidence (90°) also might improve detection of hazardous icing conditions, especially in mixed-phase clouds. These and other potential enhancements are outlined in Section 3.3, Icing Hazard Algorithm Implementation and in the corresponding Appendix B. Therefore, an optional and desirable capability for GRIDS is to transmit a vertical beam at 90° elevation angle, in addition to its primary 40° elevation transmission.

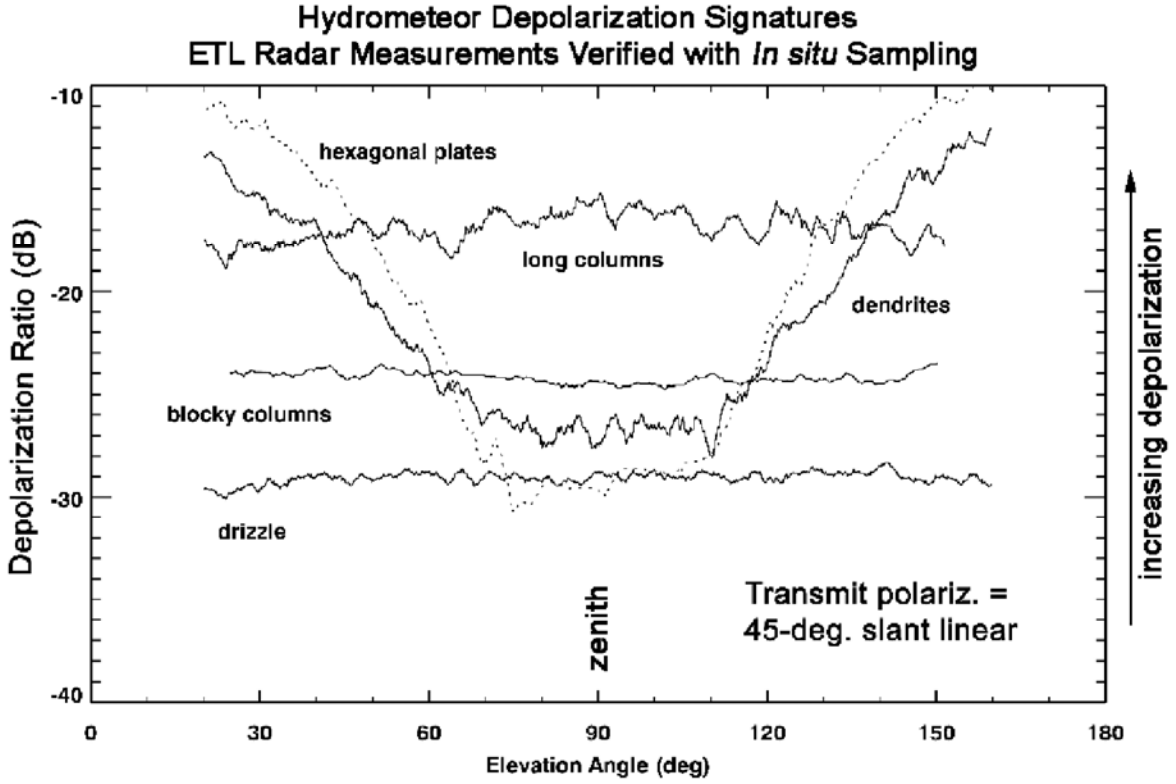

Figure 2. Radar measurement of Depolarization Ratio (DR) vs. elevation angle for various regularly shaped cloud particles during the 1999 MWISP campaign near Mt. Washington, New Hampshire (from Reinking et al. 2002).

The measurements in Figure 2 were obtained by transmitting linear polarization at a polarization rotation angle of 45° from horizontal polarization. For the purpose of the hydrometeor differentiation needed for identifying the icing hazard, this polarization is certainly superior to standard horizontal polarization used in most weather radars; the several reasons for this are detailed by Reinking et al. (2002). Theoretical studies that incorporate real-life "flutter" effects of falling ice particles (Matrosov et al. 2001, 2005) show that a circular or near-circular polarization can provide even greater and more stable separation in DR between ice particles and water drops. The collective WISP experiments demonstrated conclusively that the experimentally measured values of DR will closely match those calculated theoretically for polarization states ranging through the continuum of ellipticity, where pure circular corresponds to an ellipticity of unity and pure linear to zero. Although the 45° slant linear state (with slight ellipticity) was subjected to the most in-depth testing, circular (with slightly less ellipticity than unity) was also tested (Reinking et al. 1997a; Matrosov et al. 2001), and the principles can be merged. The introduction of ellipticity that deviates slightly from unity causes a stronger radar echo in the "weak" receiving channel. This will enable GRIDS to make meaningful measurements of even weaker reflectivity clouds. This ability comes with a price—transmitting elliptical polarization slightly diminishes DR separations between ice particles and water drops. However, this price is worth paying to achieve the enhanced sensitivity. In summation, for GRIDS we specify the antenna and feed system to have *circular polarization* within standard

limits of tolerance. But it is almost certain that the delivered antenna and the transmitted state of polarization will be imperfect, and will therefore advantageously demonstrate a slightly modified ellipticity. As part of the radar calibration, it will be necessary to measure the actual transmitted polarization state (i.e., its ellipticity) and the antenna's polarization cross-talk, and use those values to optimize the decision points in the icing algorithm.

2.2 Dual-Channel Radiometer

GRIDS' primary function is the detection of the presence of liquid water (LW) in quantities above a meaningful threshold, and in drop sizes of 50–500 microns and smaller. For GRIDS, the radar is the primary observing instrument for determining cloud particle type and identifying clouds of droplets, but it alone cannot make all necessary observations. Also required is a means to remotely sense the quantity of liquid water in the clouds, and a means to determine the temperature of that liquid water. GRIDS offers the power added by combining remote sensors.

Microwave radiometers passively receive microwave emissions from the volume of atmosphere and clouds within their "viewing" cone. From these measurements, and depending on the selection of receiving frequencies, tropospheric meteorological moisture and temperature variables can be estimated. A review of the principles of microwave radiometry has been published by Westwater et al. (2005, 2006). It is surprising that microwave radiometers, such as the GRIDS two-channel instrument, have not been deployed operationally to all first-order forecasting stations, because the *continuously available* (24 hours a day, 7 days a week) measured values and trends of total and profiled atmospheric vapor (precipitable water), plus the cloud liquid to address icing, are so fundamental to and offer so much added value to forecasts. This value and the added power of radiometer-radar combinations has been demonstrated for storm-embedded orographic gravity waves and for lake-effect storms, for example (Klimowski et al. 1998, Reinking et al. 2000a, Reinking et al. 1993a), and for many icing scenarios as shown by several of the field tests referenced in this document.

The dual-channel microwave radiometer has a well-proven capability for estimating total path-integrated LW (g m^{-2}) amount as well as the total path-integrated water vapor (WV, g m^{-2}) amount (Westwater 1972; Hogg et al. 1983; Westwater et al. 2005, 2006; Martin et al. 2006). The technique is based on deriving the optical thickness of the atmosphere at two frequencies (e.g., near 24 and 31 GHz) by measuring the corresponding radiometric brightness temperatures and relating them to LW and WV. This is possible because, at the selected frequencies, optical thickness depends nearly linearly on LW, WV, and on the amount of oxygen in the atmosphere. The oxygen component is quite stable and can therefore be accounted for with a high degree of accuracy. Selection of the two frequencies is important, since the coefficients in the linear relations between optical thicknesses and LW and WV are frequency-dependent and must be determined precisely.

Once the brightness temperatures are measured at the two frequencies, it is straightforward to derive the path-integrated amounts of both water vapor (of interest as a by-product from GRIDS) and cloud liquid water (of direct interest because this measurement helps determine the severity of the icing hazard). Ice in clouds does not contribute to the microwave signal in the frequency range below 90 GHz (Westwater et al. 2006) and does not hamper the liquid measurement. A practical liquid water detection threshold is approximately 0.05 mm for the dual-channel microwave radiometer. Recent advances in receiver technology make it practical

to receive multiple frequencies sequentially, and commercial radiometer products are available that use this capability to improve accuracy and versatility.

As reviewed by Reinking et al. (2000a), the microwave radiometer's measurement of LW is most accurate when droplet sizes are such that their scattering is in the Rayleigh regime (small compared to the radiometer wavelength). As droplet diameters exceed about 100 microns, the radiometric retrievals begin to break down. However, the degradation is not significant unless considerably larger droplets occur. The measurement is not significantly degraded by drizzle on the antenna, even though the drops can be several hundred microns in diameter. A uniform water coating or sprinkling of drops on the antenna will not degrade the measurement.

Since a microwave radiometer passively receives the emissions from the clouds, its signal reception is degraded when the rain rate is sufficient to cause rivulets on the antenna. This degradation is minimized by using a spinning-disc antenna or an integrated blower system to dry a viewing window. The latter is employed in commercial versions. Meteorologically, many documented cases of severe icing, including meteorologically analyzed cases that actually caused aircraft crashes have happened in stratiform clouds of supercooled liquid, where the introduction of ice particles to initiate rain processes has not yet occurred, and where drizzle-sized droplets dominated (Cober et al. 1995; Politovich 1989; Ashendon et al. 1996; Ashenden and Marwitz 1997). In such clouds, GRIDS will readily measure the hazard. The radar-radiometer combination also will readily identify glaciated clouds, i.e., those with insignificant liquid and no icing hazard.

Icing has been encountered by research aircraft in mixed-phase—liquid plus ice—clouds, some producing rain (Riley and McDowell 1998). Statistically, the liquid fraction increases with temperature but has a minimum around -15°C, where competition for ice crystal growth is a maximum (Boudala et al. 2004). Also statistically, *in situ* measurements have shown that there is no correlation between ice and liquid content in mixed-phase clouds at a given temperature; however, the same experimental evidence also indicates that ice and liquid in natural clouds can be well separated in space and located in single-phase clusters, and that such clusters exist on a scale of the order of kilometers (Korolev et al. 2003). Such distributions are readily detected in the DR measurement with the GRIDS radar to identify the potentially hazardous liquid zones, and the radiometer will measure the liquid in either situation. However, rain rates sufficient to contaminate the radiometric LW measurement will complicate the detection. GRIDS' first line of defense is to rely on the rain-shield window-blower system of the radiometers. Furthermore, the core algorithm is required to recognize periods of rain, and to automatically make a rain-no rain decision to flag the estimate of the icing warning level when rain is occurring.

Further enhancements to the core algorithm, to make weighting adjustments to other parameters in the icing algorithm during substantial rain events, are also possible using additional GRIDS measurements, as discussed in the design section on algorithm implementation.

2.3 Temperature Profiling

In addition to identifying the presence and altitudes of liquid water through radar and radiometer measurements, GRIDS must determine whether the detected liquid is supercooled. Timely information about the local vertical profile of temperature is therefore required. Foremost, the system therefore must determine the altitude of the 0°C level, and the altitude of

the clouds relative to that. Although the GRIDS radar makes continuous measurements of base and top altitudes of cloud layers, accurate means are required to estimate the temperatures within those layers. As enhancements to the core icing algorithm are developed, the full tropospheric temperature profile will be useful since most severe icing occurs between 0°C and -10°C, and thermodynamic instability determined from the profiles can indicate forcing to produce the condensation of liquid.

The options for determining temperature include radar estimation of the height of the melting level, nearby radiosondes, output data from numerical weather prediction (NWP) models, and measurements from microwave radiometers operated at an additional frequency. Radiosonde data and NWP model outputs are both routinely and reliably available from NOAA Internet sites.

2.3.1 Radar Detection of the Bright Band

Within clouds, the region where the temperature is approximately 0°C is where falling ice particles melt and become water droplets; this can be readily observed as the "bright band" with the GRIDS radar. Here the cloud reflectivity is enhanced, and the fall velocity, as measured in the Doppler signature, is accelerated as the snow is converted to drizzle or rain. However, the bright band, even when weak, is unmistakably and conveniently depicted in the DR signature, even when it is not evident in reflectivity, because the depolarization is enhanced by melting hydrometeors. Substantial gradients of 2-5 dB in DR have been measured between the edges and the core of the bright band, and the bright band has been observed to be 100m or more deep even when melting crystals are only producing drizzle (Reinking et al. 1996b). Thus, an algorithm that recognizes time-persistent gradients such as these along the fixed GRIDS radar beam will readily identify the bright band. Liquid water detected more than about 200 m above the height of the bright band is almost certainly supercooled. Unfortunately, bright bands can be ambiguous or not present at all, such as when the cloud is totally composed of liquid and there is no precipitation to melt, or the freezing level is at or just above ground level, or convective drafts mix melting through a deep volume. Thus, additional sources of local temperature information are required.

2.3.2 Temperature Profiles from Radiosondes

Radiosonde launches typically occur only twice per day, require 1–2 hours of flight time to profile the entire troposphere, and may be launched from sites 200–300 miles apart. Temperature fields aloft are less variable across large horizontal distances than surface temperatures or cloud fields. Thus, standard network radiosondes provide good reference data that are necessary for calibrating the GRIDS microwave radiometer, but the data are too coarse to be counted on to provide the timely and local temperature profile that GRIDS requires to determine cloud liquid cooling. Therefore, the GRIDS design allows ingest of the closest radiosonde data for calibrations, and these temperature data will be available as backup information. For GRIDS temperature profiling, the NWS network radiosonde data are best used as assimilated in the operational Rapid Update Cycle (RUC) numerical observation and forecast model.

2.3.3 RUC Model

The Rapid Update Cycle (RUC) atmospheric prediction system has been chosen as the primary source of temperature profile information for GRIDS, and allowance is made for checks of this value via the other options for determining temperature. The RUC is maintained by NOAA Forecast Systems Laboratory (FSL) and runs operationally at the National Center for Environmental Prediction (NCEP).

The RUC produces updates with the highest frequency of any forecast and assimilation model in the United States. This system is a combination of a data assimilation tool and a sophisticated mesoscale forecast model. A 20-km 50-level hourly version of it was implemented in 2002 (Benjamin et al. 2004b). The RUC uses a hybrid isentropic-sigma vertical coordinate, which improves accuracy for moist reversible processes. Thus, the moisture environment for areas of cloud development and precipitation may be forecast with better coherence. Also, isentropic coordinates are advantageous in that they "provide adaptive vertical resolution, greater in layers of higher static stability where strong vertical gradients of other variables are likely to occur" (Benjamin et al. 2004a). The RUC parameterizations include mixed-phase cloud microphysics. The combination of these features makes it the optimal model for obtaining temperature soundings in potential icing conditions. The regional analyses are based on data assimilated from multifarious sources including surface (land-based and ship-borne), upper air (balloon-borne radiosondes), and commercial aircraft flight-level (*in situ*) observations. The assimilation is performed via an optimal interpolation multivariate analysis procedure. Every hour, RUC issues updated meteorological analyses and forecasts, thus allowing extraction of site-specific temperature soundings with reasonable temporal resolution. GRIDS will extract these soundings to sites that are selected for deployment.

2.3.4 Radiometric Temperature Profiling

Microwave radiometry offers a means to provide temperature profiles continuously, at least in the lower troposphere. Radiometric temperature profiling can be accomplished by measuring the emissions through a band around 50–60GHz. Scanning through a narrow spectrum here will allow receipt of emissions from a range of distances into the atmosphere. The emission at any altitude is proportional to the temperature, so the profile can be obtained. However, microwave temperature profiling is most accurate in the atmospheric boundary layer, below about 2 km Above Ground Level (AGL). A comparison to radiosondes in the winter atmosphere shows that temperature retrieval accuracy is best near the surface and degrades upward to a standard deviation of 1.5°K at 3 km AGL. Also, the effective vertical resolution of the temperature measurement degrades linearly with increased altitude at 0.44z, where z is AGL height (Cimini et al. 2006). Thus, at 1 km it is ~440 m and at 3 km it is ~1,320 m. Temperature profiles to higher altitudes were measured by spiraling aircraft and a radiometer during the second Alliance Icing Research Study (AIRSII; Reehorst et al. 2005). The radiometer provided profiles to 10 km AGL, but the aircraft provided measurements only through cloud layers below 4 km AGL. Taking the aircraft measurements as "truth", the radiometer estimates differed by as much as 3–6°C in each of several test soundings, with these greater errors occurring within temperature inversions. Comparisons of radiosonde and radiometer data indicated temperature differences with standard deviations of 1.5–2°C (e.g., Chan and Tam 2005).

Thus, the temperature profiling radiometer is limited in measuring detail, generally overestimating temperature in the upper reaches of inversions, and underestimating in the lower

regions, but it can provide a good smoothed temperature profile that is continuously available with a temporal resolution of seconds, to verify and compare to the RUC output. This will be particularly important in situations with frontal activity where the 1-hour resolution and time-interpolation of the RUC may become too coarse. These radiometric temperature data are not included in the GRIDS core algorithm, but development as an enhancement is recommended.

As an interim development, it is possible to estimate the layer-mean temperature of cloud liquid using two channels: ~30 GHz and ~90 GHz (Schneider et al. 2004). This radiometric approach was first suggested by Koldaev et al. (1998). This approach was adopted and modified for use with GRIDS to provide the additional information in remote sensing of icing conditions. The exact microwave frequencies of the NASA-Glenn radiometric system used with this approach during AIRSII were 89 and 30 GHz. Optical thicknesses at these two frequencies obtained from measured brightness temperatures are the sum of the cloud optical thicknesses (τw) and optical thicknesses due to water vapor (τv) and oxygen (τo). After removing the gaseous components τv and τo using the value of the total integrated water vapor from standard radiometric retrievals and surface values of temperature and pressure, the time series of the ratio τw (89 GHz) / τw (30 GHz) is calculated. This ratio depends on the cloud liquid water temperature as shown in Figure 3, which shows that the condition $\tau w(89\ GHz) / \tau w(30\ GHz) < 5.6$ (or $\tau w\ (30\ GHz) / \tau w\ (89\ GHz) > 0.18$) corresponds to supercooled water temperatures.

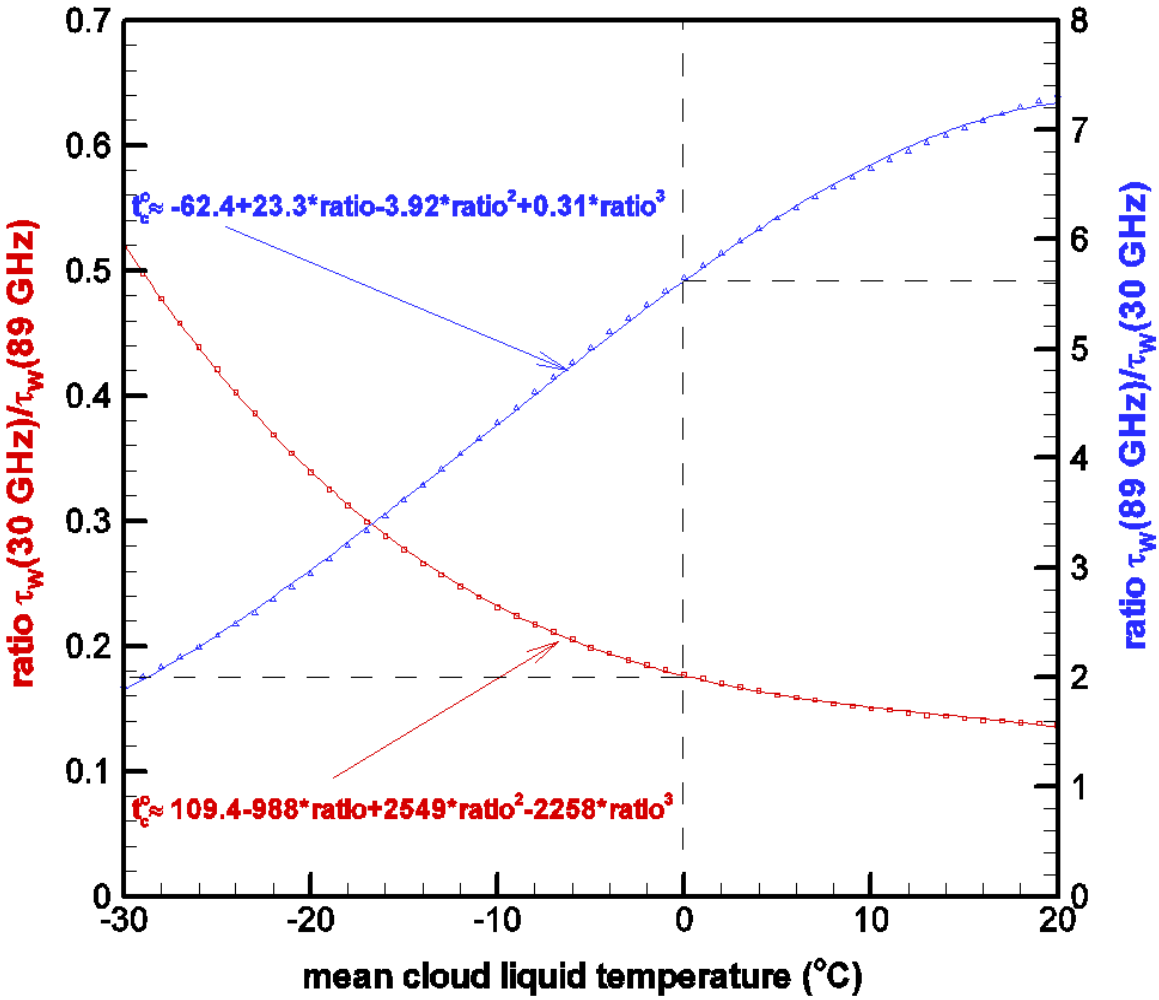

Figure 3. Ratios τ_w (89 GHz) / τ_w (30 GHz) (blue) and τ_w(30 GHz)/ τ_w(89 GHz) (red) as a function of temperature (from Schneider et al. 2004).

Figure 4 shows results of estimation ratios in layers of "warm" (red) and "cold" (blue) liquid water stratus clouds, as a test of the technique during AIRSII. Average slopes of the best linear fit equations represent a mean value for the optical thickness ratio τw(89 GHz)/ τw(30 GHz) and thus can be used for estimating mean cloud liquid temperatures. These temperatures are about +7°C and -12°C for the "warm" and "cold" stratus cases, respectively. The fact that the best linear fit lines approximately cross the (0, 0) coordinate origin point indicates that the removal of the gaseous optical thicknesses τv and τo was generally accurate. This technique will be most helpful if the cloud liquid is entirely supercooled. However, when a cloud layer harbors both warm and supercooled liquid, a mean temperature warmer than 0°C can be deceiving, so care must be exercised to recognize that part of the cloud is supercooled and potentially hazardous.

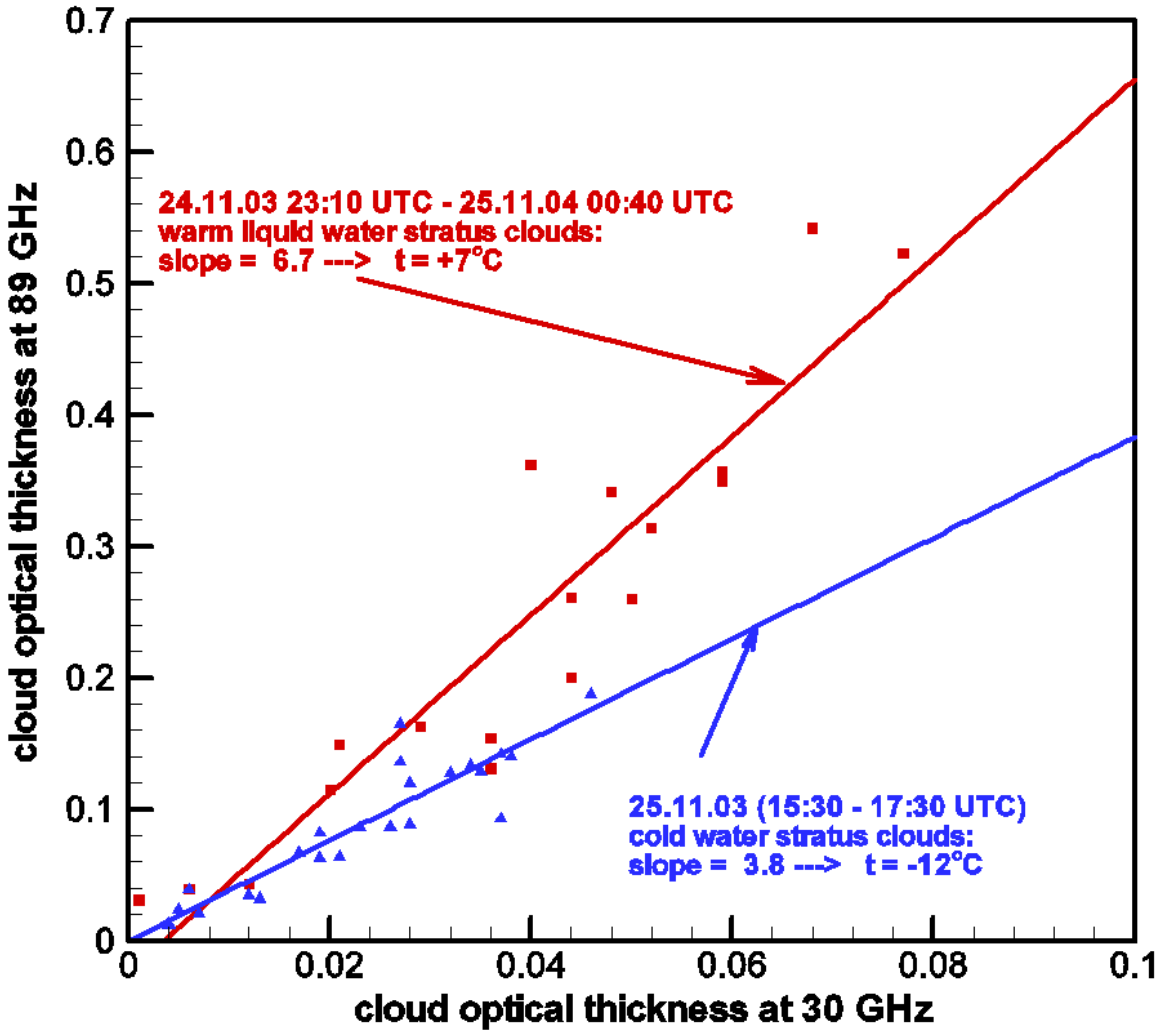

Figure 4. Illustrations of the mean liquid water temperature retrievals in "warm" and "cold" stratus during AIRSII (from Schneider et al. 2004).

2.4 Icing Hazard Algorithm

The several measurements and data ingests designed into GRIDS must be integrated in a meteorologically and technologically sound way to provide an output that will identify and warn of potential aircraft icing hazards. The icing algorithm brings together all the relevant measurements from GRIDS to make and issue a decision about the current icing hazard. GRIDS can address all-liquid clouds, mixed-phase clouds, and glaciated clouds.

Some perspective on the expected values is helpful. Pilot report (PIREP) statistics (Schultz and Politovich 1992) and many other more recent studies with instrumented aircraft indicate that about 90% of icing events occur in clouds with temperatures between 0°C and -20°C, below 6 km MSL, or within 9.3 km range for a radar elevation angle set at 40°, the fixed-beam selected for GRIDS. The required measurements are easily achieved through this short range with the GRIDS radar. The 50–500 μm droplets defined as supercooled large droplets (SLD) generally

cause reflectivities between -15 and +5 dBZ, a range readily handled with a large margin with the GRIDS radar, and use of the K_a-band radar allows a good margin for detection of high concentrations of still smaller droplets (<50 μm diameter).

Heggli and Rauber (1988) established a climatology of LW in mountain-forced winter clouds, including those events driven by storms. They found that the column-integrated LW was less than 0.2 mm 85% of the time, but storm periods produced many hours in the 0.5 – 1.0 mm range. This range is generally supported by other studies. Some values reaching as high as 2.0 mm can be expected; some column liquid values of this order were measured under wave forcing (Reinking et al. 2000a) and during the second Alliance Icing Research Project (AIRSII) with ETL and NASA radiometers in 2003.

The core icing algorithm uses four decision points based on the slant-path, fixed beam measurements of liquid water (LW), radar reflectivity Z_e, radar depolarization ratio (DR), and on the ingested temperature profile. The following parameters and values have been incorporated into the GRIDS core icing algorithm. A hazardous region within a cloud is identified as one that exhibits a temperature low enough to cause droplet supercooling ($T < 0°C$), a reflectivity large enough to warrant consideration ($Z_e > -23$ dBZ), and a DR that matches the spherical hydrometeor signature (± 2 dB), all while the radiometer indicates significant liquid water along the path (LW > 0.05 mm—the minimum detection threshold). A reflectivity Z_e of -23 dBZ approximates that point where the minimum threshold for moderate icing conditions is met at the smallest effective droplet diameter, D_e, considered in the Federal Aviation Regulations (FAR) Appendix C icing envelopes. That point is (LWC, D_e, T) = (0.3 g m^{-3}, 15 μm, -20º C). The lower-threshold value of the depolarization ratio, DR_{th}, depends on the properties of the antenna; it is a few decibels more than the antenna cross-talk, which is nominally specified for -30 dB. The GRIDS core icing algorithm, as derived from these decision points is summarized in Figure 5. The icing potential is indicated in a continuous time-altitude display (as schematically depicted in Figure 1) updated every minute, such that the real-time conditions and a short history (e.g., several hours) are presented as an evolving profile through all clouds in the radar beam. Thus, the core icing algorithm uses four decision points based on the slant-path, fixed beam measurements of liquid water (LW), radar reflectivity Z_e, radar depolarization ratio (DR), and on the ingested temperature profile.

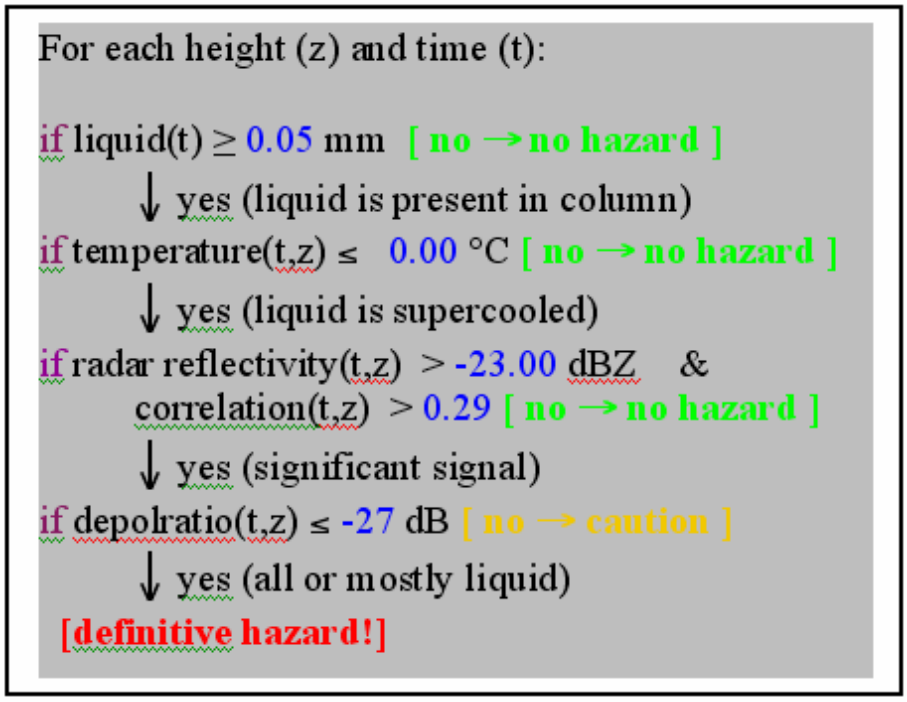

Figure 5. The decision points for the GRIDS core icing hazard (from Schneider and Campbell 2006).

The GRIDS algorithm is a vital, evolving decision-making tool. This perspective for the GRIDS core algorithm must be recognized. The core algorithm is an effective beginning, with much potential for enhancements. Just as algorithms for the NEXRAD have been continuously improved since that system was made operational, the GRIDS algorithm can gain power with continuing upgrades. Further, GRIDS or any other measurement or modeling system can only warn of a potential hazard. An accident-causing hazard is dependent on the aircraft and its deicing capabilities as well as the cloud environment. An aircraft may collect too much ice very rapidly in a high liquid, SLD cloud, or by flying too long, e.g., in a holding pattern, in a low-liquid small-droplet cloud. GRIDS will detect both and warn of the general hazard, but cannot include characteristics of individual types of aircraft.

The specifics of the implementation of this algorithm, including the core algorithm and enhancements thereto, are outlined in Section 3.3 and discussed in more detail in Appendix B.

2.5 GRIDS Operational Experience

The GRIDS design described in this document is based on tests with ETL's scanning K_a-band radar (NOAA/K), a fixed-beam K_a-band radar (MMCR), and on component design and construction selected specifically for an operational GRIDS. NOAA/K was operated in the series of WISP and related experiments and has provided the proof of concept. Thus, the fundamental icing-detection algorithm was derived from the evolving polarization theory and field testing which has been extensively referenced in this document. ETL's Millimeter-wave Cloud Radar (MMCR), a vertically pointing, fixed-beam system that is in continuous operational use at the several DOE Atmospheric Radiation Monitoring (ARM) sites, has provided a

hardware prototype for the operational GRIDS. Tests of the algorithm were conducted by operating NOAA/K in the same mode as planned for GRIDS in order to validate the concepts that integrate the data from the separate systems and inputs. Two experiments were performed, AIRS II and WISP04, and both incorporated a radiometer measuring LW and WV and the RUC model. The icing algorithm was calculated in real time and data were sent via the Internet to ETL, where it was archived and displayed. The temperature profile was taken from the RUC model.

Analyses of two field tests, one from AIRS II and one from WISP04, as analyzed by Schneider et al. (2005) and Bernstein and Schneider (2004), respectively, demonstrate the functionality of GRIDS.

2.5.1 AIRS II—Essence of Case of 11 November 2003

Meteorologically, deep, glaciated, snowing clouds early in the period contributed minimal icing threats over Mirabel Airport, Montreal, the site of the AIRS II experiments. Later, mid-level drying occurred, leaving lower, water-dominated clouds with warmer (but still sub-zero) tops that were being lifted over a warm frontal surface. These clouds carried significant water contents and SLD, which resulted in moderate to severe icing conditions. GRIDS documented the fine structure of clouds throughout the period and recorded signatures of the SLD, the presence and timing of which were verified by three research aircraft in coordinated flight. The aircraft samples reported here are mainly from a NASA Twin Otter aircraft.

Early in the period, the aircraft found cloud above the melting level to be dominated by snow, with most liquid well consumed by the crystal growth processes (Figure 6). From vertical profiles prior to ~2000 UTC, the various aircraft sampled low liquid water contents (LWC), in the range of 0.1 to 0.25 g m^{-3}.

However, samples with one aircraft after ~2009 UTC found rapid change resulting in LWC of 0.15 – 0.5 g m^{-3}, and freezing drizzle around -2°C between 1.7 and 2.3 km AGL (top of the profile) at ~2018 UTC, and recorded 100–300-micron-diameter SLD (Figure 7). The pilots reported ice accretions aft of the ice protection system in moderate-to-severe conditions, while other aircraft found icing up to 3.7 km AGL. Cloud tops continued to descend and eventually became too warm for icing, but the drizzle formation process continued, as documented by the Twin Otter aircraft.

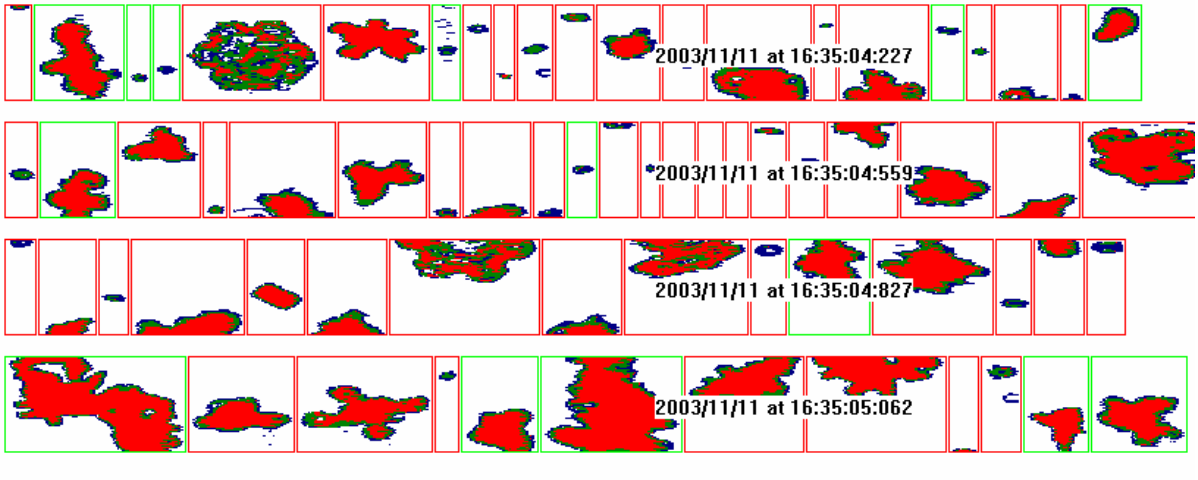

Figure 6. Individual ice crystal images observed by the NASA Twin Otter 2DC-Grey probe at 1635 UTC.

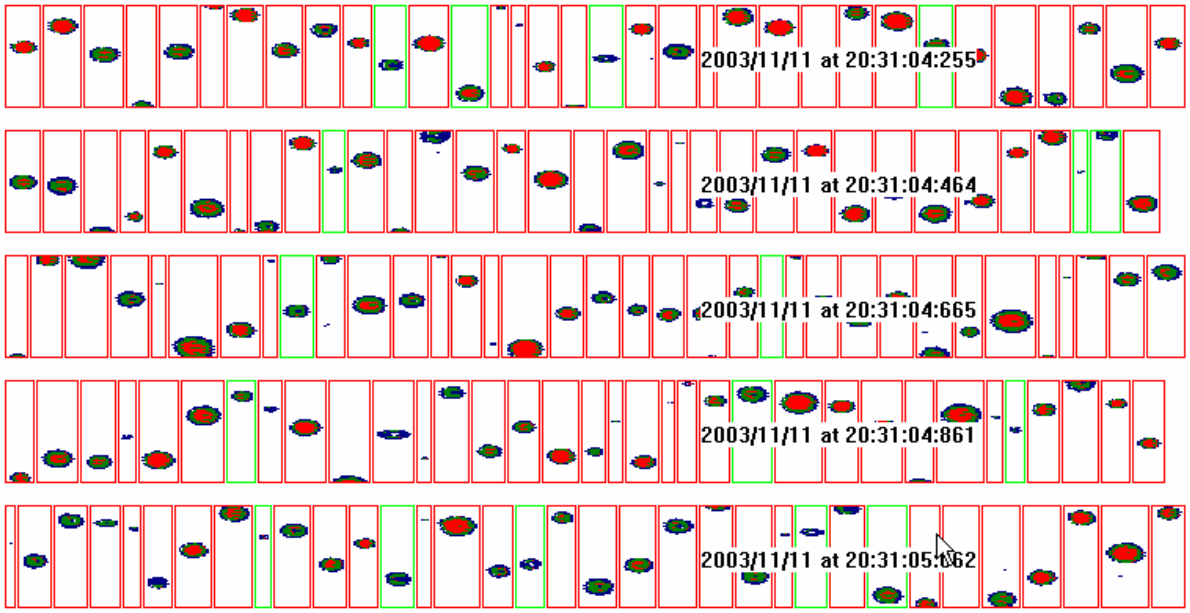

Figure 7. Individual freezing drizzle droplet (SLD) images observed by the NASA Twin Otter 2DC-Grey probe at 2031 UTC.

At ~1900 UTC, the RUC model and the aircraft, in reasonable agreement, placed the melting level at ~1.5 km. The RUC held the melting level constant throughout the period of interest, 1900–1945 UTC. During AIRS II, and including this case, the GRIDS radar was operated nominally on a 20-minute cycle, with 18 minutes staring at 40° elevation with a fixed azimuth, followed by two orthogonal RHI (vertical-slice) scans to provide spatial context and information on the angular dependence of DR. The GRIDS icing hazard product for the period of interest is shown in Figure 8.

The extensive yellow areas denote regions where caution was advised within the changing boundaries of the clouds; during these periods the GRIDS microwave radiometer confirmed supercooled liquid above the algorithm threshold, but due to the mixed phase, the radar did not determine where within the cloud the liquid actually resided. The depolarization measurements from the radar, combined with the radiometer, did indicate dangerous SLD (DR < ~ -28 dB) at times and altitudes indicated in red (Figure 8). Included here are red conditions that began at 2017 UTC, between 1.5 and 3.5 km AGL. This warning, which persisted through 2045 UTC, was consistent with data from the Twin Otter aircraft, which detected significant SLD on climb-out at 2009 UTC and during its 2015–2031 period of level flight at ~2.3 km, as reported in Figure 7. This is *in situ* confirmation of the GRIDS algorithm.

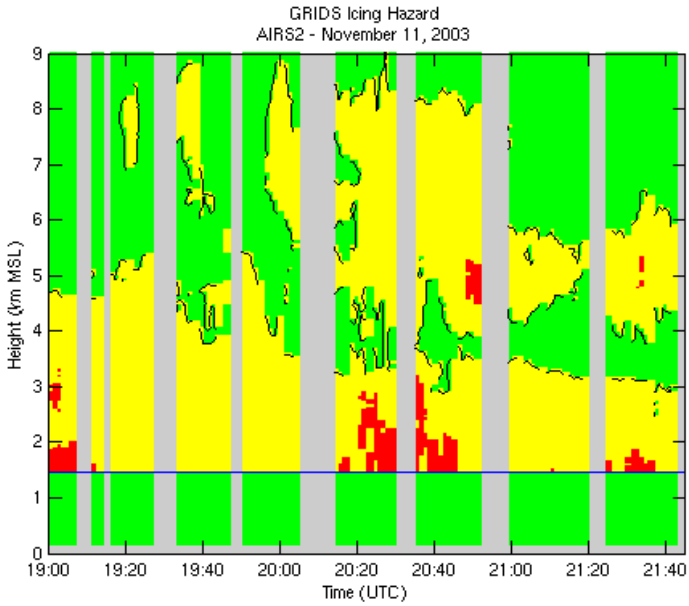

Figure 8. Time-height image of the GRIDS icing hazard. Green=safe; yellow=caution; red=definitive hazard. The blue horizontal line at 1.5 km altitude indicates the freezing level determined from the RUC model. The vertical grey bars are periods where the radar was scanning or pointing vertically.

The location of predominant LWC within the vertical column, even though not specifically identified in the DR signature, is potentially measurable using vertical Doppler spectra. Spectral information would be an enhancement to the core GRIDS algorithm. When any of the aircraft were sampling in vertical profiles over the Mirabel Airport, the GRIDS radar was sometimes operated in a vertically pointing time series mode, in order to measure the spectra of cloud particle fall speeds. An exemplary set of measurements was taken between 2007 and 2011 UTC during this case study (Figure 8 shows a vertical grey bar for this period). In Figure 9, five-second time-averaged spectra that were sampled three times in this 4-minute period are presented at selected altitudes through the cloud layers.

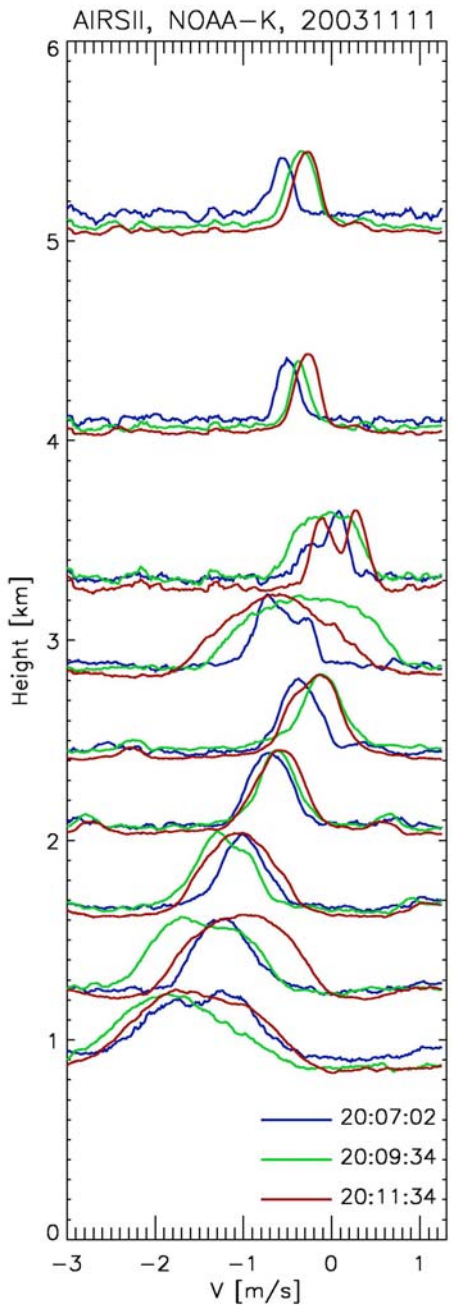

Figure 9. Spectra of vertical velocity as a function of altitude from 4-min time series measurements with GRIDS, 2007–2011 UTC. The minimum value in each spectrum indicates the corresponding altitude.

The Twin Otter aircraft generally encountered an ice-dominated environment during a descent just prior to 2009 UTC and a liquid-dominated environment during its foray after 2009 UTC. The GRIDS radar spectra were centered on this time. The spectra above 4 km have narrow peaks and a downward motion of ~0.5 ms^{-1}; these are characteristic of settling ice crystals. The aircraft found ice crystals and minimal LWC above 3.5 km. Between ~2.8 and 3.3 km altitude, the spectra vary considerably and are mostly characterized by their breadth and/or

bimodality straddling the 0 ms^{-1} boundary separating upward from downward motion. These features suggest the generation of liquid, i.e., small droplets with negligible fall speeds carried with cloud motion, in the presence of settling ice. Some 14 min earlier, the aircraft found crystals and their aggregates here, but essentially no liquid. The time difference is significant. Supercooled liquid water (SLW) became evident again in the aircraft samples below 2.5 km at 1953 UTC in mixed-phase clouds. The spectra show downward increases in hydrometeor fall speeds below this level, indicating growing ice crystals. However, bimodalities again appear between 1 and 2 km, corresponding with the aircraft detection of drizzle-sized droplets (SLD).

This case is presented in more detail by Schneider et al. (2005). More about the addition of Doppler spectral measurements to enhance the GRIDS algorithm is discussed in Appendix B.

2.5.2 WISP04—Essence of Case of 10–11 March

The following test case illustrates not only the performance of GRIDS but the synergy with the Current Icing Potential Model (CIP; Bernstein et al. 2004), which was also developed under the FAA's Aviation Weather Research Program over the same years as ETL's GRIDS. Since each integrates different sources of icing-related data to indicate the presence of supercooled water drops, both at small and large sizes, they can provide largely independent and complementary assessments of the hazard and thus add (or subtract) confidence in the combined result. During WISP04, GRIDS operated out of its base at Erie, CO, while CIP was running in real time at NCAR. This test case is taken from WISP04, as analyzed by Bernstein and Schneider (2004). Additional such studies can be found in the analyses of Schneider et al. (2004) and Schneider and Campbell (2006).

This icing event, which occurred on 10–11 March 2004, manifested itself as post-frontal, upslope stratus with some embedded showers, and impacted the plains of northeastern Colorado. Both GRIDS and CIP diagnosed the presence of icing and provided unique perspectives on the event. These diagnoses were verified by comparison to aircraft observations of in-cloud "truth" from the North Dakota Citation.

GRIDS measurements are nominally averaged to provide 1-min resolution data (higher temporal resolutions are possible). The spatial resolution of GRIDS is nominally 37.5 m. CIP uses GOES satellite data and surface observations to find clouds and identify their bases, tops, and cloud top temperatures. It combines this information with a mosaic of NEXRAD radar reflectivity, surface observations of precipitation, observations of lightning from the national lightning detection network, recent pilot reports, and 3-hr RUC model forecasts of temperature, relative humidity, vertical velocity, and supercooled-liquid water to estimate the potential for icing and SLD conditions across the contiguous United States and southern Canada.

During WISP04, an operational, 40-km-resolution version of CIP ran at NOAA's Aviation Weather Center (AWC) and a then-experimental, 20-km version ran at NCAR. The 20-km version, used here, contains many important upgrades and was implemented in 2005 at AWC.

The University of North Dakota's aircraft was flown to document the microphysical characteristics of clouds and precipitation over the WISP04 domain. The Citation carries an array of probes to record state parameters and cloud physics fields.

Early in the test period for this case, little or no supercooled liquid water was present in the clouds, as evidenced in the intermittent, low integrated water contents measured by the GRIDS radiometer through ~2000 UTC (Figure 10). Following a secondary frontal passage,

temperatures dropped rapidly toward freezing and low stratus clouds moved into the WISP04 domain. These clouds contained significant amounts of supercooled liquid water which impacted the area between 2100 and 0400 UTC (Figure 10), resulting in numerous reports of light and moderate icing. Water contents dropped to near zero by 0400, although skies did not clear immediately.

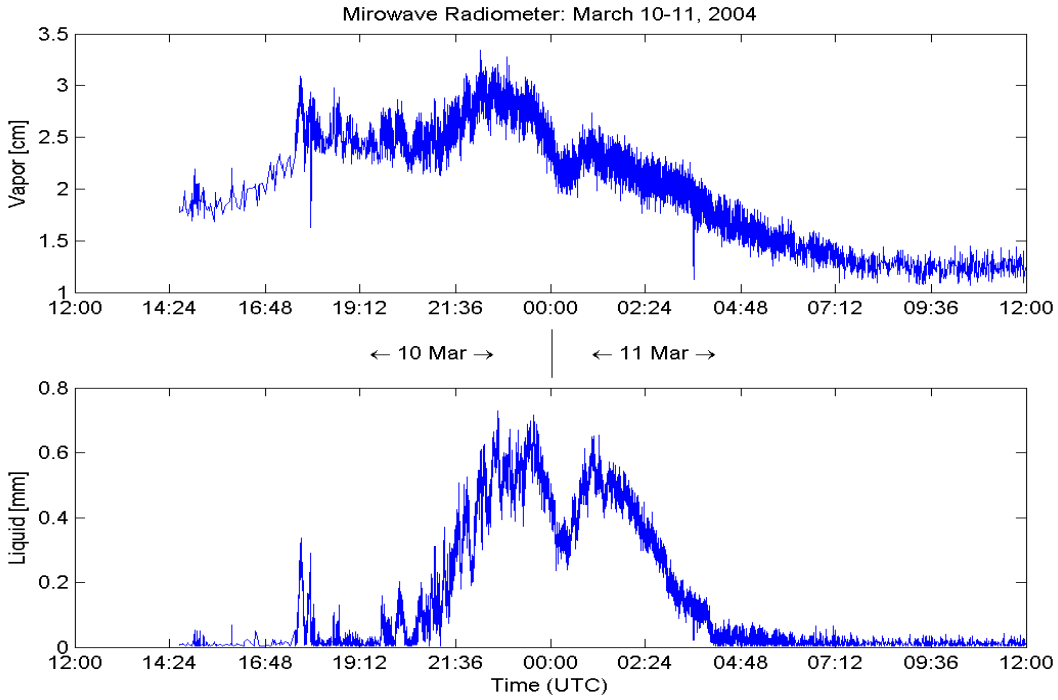

Figure 10. Integrated vapor and liquid values measured by the GRIDS radiometer for the period 1200 UTC, 10 March through 1200 UTC, 11 March.

In accord with the GRIDS radiometer, the UND aircraft measured LWC during climb out at ~2230 UTC (Figure 11a), and during a subsequent series of flight legs at stepped altitudes (Figure 11b) ending at 0001 UTC. Cloud base and top were found near 2.3 and 3.6 km (all heights MSL). Cloud top and base temperatures were -7.7°C and -2.5°C, respectively, which were ideal for icing conditions. Measurable LWC was found throughout this cloud layer, with the most significant concentrations consistently near 0.35-0.55 g m^{-3} and peak values to 0.8 g m^{-3} in the upper part of the cloud. During a brief second flight (not shown), uniform icing conditions with LWC of 0.5 g m^{-3} were found near 3.0 km MSL between 0100 and 0200 UTC.

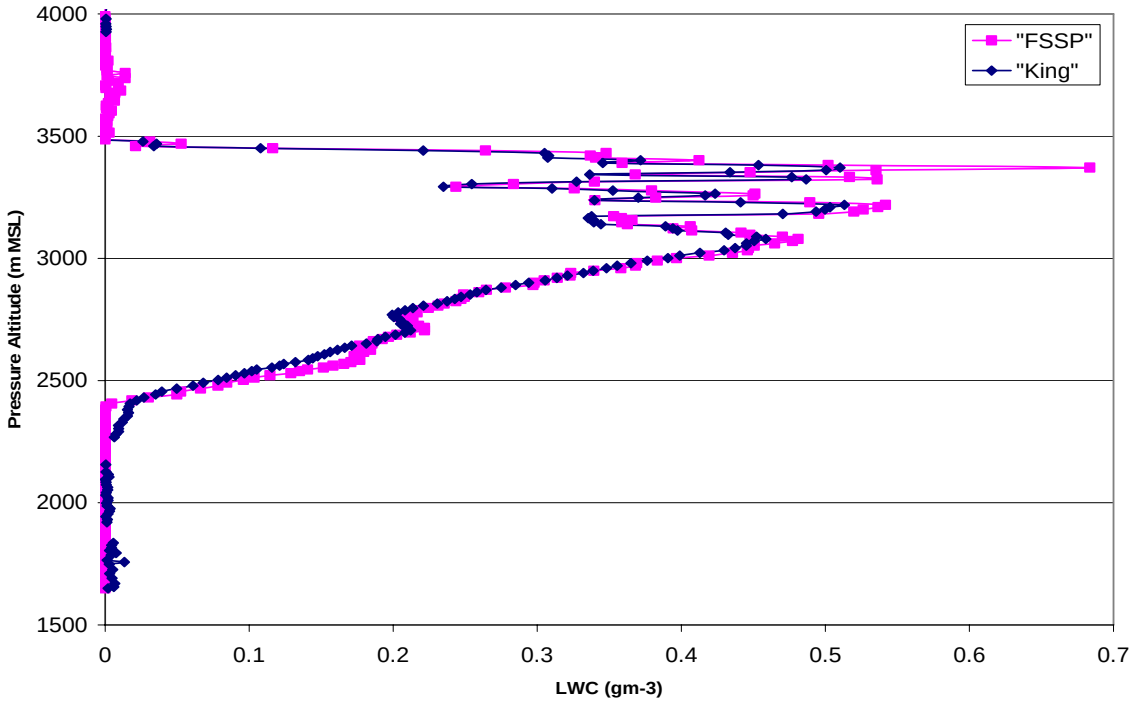

Figure 11a. Liquid water content measured during climb out at ~2230 UTC. Altitudes are in meters above MSL. Magenta and blue lines trace water contents measured by two different probes.

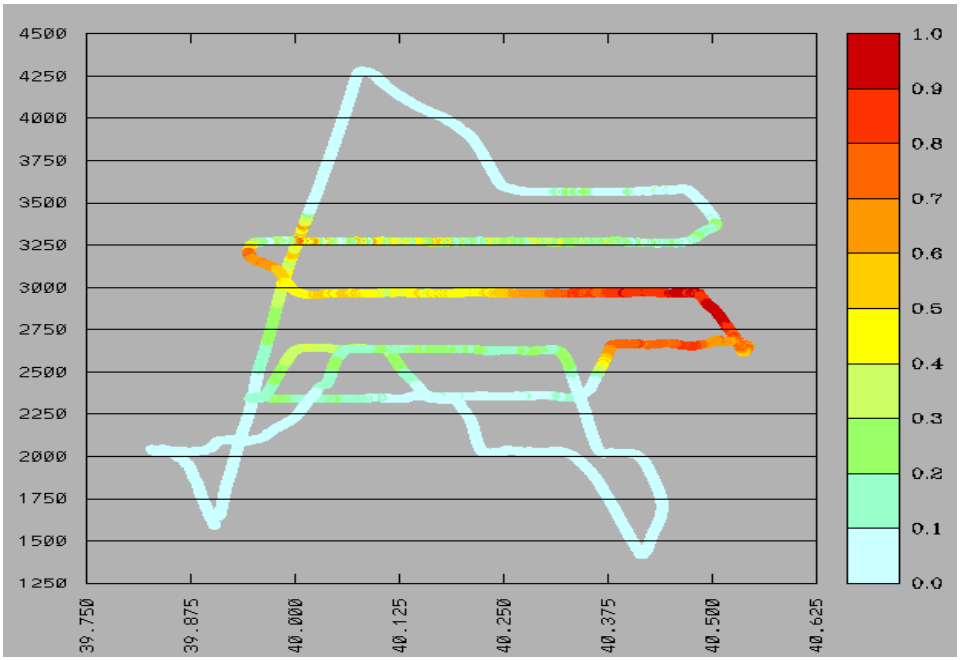

Figure 11b. Liquid water content measured during climb out at ~2230 UTC in a distance-height cross section. Color scale shows water content in g m^{-3}. Altitudes are in meters above MSL. The horizontal axis is in degrees of latitude.

The GRIDS K_a-band radar depiction of the clouds during this case showed relatively dynamic clouds for the first half of the event, then weaker, more stratiform clouds during the second half. Depolarization ratio measurements indicated that cloud ice was present somewhere in the column throughout the duration of this case. Prior to 2100 UTC, the K_a-band radar indicated that there were ice clouds between 2 and 5 km MSL (Figure 12). By 1915 UTC there was a bright band which persisted until 2050 UTC, showing the melting level to be just over 2 km MSL during this period. The GRIDS icing algorithm (Figure 13) issued icing cautions (yellow) throughout most of the duration of the case until the system dissipated, including and in accord with the *in situ* truth of SLW measured during the 2230–0000 flight of the UND aircraft. The radar was documenting the presence of ice and the radiometer was documenting the presence of liquid, thus confirming mixed-phase clouds observed by the aircraft. The yellow warning was intermittent prior to ~2045 UTC, reflecting the intermittent LW measured with the radiometer (Figure 10). Interspersed were three zones with red warnings of icing, including very two slight ones at ~1945, at ~0200 UTC, and a very significant one between 2230 and 2300 UTC below ~3.5 km MSL. Notably, the algorithm appropriately flagged the main "condition red" as the aircraft confirmed the significant SLW during and following climb out (~22:30 UTC, Figure 11a).

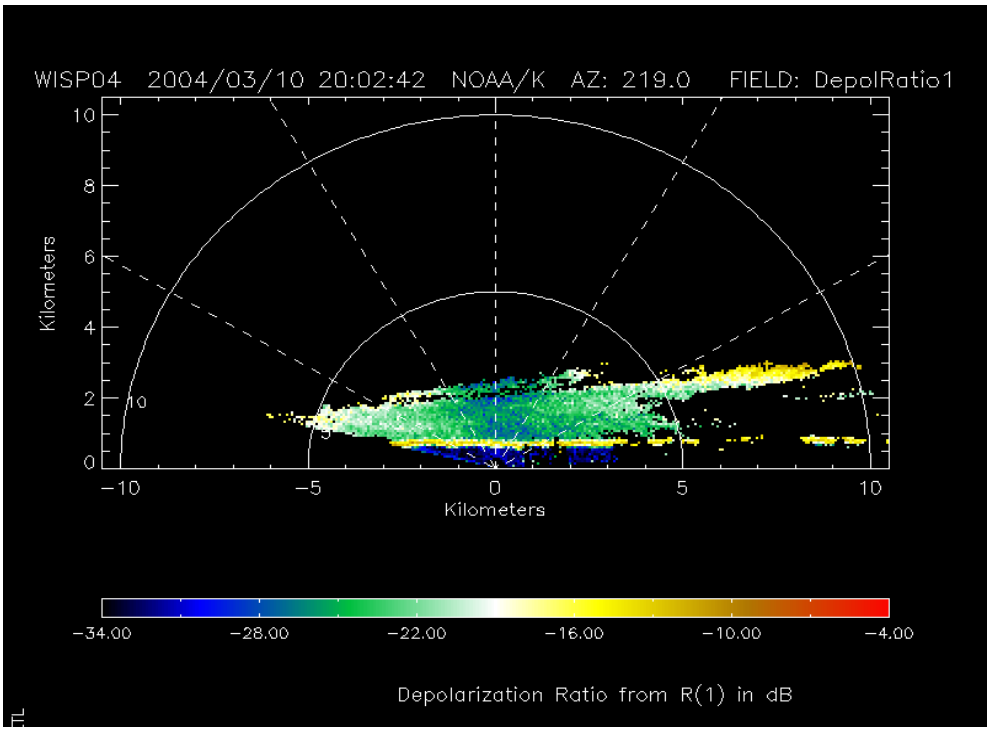

Figure 12. Vertical slice (RHI scan) of the depolarization ratio (DR) at 2002 UTC, parallel to an aircraft transect. The DR clearly shows the bright band at ~2 km MSL (~0.5 km AGL). DR > -32 dB indicates the presence of ice. Range is relative to radar.

During the 1915–2050 UTC period, when the radar documented the bright band at 0.8 km AGL or 2300 m MSL, the RUC model had the freezing level at 2800 m MSL, nearly 500 m higher (Figure 13). The GRIDS algorithm most likely missed lower-level icing hazards because of the RUC model error, as determined by the radar bright-band truth. The incorporation of the

bright-band altitude enhancement to the algorithm (as outlined in Appendix B) and use of the additional, 55-GHz radiometer channel to determine low-altitude cloud temperatures (as in Section 2.3.4 and Appendix B) to serve as cross-checks on the RUC, will certainly increase the accuracy of the GRIDS algorithm. These can be readily implemented.

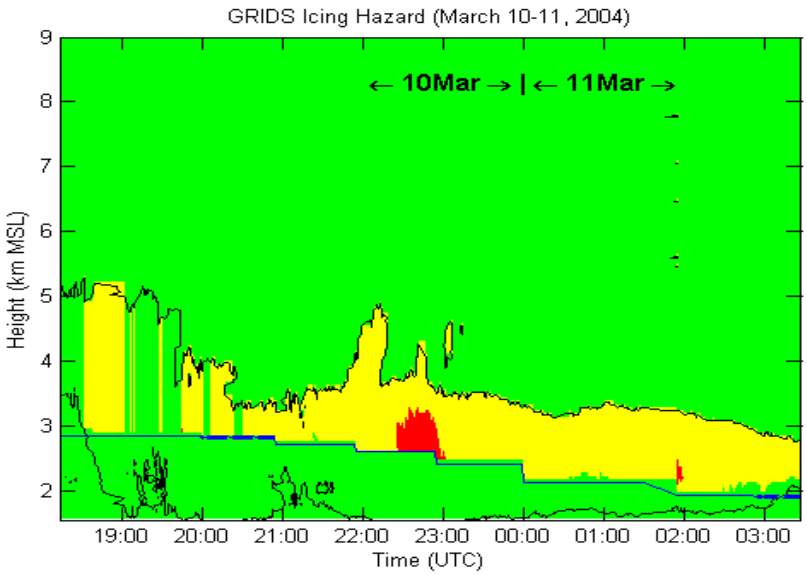

Figure 13. Time-height (MSL) image of the GRIDS icing product (green=safe; yellow=caution; red=serious hazard), with a cloud boundary overlay (black contour) and the zero degree isotherm (blue line) from the hourly RUC product.

The CIP model diagnosed icing conditions across northeastern Colorado throughout the period of the flights. At approximately the time of the aircraft climb out, CIP indicated potential for icing between 2.5 and 4.3 km, with high potentials (0.8–1.0 on a scale of 0.0–1.0) between 2.8 and 3.7 km (Figure 14). This range of altitudes very closely matches the core icing altitudes observed by the aircraft and GRIDS, both during its climb and during the horizontal flight legs, but generally overestimated the total depth of the icing layer (see Figure 11a and Figure 13). Using GOES observations of clouds with -9°C cloud-top temperatures in combination with the RUC profile of temperature (compared to the -7.7°C value observed by the aircraft), CIP overestimated the cloud-top height by ~0.5 km (~1500 ft). The overestimate was caused by a combination of slightly cold satellite-measured cloud-top temperature (CTT), slightly warm RUC forecast temperatures which also affect the GRIDS algorithm, and CIP's conservative method of cloud-top height estimation, which places the cloud top at the first vertical level that is colder than the satellite-observed cloud-top temperature.

Local ceiling observations indicated a cloud base of 2.6 km MSL, which CIP brought down to the next lower grid point, vertically, at 2.5 km. Ideal icing temperatures (-3°C to -9°C), satellite-indicated cloud top at -9°C, plus both high relative humidity (>90%) and weak upward motion from the RUC all contributed to the high icing potentials. Although the cloud top height was overestimated by 0.5 km, low relative humidity values and slight downward motion at altitudes between the actual and the CIP-diagnosed cloud tops resulted in low (0.1-0.4) icing

potentials there. Warm RUC temperatures also resulted in low icing potentials (0.35) near cloud base.

CIP diagnosed icing all along the flight track, and continued it southwestward into the Colorado foothills and northeastward to the Nebraska border (Figure 14). Icing was consistently depicted during the hours of flight, when icing was encountered aloft and the GRIDS radiometer showed significant amounts of integrated liquid water (Figure 10).

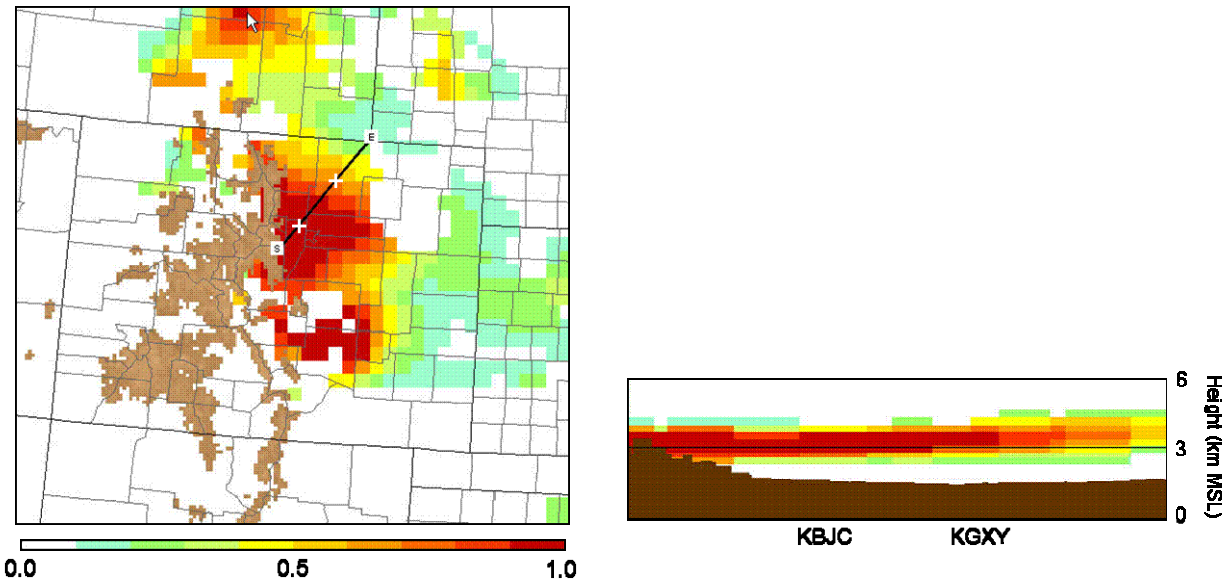

Part a Part b

Figure 14. Horizontal and vertical cross sections of CIP icing potential for 2300 UTC a) at ~3.0 km (700 mb) altitude and b) vertically, along the black line in part (a). White crosses in part (a) indicate the locations of the aircraft flight legs. Brown filled areas indicate topography.

In sum, both GRIDS and CIP were able to diagnose the icing potential that occurred on this day. As with all systems, the GRIDS and CIP methods each have their strengths and weaknesses affecting diagnoses for different icing events. While CIP consistently depicted icing throughout the ~7 hour event, it provided relatively coarse, hourly output with 20 km horizontal and 0.3 km (1000 ft) vertical grid spacing. GRIDS demonstrated the ability to diagnose the icing on very fine time (1 min) and space (0.1 km) scales, accurately portraying the regions which contained icing, as would be appropriate in the immediate airspace of an airport.

GRIDS can accurately identify the altitudes of clouds and provide estimates of their phase and liquid water content. CIP's satellite- and surface-observation based cloud scheme can help to fill the gaps in GRIDS' cloud field when radar signals are weak or when heavy precipitation saturates the K_a-band signal, and to extend GRIDS' point-like measurements over a broader region. These two systems can complement each other particularly well in a terminal-scale setting, especially when development of the new terminal-scale version of CIP, running at 5 km and 15 min resolution, is completed. In all, GRIDS and CIP operated simultaneously would enhance the total icing product.

The field tests from these case studies further validate the fundamentals of the algorithm and GRIDS. Note that the GRIDS design calls for a much more sensitive K_a-band radar (work in progress) than was used during WISP04, which will improve the hydrometeor discrimination and extend the range of application of GRIDS. Full construction and operational implementation of GRIDS on a prototype basis is the next step, and is left to the discretion of potential users.

3. DESIGN OF GRIDS

General requirements for GRIDS are given in Appendix C, as well as a table of operating modes. In the following sections we divide the overall GRIDS design into its major components and discuss each individually. Below, in Figure 15, is a simplified block diagram that shows how the various sub-systems of GRIDS interconnect. For a more comprehensive block diagram of GRIDS, see Appendix D. Appendix E gives a list of GRIDS Features and Benefits.

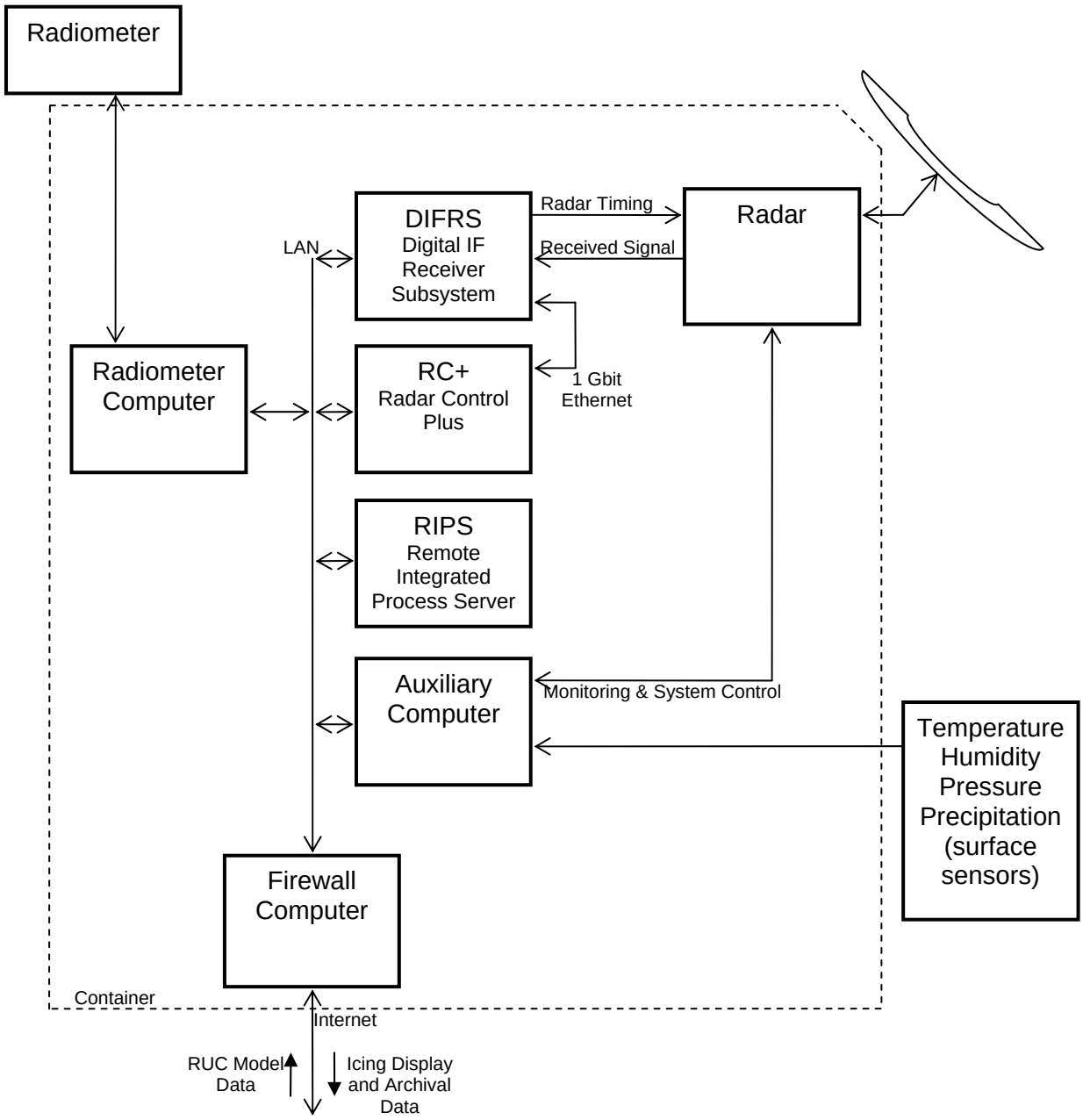

Figure 15. Simplified block diagram of GRIDS showing major sub-systems. For a detailed block diagram, see Appendix D. DIFRS, RC+, and RIPS are each Linux-based computers.

3.1 Sensors

Research leading to GRIDS indicates that the icing hazard within a cloud can be ascertained by combining three measurements: 1) depolarization of microwave energy scattered from cloud particles, 2) liquid water content along the path containing the scattering particles, and 3) the temperature profile within the cloud. These three measurements can be made using currently available technology, and are discussed in the following sections.

3.1.1 Radar

Our design of a radar suitable for operational use is based upon an award-winning design by ETL (Moran et al. 1998) that has proven its power, flexibility, and robustness with nine years of continuous operation at a number of remote Department of Energy (DOE) climate-observing field sites worldwide. It will be discussed here only in a cursory manner since its design is well documented in the Moran paper. The final transmitter stage in DOE's Milli-Meter Cloud Radar (MMCR) systems, and in GRIDS, is a low peak power, but high average power Traveling Wave Tube Amplifier (TWTA), designed originally for use in satellites. Average power is increased in one of two ways (or both) with respect to more conventional final transmitter stages such as magnetrons: high pulse repetition frequency (PRF), and/or transmitting pulses of long duration with embedded pulse coding (to maintain range resolution), which is known as pulse compression. For GRIDS, no pulse coding will be used to increase power (and hence sensitivity) because of the complicating range-velocity sidelobes that can result, and because adequate sensitivity can be obtained by other means. However, the design will accommodate the addition of pulse compression in the future if it is determined that more sensitivity is required.

GRIDS will have a TWTA with a peak transmitted power of 1000 watts. TWTAs are designed to operate unattended for long periods of time, with the manufacturer stating an expected lifetime of 2.3 years at continuous operation. However, experience with DOE radars indicates that the actual lifetime of these devices is considerably longer.

All of the radar components are designed to function in a standard laboratory environment (76 degrees F, low relative humidity). The radar is therefore housed in two racks inside an environmentally controlled transportable container, with the antenna mounted outside but as close as possible to the transmitter. The antenna will point the radar beam at an elevation angle of about 40º above the horizon, and (optionally) in the zenith direction (elevation angle of 90º).

The radar will have an adjustable pulse width with 1.55 and 1.00 μs pulses planned for first use, giving range resolutions of 232 and 150 meters, respectively. It is planned to use the 1.55 μs pulse width for the 40º elevation angle, and the 1.00 μs pulse width for possible zenith operation, giving a height resolution in both cases of 150 m. Thus, sensitivity at a given height above ground and height resolution will be approximately equal for the two elevation angles.

The desired minimum detectable signal at a height of 5 km above the radar is -140 dBm for GRIDS, which corresponds to an equivalent radar reflectivity factor (Z_e) of -65 dBZ. (Henceforth, we will refer to Z_e simply as reflectivity.) The present GRIDS design allows the antenna elevation angle to be manually adjusted between 30º and 90º. It would be desirable for GRIDS to have the capability for automatic angle changes commanded by computer to one of two positions (most likely 40º and 90º). For this capability, simple motors and stops would be added, at some added cost.

The microwave portion of the radar is shown in Figure 16 in block diagram form. The transmit pulse originates as a digital pulse in the Radar Timing Generator (not shown). From it, a 60 MHz pulsed IF signal is generated in the IF Modulator and sent to the Coherent Up/Down Converter (CUD). The CUD contains a solid state source whose output is used to synthesize all the frequencies needed to up-convert the transmitted signal and down-convert the received signals. The pulsed IF signal is then converted to RF (34.8 GHz) and then amplified by the TWTA to a 1000-watt pulse. The pulse is then sent through the Circulator Assembly, which functions mainly as a transmit/receive switch. The Circulator Assembly also serves to switch a

noise source into the receiver channel during calibration. The pulse then passes through the Ortho Mode Transducer (OMT), which transitions it to the circular waveguide, and then to the polarizer, which converts the linearly polarized wave to circular polarization. This signal is then radiated by the antenna as a circularly polarized wave.

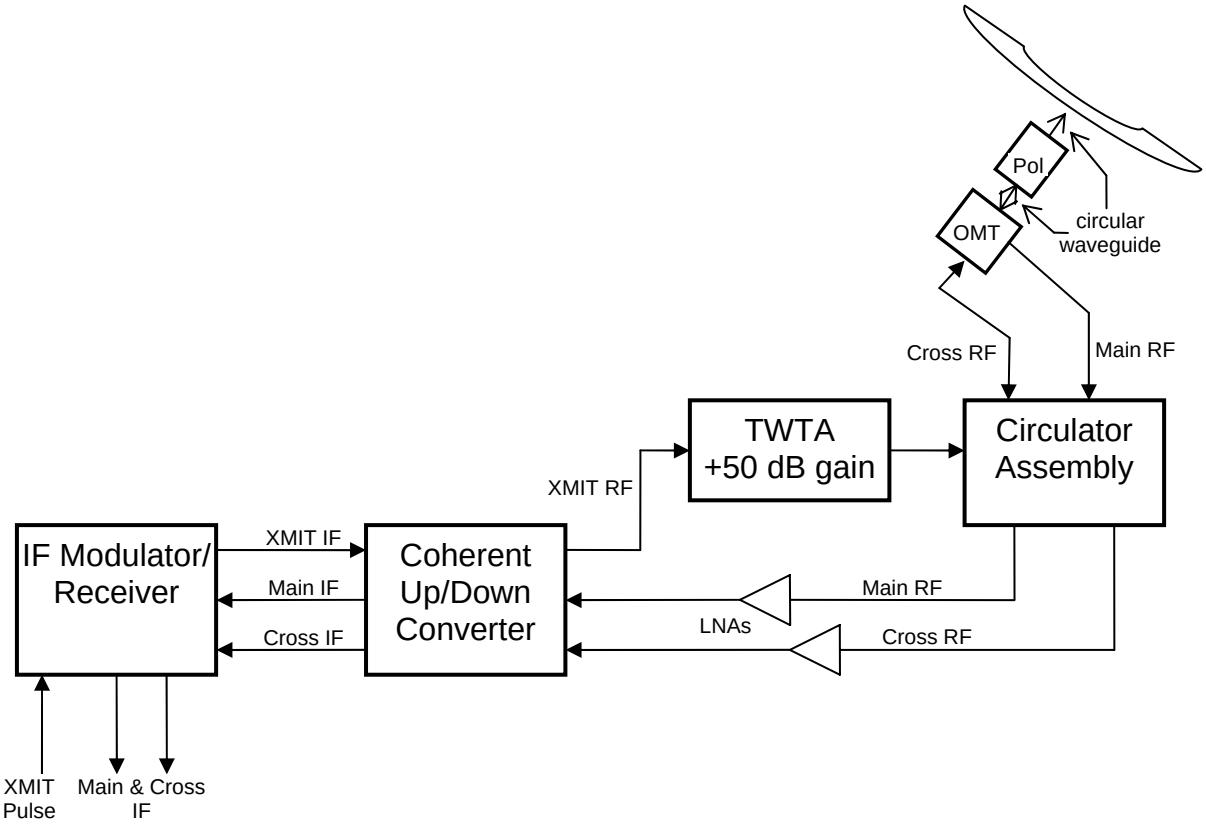

Figure 16. Diagram of radar in GRIDS showing the major components. The Circulator Assembly functions as a transmit/receive switch and also allows for injection of a noise source for receiver calibration.

When the radiated pulse strikes a scatterer, it is reflected back to the antenna. Specular (mirror-like) reflection will cause a polarization reversal (in circularly polarized waves) of the backscattered signal. So, for instance, if right-hand circular polarization (RHCP) were transmitted, then left-hand circular polarization (LHCP) would be received at the antenna from a non-depolarizing target. The received energy passes through the polarizer which converts it to linear polarization, and then into the OMT which separates the energy out into horizontally and vertically polarized waves at the two linear ports. These two ports are designated Main and Cross, with the Main port having the generally stronger signal because it is the cross-polarized port from the transmitted signal.

The two receive channels now enter the Circulator Assembly, pass through transmit/receive switching and are routed to the low-noise amplifiers (LNA), where they are amplified and passed to the Coherent Up/Down Converter (CUDC). The CUDC mixes the signals down to the 60

MHz IF frequencies, which are passed to the IF Modulator/Receiver where they are amplified to a suitable level to drive the A/D converters in the digital receiver (not shown).

Table 2 shows the characteristics of the radar portion of GRIDS when operating at 40° elevation and with 64-point Fast Fourier Transforms (FFTs). For characteristics in other modes, refer to Appendix C.

Table 2. Radar characteristics of GRIDS operating at 40° elevation

Physical characteristics	elevation angle	40 deg
	radar wavelength	8.6 mm
	antenna diameter	3.0 m
	peak transmitter power	1000 watts
	elevation angle	40.2 degrees
	transmitter path loss	2 dB
	receiver noise figure	5.5 dB
Parameters alterable by software	pulse repetition period	110 μs
	pulse width	1.55 μs
	number of FFT points	64 points
	dwell time	60 s
	range gate spacing	1.55 μs
	number of range gates	69
	receiver bandwidth	0.645 MHz
Dependent characteristics	unambiguous radar range	16.49 km
	minimum height	68 m
	maximum usable height	10.2 km
	maximum unambiguous radial velocity	±19.55 m/s
	maximum unambiguous horizontal velocity	±25.60 m/s
	time available for one spectrum computation	51 μs
	number of spectrum averaged per gate per dwell time	8523
	duty cycle	1.41%
	average power	14.1 watts
	range resolution	232.3 meters
	height resolution	150.0 meters
	radial velocity resolution	0.611 m/s
	Estimated sensitivity at 5 km AGL using spectral processing (0.2 m/s spectral width)	-69.4 dBZe
	Estimated sensitivity at 10 km AGL using spectral processing (0.2 m/s spectral width)	-63.4 dBZe

3.1.1.1 Calibration Checks

One planned difference between the GRIDS radar and DOE's MMCRs is the manner in which calibration checks will be performed. For MMCRs, about once every 10 days, a lengthy process is undertaken whereby radar operations are halted and many different levels of white noise are injected into the receiving channel, a transfer curve is produced (signal in vs. detected power) for the entire dynamic range of the receiver, and the radar constant is re-derived and compared to the default value. All measurements are saved. Only if the new radar constant differs markedly from the default value is action taken. For GRIDS we will perform calibration checks much more frequently, at least once per day. Instead of regenerating the entire transfer curve, however, we will check only two points on it – one point near the center of the receiver dynamic range and one point at the bottom (no signal in).

The receiver design will allow this calibration to be done automatically, and it will be controlled and scheduled by the GRIDS software. Action will be taken only if the transfer values differ markedly from the current "correct" values. If the expected values from the calibration are off by only a small amount, then the calibration constants will be changed automatically. Large errors would indicate a severe problem and require service by a maintenance technician. Several years' experience with five MMCRs has led us to take this simpler approach. The more thorough and time-consuming procedure has no additional practical benefit. Either procedure checks only the receiver's calibration; it does not check calibration of components "outside" the receiver, such as the waveguide between the antenna and the radar's electronics, and the antenna itself. These components typically remain stable unless damaged. The other variable is the transmitted power, which will be monitored automatically.

3.1.1.2 Radome

Radomes are antenna covers designed to protect the antenna from water buildup (snow/slush) and from birds and dust/dirt which are often a problem in unattended operation. The radome introduces a small loss by attenuating the radar signal on both transmission and reception (about 1 dB, two-way). This loss is normally accounted for in the antenna calibration, but additional loss will occur if the radome surface is coated with water or wet snow, perhaps during and after local events of precipitation. The amount of loss depends on the amount and thickness of water on the surface. For a vertically pointing antenna the radome surface is nearly horizontal. Often such radomes are designed with a 5º tilt, to allow water to run off. Still, attenuation values range from a few dB to 10 dB, for radome surface wetness ranging from a thin film of water to puddles of water. For wet snow, several inches can add more than 20 dB of attenuation to the radar signal.

For unattended operation, the GRIDS' antenna must have a radome to protect the surface of the dish from weather, birds, insects, etc. Since the antenna will be tilted at an elevation angle of 40º either permanently or cyclically with 90º, the likelihood of water/snow buildup is reduced. Experience shows that dry snow will be shed from the radome with negligible impact. The radome may, however, still have a water film buildup during and after wet precipitation that can introduce up to 10 dB additional attenuation (two-way). The sensitivity of the radar will be reduced by this loss. The water film loss will not affect the depolarization ratio (DR) measurements since the loss is the same for both polarizations. Since the water film will affect the reflectivity measurement, calculated reflectivity will be lowered by the amount of this loss. But this can be mitigated somewhat by using the radar data itself and data from a rain gauge to

estimate and correct for the additional loss. The data will also be flagged to indicate that the accuracy of the reflectivity is suspect.

3.1.1.3 Receiver Channels

GRIDS will use two independent receiver channels, each dedicated to one of the polarization states. This increases the sensitivity of each polarization channel by 3 dB, equivalent to doubling the transmitter power, as compared to having one receiver channel that is multiplexed between the two polarizations. The output of the two receiver channels is at IF frequencies, which is then digitized by a digital receiver card.

3.1.2 Radiometers

The GRIDS icing algorithm (Section 3.3) requires a measurement of integrated liquid water along the radar beam, as well as a frequent if not continuous temperature profile. These needs can be met by radiometers operating at both 20–30 GHz and around 55 GHz, although the 55-GHz temperature profiling has limitations as well as the advantage of continuous monitoring, as detailed earlier. Through core algorithm upgrades, the 55 GHz temperature profiler readings can be integrated with RUC model temperatures and bright-band recognition to achieve a best estimate. Frequencies around 20–30 GHz yield integrated liquid water and water vapor measurements. Although water vapor is not required by GRIDS, it is available as a by-product of the liquid water measurement. Frequencies around 55 GHz are used to provide a temperature profile.

A single enclosure housing all the radiometer equipment will be mounted on the roof of the GRIDS container. The radiometer system will be controlled by a PC inside the GRIDS container.

Radiometers are available from ESRL/PSD, which, operating as ETL, developed the technology in the late 1980s and continues to improve microwave radiometry, or from commercial sources such as Radiometrics, Inc. (http://www.radiometrics.com/) whose model TP/WVP-3000 has the needed capabilities.

3.1.3 Temperature profiles

The RUC model analysis produces a self-consistent statement of the current state of the atmosphere. The operational version used in GRIDS algorithm testing (Section 2.5), known as RUC-20, produced updated three-dimensional analyses and forecasts every hour, covering the lower 48 states at 20-km horizontal resolution through 50 vertical layers.

The current operational version, known as RUC-13, has 13-km horizontal resolution through 50 vertical layers. This version of RUC has improved numerics in the assimilation package, as well as improved physics in the mesoscale model. RUC is scheduled to be improved again by 2008 with an enhancement called Rapid Refresh. Real-time access to RUC data is available from NCEP (http://ruc.fsl.noaa.gov/). These data will be ingested into the GRIDS system via an Internet connection at hourly intervals.

Temperature profiles from the network rawinsondes at 00Z and 12Z are assimilated into the RUC, so the RUC is most accurate near the times and locations of the sonde launches—normally first-order stations at or near airports, where GRIDS units also will be most appropriately located. Temperature profile and melting level data from any radar signatures of the bright band

when available, and the 55 GHz radiometer will be compared to produce an algorithm for the most accurate profile possible. In this way, a temperature decision protocol will be established.

3.1.4 Surface Meteorological Sensors

Commercial off-the-shelf sensors (COTS) are used to furnish GRIDS with surface meteorological data consisting of temperature, relative humidity, atmospheric pressure, and rain rate. These data are used for station maintenance, radiometer calibration, diagnostic purposes, and data-quality assurance.

3.2 On-Site Computer Systems

There are six computers in the GRIDS container, all connected by a Local Area Network (LAN). This section describes both the hardware and software architecture of these computers.

Below we describe the design for the GRIDS system of computers, what they do, how they do it, and how they communicate. We believe this design will result in a robust unattended instrument at minimum cost and effort.

3.2.1 GRIDS Software Architecture

The GRIDS Radar Acquisition and Display System (GRADS) is the heart of the GRIDS real-time data-processing system. It is named GRADS, as a combination of GRIDS and RADS. RADS is a computer system that has been used reliably on the ETL scanning radars for the past ten years. It is described by Campbell and Gibson (1997) and by Gibson et al. (2004). The GRADS is a multi-level distributed software architecture that has been custom-designed for the GRIDS. Its design allows for significant changes in the hardware and operating system. It consists of several distributed processes that allow for acquisition of four separate data streams, data integration, archival, and display. The system produces data files as well as graphical products in real time and has a Web server component as well.

The top level GRADS is made up of two levels of distributed components, as shown in Figure 17. The next level is made up of the eXtended RADS or XRADS and the Remote Integrated Product Server, RIPS. XRADS acquires, processes, displays, and writes radar data and controls the radar. It is also composed of three distributed modules. The first is the Digital IF Receiver Subsystem or DIFRS. It is this part of the system that queries the Digital IF Receiver, services interrupts and acquires the data. It then sockets the data to the second module, Radar Control Plus, known as RC+. RC+ not only reformats the data, displays it and writes it to disk, but it also sockets the radar data to RIPS for integration with radiometer, RUC, and surface data. RIPS calculates the icing product and generates icing hazard, radiometer, RUC, surface met and radar displays in near real time. It archives the data and selected images and serves the data via HyperText Transport Protocol (HTTP) to a Web server. In addition the AUX computer controls and monitors radar hardware, such as the TWTA transmitter and the Pulse Controller.

All of the modules which compose the GRADS, except for the AUX computer, run on Linux operating systems. They are implemented in object-oriented C, C++, and Java, as a number of independent processes that communicate via shared memory, sockets, Remote Method Invocation (RMI) and HTTP. The AUX Radar Monitor program uses LabView running on Windows 2000 and communicates with RIPS via TCP sockets.

See Appendix F for a complete listing of existing software.

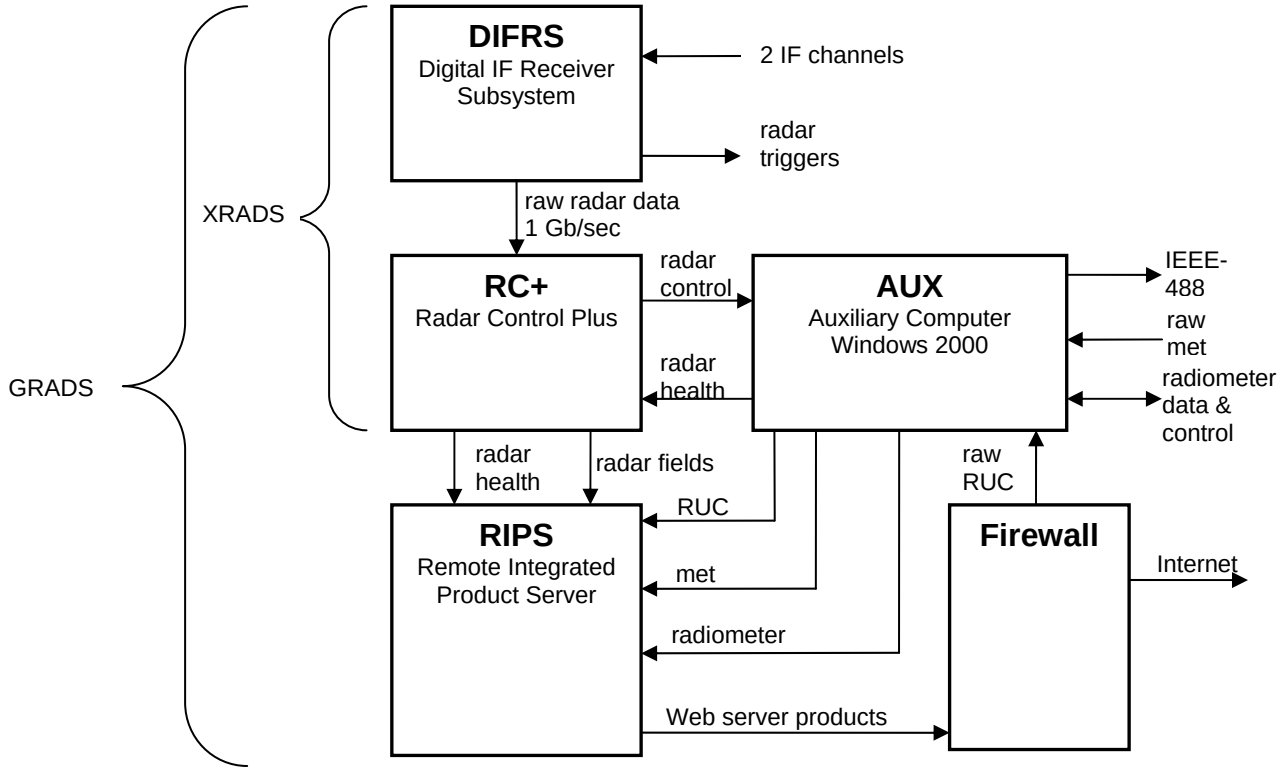

Figure 17. Software architecture diagram showing information flow. Each block represents a different computer.

3.2.2 GRIDS Computer Architecture

The GRIDS is designed to distribute data acquisition, data stream integration, processing, icing hazard calculation and display functionality across several platforms. It is currently designed with five computers, excluding the radiometer computer, which is part of a COTS radiometer system, and the off-site archival system/Web server. These five computers are connected with a Local Area Network (LAN). More detail on this, including a complete system block diagram and a GRADD data flow diagram, is available in Appendix D. The GRADS computers are rack-mountable PCs running the Linux operating system; they perform the functions of radar control, data acquisition, and data fusion. Another computer, called AUX, is a rack-mountable Windows PC that runs the Radar Monitor process that performs additional radar control functions and monitors the system health. The last computer is a Linux PC that functions as a network firewall. Because of the modest demands made upon it, it could be an older PC. In order to allow for flexibility in the chosen radiometer subsystem, the GRIDS software requires from the radiometer only a data stream of brightness temperature from the three radiometer frequencies, integrated liquid water, integrated water vapor, and the temperature profile.

It may be possible to combine some of the functions to eliminate one or two of the computers and thus reduce the cost. This decision can be made when the system is running and the computational loads can be assessed. Because of the way processes communicate, the software effort to combine functions is quite small. However, because of the low cost of PCs, the simplicity of distributed functions and the redundancy provided by multiple systems, it was decided to use five computers in the initial design.

3.2.2.1 Digital IF Receiver Subsystem (DIFRS) Computer

The Digital IF Receiver Subsystem, commonly referred to as DIFRS, is a Linux-based computer system. It incorporates a two-channel digital receiver card (ICS-554B), a Radar Timing Generator (RTG) card, and a frequency synthesizer card. All cards are Commercial-Off-The-Shelf (COTS) products, but the RTG is programmed by ESRL/PSD. The frequency synthesizer card is used to generate a needed frequency (80 MHz) for the digital receiver card, which takes signals at IF frequency (60 MHz) and digitally produces the baseband signals.

The RTG card generates various radar timing signals such as the radar trigger, range gates, and receiver blanking signals. Since the card uses programmable FPGAs, this allows it to be reprogrammed when required.

Software running on the DIFRS is written in C++ since speed is important here. There is no graphical user interface (GUI) used on this computer since its control comes from RC+ via a TCP socket. This is purposely done in order to remove the computing load associated with GUIs from this machine.

In time-series or spectrum mode, raw data will be transferred to RC+, but in pulse-pair modes, DIFRS will implement the pulse-pair algorithm and send the resulting products to RC+. Whether DIFRS or RC+ will implement spectral processing in those modes will be determined by computational load.

3.2.2.2 Radar Control + (RC+) Computer

The Radar Control+ (known as RC+) computer provides an operator's graphical interface panel for the radar control, acquisition, display and archival of GRIDS. It is Linux-based and contains a GPS receiver card and functions as a time base for the entire system. It is on this machine that the real-time displays are created, images are captured, and data are written to local disks. This machine also runs processes that serve images and data to local client processes, which include data archival and the RIPS processes described below. This code is written in C++ and uses Motif libraries. When antenna scanning is implemented, the motion controller and antenna encoder cards will be interfaced into this machine. For additional detail on the RC+ processes, see Section 3.2.3.3 and Appendix G.

3.2.2.3 Auxiliary Computer (AUX)

The Auxiliary computer (known as AUX) is a rack-mountable Windows-based computer. It performs the functions of monitoring and controlling equipment, and retrieving and pre-processing the data from the RUC model. For additional detail on monitoring, see Section 3.4. Almost all programs on this computer are implemented in LabVIEW.

3.2.2.4 RIPS Computer

The RIPS computer is another Linux PC. This computer integrates and archives data from the various sensors and information sources: radar, radiometer, surface meteorological sensors, and the RUC model. It performs the icing algorithm and displays all of the raw and derived products in graphical format. Code on this machine is written in Java and uses the Abstract Window Toolkit (AWT) and Swing Java Foundation Classes. AWT and Swing are Java user interface toolkits which are commonly used to develop GUIs in Java. In order to serve data to a Web server it needs to be connected to the Internet through a firewall computer. The RIPS software and the RC+ software could be run on the same computer, although operational experience has shown that separate computers (or at least separate monitors) make viewing the numerous displays easier.

3.2.2.5 Firewall Computer

The firewall computer acts as a gateway to the Internet for the other GRIDS computers. It centralizes security problems and provides system security for the other computers, protecting them from hackers. This is a very important function, because it removes the burden of keeping the operating systems on the other computers up to current levels. Because of special hardware drivers on some of the computers, it is not possible to keep software current without rewriting drivers. This computer is also a rack-mountable PC with a Linux operating system. Because it is the same style computer as the other PCs, it can also function as a spare or redundant computer.

3.2.3 Radar Data Acquisition and Processing

3.2.3.1 Data Acquisition

The radar is a dual-polarization, pulsed Doppler radar with a high duty cycle. A single circular polarization is transmitted, and two polarizations, designated main and cross, are received simultaneously. The radar receiver provides two channels of analog output (main and cross) at the IF frequency of 60 MHz which feed the digital receiver card in the DIFRS computer. The digital receiver card's 14-bit A/D converters are driven by an 80 MHz sampling clock from the frequency synthesizer board. The 60 MHz IF frequency and the 80 MHz sampling rate results in a signal frequency of 20 MHz in the digital signal. This is digitally mixed with a 20 MHz signal from a Numerically Controlled Oscillator (NCO) to deliver a signal at baseband. The baseband signal has two channels; they are referred to as I and Q for in-phase and quadrature. The signals are digitally filtered to the appropriate bandwidth and are then input into the computer's memory. After filtering, there are about 69 samples (range gates) after each radar pulse, depending on the operating mode. Appendix H describes in detail the digital filters used in the digital receiver card.

3.2.3.2 Front-end Processing

The DIFRS computer performs the calculations described in the GRIDS Covariance Algorithms document (Appendix I). Note that there are two classes of results from these calculations: recorded data products and display products. Because the display products can be recalculated from the recorded data products, they are not recorded. They are calculated solely for the purpose of providing real-time displays and as input for the icing algorithm. After the

covariance algorithms have been implemented, we intend to implement spectral processing in order to improve the GRIDS algorithm's performance in mixed-phase clouds.

These processed data are then sent via 1 Gbit Ethernet to the RC+ computer using TCP sockets.

3.2.3.3 Back-end Processing

This section describes the processing on the RC+ and RIPS computers. When RC+ receives data from the DIFRS computer, it is ingested by a process called readSock. It then calculates and appends header information and sends the recorded data products through shared memory to another process, writeDisk, which writes these records to disk. At the same time the readSock process sends the display data products to another process, xDisplay, which displays the radar data. Simultaneously, a relay process sends reflectivity and polarization products to RIPS.

There are RIPS processes that ingest radar data from RC+, surface data from the AUX Radar Monitor, radiometer data from the radiometer computer, and RUC data which have been FTPed from the AUX Radar Monitor. Another process calculates the icing hazard every minute throughout all portions of detected clouds and sends the results for display. Two additional processes display the products in real time. Yet another process posts data to an HTTP server for remote display and archival.

For more details, see Appendix G (GRADS Software Specifications).

3.2.4 Radiometer Data Acquisition and Processing

A computer associated with the radiometer calculates liquid water and water vapor column amounts and vertical temperature profiles. It then sends the data to the RIPS computer via a TCP socket, where the data are ingested, written to disk (one file every hour) and displayed in real time by RIPS.

3.2.5 RUC Model Data Processing

The Radar Monitor process acquires RUC model data from a Web site approximately once an hour and then reformats the data. It then writes time-stamped files on the RIPS internal disk via FTP. Separate RIPS modules process, display, and archive those files.

3.2.6 Surface Met Data Processing

The Radar Monitor process acquires surface meteorological data from GRIDS sensors and sends surface temperature, humidity, and rainfall data to RIPS via a TCP socket. Separate RIPS modules read, display, and archive the data stream in real time whenever new data are acquired (typically every minute). The logged data are useful for research purposes as well as diagnostic purposes, and for detecting water on the radome.

3.2.7 Icing Algorithm Processing

There is a RIPS module which accesses the latest radar, radiometer, surface meteorological, and RUC data and calculates the icing hazard potential. Once that calculation has been made, the numerical information needed to color-code icing hazard displays is sent to the icing display module, icingGui. Here data are displayed and communicated externally. Implementation of the icing algorithm is discussed more thoroughly in Section 3.3.

3.2.8 XRADS User Interface

The Extended RADS or XRADS user interface is called RCP (Radar Control Program) and runs on the RC+ PC. It communicates with the rest of the GRADS processes in RC+ via shared memory. RCP communicates with the GRIDS-AUX and radiometer computers, and the RIPS process via TCP sockets. An operator can view, build, modify, check, save, load, and run control tables and queues of control tables. It allows the operator to start, stop, and position the radar and radiometer antennas (if applicable), to tell the AUX machine to stop sending RUC and surface data, and to turn data archival on and off. Status messages and a help menu will be available via the user interface. See the GUI prototype in Appendix G.

For autonomous operation, no operator will be routinely exercising the user interface; instead, control tables will be read via configuration files. The user interface will be available for intervention (if needed) and to display health and status information to personnel visiting the container.

3.3 Icing Hazard Algorithm Implementation

3.3.1 Core Algorithm Implementation

The core icing algorithm has been described in Section 2.4. As noted, it uses four decision points based on the slant-path, fixed-beam measurements of liquid water (threshold LW > 0.05 mm), radar reflectivity (threshold Z_e > -23 dBZ), radar depolarization ratio (threshold DR_{th} = -30 ± 2 dB), and on the ingested temperature profile (threshold T < 0ºC) to identify hazardous regions within the clouds. Table 3 and Figure 18 depict how the thresholds of these four parameters are applied in the decision tree used to determine the warning level for icing potential as a function of altitude (H_i).

The icing potential is indicated in a continuous time-altitude display updated every minute (as schematically depicted in Figure 1 and in actual application in Figure 13), such that the real-time conditions and a short history (e.g., several hours) are presented as an evolving profile through all clouds in the radar beam. The warning of icing potential is scaled as follows: red for probable, yellow for caution, green for no threat. The appropriate color, or warning level, appears at the time and altitude of the condition.

This core algorithm is conservative and may over-warn. The performance of the core algorithm will be assessed during field trials, and adjustments made later to the decision points, if needed.

Table 3. Icing algorithm thresholds

Condition Red: All four of the thresholds are affirmed.
Condition Yellow: Only the first three thresholds are met (LW > 0.05 mm, T < 0°C, Ze > -23 dBZ), but DR > DRth + 2 dB. This indicates the co-existence of liquid and ice particles, a mixed-phase condition. Caution is warranted.
Condition Green: Clear skies obviously represent the first order condition green. Within clouds, green is established if T > 0°C; or if cloud is supercooled (T < 0°C), but either LW ≤ 0.05 mm, or Ze ≤ -23 dBZ. Low Ze means that the combination of droplet sizes and concentrations are insufficient to produce an icing threat, even if DR ≤ DRth ± 2 dB. For all ice clouds DR > DRth and LW < 0.05 mm, establishing condition green by default.

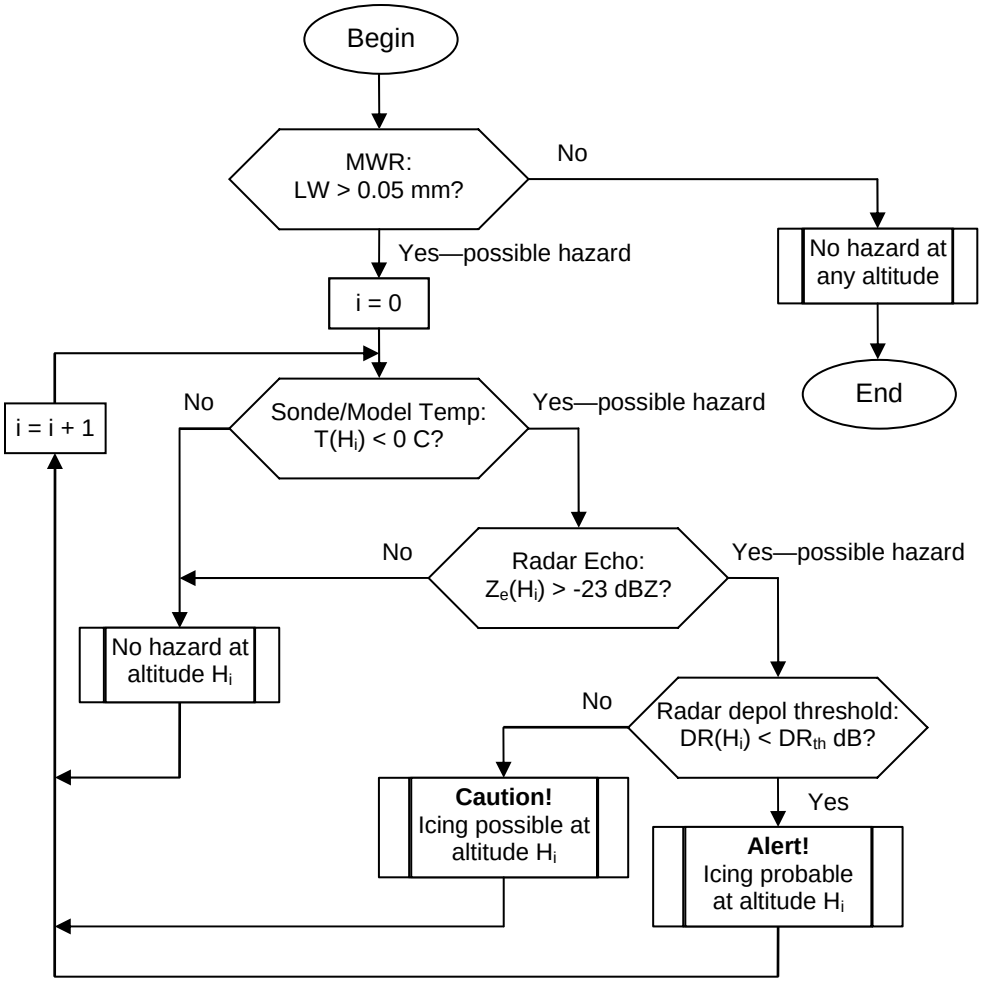

Figure 18. Core icing hazards algorithm.

3.3.2 Algorithm Enhancements

As noted previously, the GRIDS algorithm is an evolving decision-making tool, and as such, it is expected that many enhancements will be made to it as operational experience is accrued. The core algorithm is an effective beginning, with much potential for enhancements. GRIDS can gain power with a number of very feasible algorithm upgrades. The overall effect of these enhancements is to make GRIDS icing warnings more quantitative and robust.

The potential enhancements include but are not limited to the following; more detail is provided in Appendix B:

- Liquid water enhancements

The core algorithm can be enhanced for GRIDS by distributing the value of LW in different ways throughout the various portions of detected clouds, using better temperature profiles to refine hazard potential, using knowledge of reflectivity bright bands (if detected), and by incorporating additional information from the radar and radiometer if and when they point to the zenith. In Appendix B we discuss these enhancements in more detail, and relate them to icing hazards potentials defined by envelopes in Appendix C of the FAR.

The core algorithm operates from the detected *presence* of LW above the defined threshold, but the microwave radiometer actually measures the *quantity* of LW in the tropospheric column, and the GRIDS radar measures the cloud boundaries (top and bases), and thus cloud layer depth. Therefore, by various methods, the path-integrated liquid measured with the radiometer can be assigned to, and, with more sophistication, distributed through the cloud layer(s) and converted to a *concentration* of liquid water (Kg of liquid per m^3 of air, i.e., the liquid water concentration or LWC) to better rate icing *severity*. The supercooled LW can then be allocated linearly through the depth of cloud, but adiabatic or climatological LW profile shapes have been found to be more realistic (Politovich et al. 1995; Stankov et al. 1995). A method for making the first steps toward use of the actual LW values to estimate LWC and estimate the severity in terms of the FAR Appendix C ratings is outlined in Appendix B.

Methods to combine automated radiometric and radar measurements to *profile* cloud LW are under development, and are promising but not yet ready to apply operationally (e.g., Lohnert et al. 2001; Reehorst et al. 2005; Westwater et al. 2006). GRIDS developers should keep abreast of these developments.

- Temperature enhancements

Within a supercooled cloud, the icing potential increases with temperature, so it is possible to rate icing risk to the temperature profile from RUC or other measurements. Steps to add this *temperature classification* feature are noted in Appendix B.

The tropospheric temperature and dew point soundings, as available from the RUC, will be useful since most severe icing occurs between 0°C and -10°C, and thermodynamic instability can indicate forcing to produce the condensation of liquid. Also, thermodynamic instability, as in embedded convection, can enhance LWC. Various temperature profile scenarios can be implemented to provide a *temperature instability enhancement*.

The application of 30 and 90 GHz radiometric measurements to estimate the layer-mean LW temperature, as described in the section on radiometric temperature profiling (Section 2.3.4),

can be readily implemented with the existing GRIDS design, as a cross-check on the RUC temperature profile, especially at low altitudes.

- Bright band (melting level) enhancement

Obviously, supercooled cloud liquid can occur only at altitudes where T < 0°C, which will begin slightly above the melting level if one occurs. The melting level is detected with radars as the bright band. Freezing drizzle and rain occur at the surface when falling snowflakes melt, and the droplets they create fall into colder, sub-cooled air nearer the surface. The first indicator is evidence of a bright band, the signature of which is much more defined in the depolarization measurement than the reflectivity measurement. Thus, automated recognition of the bright band can be used to (1) estimate the altitude above which cloud liquid is supercooled, (2) cross-check the RUC melting level and correct it if needed, (3) identify freezing drizzle or rain when combined with a RUC temperature sounding, and (4) recognize rain and potential degradation of GRIDS signals when the rain rate from reflectivity is also used. See Appendix B for some approaches to adding these features to the core algorithm.

- Vertically pointing enhancements (depolarization and vertical motion measurements)

The addition of zenith pointing measurements of DR and the vertical velocity parameters are expected to provide significant additional value to the GRIDS measurements, not only by enhancing the estimate of the potential icing hazard through better identification of the prevailing ice and liquid processes, but also by indicating the vertical atmospheric forcing and turbulence that produces those conditions.

To these ends, more specific identification of the different ice particles by their depolarization in itself can add another level of confidence to detection of an icing condition, especially in those clouds of mixed phase. The GRIDS capability to do this has been thoroughly demonstrated (Reinking et al. 2000a). Also, GRIDS is a Doppler radar, so estimates of the beam-radial velocity, V_e, of reflecting hydrometeors are also routinely measured. The cloud motion and hydrometeor settling measurements can be greatly enhanced using the optional addition of the vertically pointing radar beam.

Since cloud physics principles dictate that cloud ice particles will rapidly consume liquid droplets, the LW component in mixed-phase clouds can only present a lasting icing hazard if the dynamics support continued condensation. Mixed-phase icing hazards may occur, especially when embedded convection is involved to force continued condensation of new liquid in the presence of ice particles. Measurements of vertical motion along with DR, including the spectra of vertical motion, can be used to identify mixed-phase clouds through the differences between cloud droplet and ice particle fall speeds and to note rain in the signature of accelerated fall velocities. This has been demonstrated, as discussed with the case study in Section 2.5.1, and in Appendix B. Thus, utilization of the radar's measurement of vertical motion can enhance the algorithm in and without the presence for rain.

- Rain Recognition Enhancements

As noted previously, the core icing hazards algorithm does not incorporate rainfall directly because the commercially available microwave radiometers integrate a blower system to dry a microwave-transparent window that protects the antenna. However, experiments by NASA with these drying devices during the 2nd Alliance Icing Research Study (AIRSII 2003)

indicate that unreasonably high values of LW are obtained during significant rain, so this window-blower approach is not fail-safe. Drizzle is unlikely to induce false readings (Reinking et al. 2000a), but at this writing a rain-rate threshold above which the dryers fail has not yet been established. GRIDS can be more stringently required to recognize periods of rain, and to define alternate paths for identifying the hazard or to automatically make weighting adjustments to other parameters in the icing algorithm during substantial rain events.

Approaches to rain recognition include the following: 1) use of the surface rain-rate sensor, 2) use of the value and variance of the microwave radiometer LW measurement itself to identify unreliable estimates, 3) use of the GRIDS radar measurements reflectivity-rain-rate (Z-R) estimate from the GRIDS radar, and 4) use of the Doppler vertical velocity and velocity variance to identify times of likely production of high LW when radiometer measurements are made uncertain by substantial rain. Due to the short propagation path below normal bright bands in winter precipitation, attenuation of the radar's signal by rain is minimized. These approaches and factors are examined in Appendix B.

- GRIDS-CIP Synergy

The noted enhancements to the GRIDS algorithm begin a list that will add to the power of GRIDS. As new developments in instrumentation, measurements, and modeling that could support GRIDS come online, they would logically be examined and incorporated as appropriate. Integration of the Current Icing Product (CIP; Bernstein and Schneider 2004) could be one such strong addition. The CIP integrates several network data products to produce mapped estimates of icing and SLD potential. GRIDS and CIP are each a stand-alone system, but together the power for identifying the real icing potential can be greatly enhanced. CIP is explained and this is discussed further in Appendix B.

3.3.3 Important GRIDS By-products

It should be evident at this point that the many radar and radiometric measurements made by the GRIDS multi-sensor system have numerous applications to broader weather forecasting. With certainty, this will greatly increase the GRIDS benefit-to-cost ratio. Some of the GRIDS by-products—precipitable water, cloud boundaries and thicknesses, multiple ceilings, turbulence from radial velocity variance, detailed cloud microphysics, all in data streams suitable for integration into the national network—can support many fundamental aspects of National Weather Service operations if implemented. Assimilation of these data into the network modeling product, and continuous measurement of all these parameters through the depth of the troposphere for the weather and climate assessment databases, provide not-to-be missed opportunities.

3.4 Monitoring and Calibration

The monitoring and calibration functions are largely performed by the Radar Monitor process which will run on the Auxiliary Computer (AUX). Several analog and digital signals will be monitored, a radar health status log will be generated, and certain radar functions will be controlled either under human control, or automatically in response to a radar system or power failure.

Industrial Packs (IPs) will be used to interface the radar system to the AUX system. IPs are small modular circuit boards that each perform a specific function. Four IPs are mounted on an IP carrier board which occupies one slot on the PCI backplane. This technology allows the system designer to "mix and match" multiple I/O functions while using a minimum number of backplane slots. In the AUX system, an A/D IP will be used to sample analog signals and digital I/O IPs will be used to sample and drive TTL-level digital signals. Future I/O requirements can be easily addressed by adding IPs with whatever functionality is needed.

Several analog signals will be sampled hourly. Acceptable operating ranges will be established for each of these signals. Any readings that are outside the acceptable operating range will be documented and time-stamped in a status file that will be updated daily at 12:01 AM. Criteria will be established for taking action based on readings that are out of range, ranging from simple reporting within 24 hours to immediate shutdown of sub-systems or the entire GRIDS. For example, the radar transmitter may be automatically shut down if certain power-supply failures are detected. The analog signals which will be monitored are listed in Table 4.

The Radar Monitor process is written in LabVIEW, which is a graphical programming language designed for instrumentation control.

Table 4. Analog Signals monitored by Radar Monitor process

CH #	I/O connector pin #	Signal Name	Units
1	1,2	Transmitted RF power	watts
2	27,28	Outdoor temperature	°C
3	3,4	Outdoor humidity	%
4	29,30	Indoor temperature	°C
5	5,6	Indoor humidity	%
6	31,32	Pulse controller +5V #1	volts
7	7,8	Pulse controller +5V #2	volts
8	33,34	Pulse controller +28V	volts
9	9,10	Pulse controller +15V	volts
10	35,36	Pulse controller –15V	volts
11	11,12	RF CUD +12V (mon)	volts
12	37,38	RF CUD TX +12V (mon)	volts
13	13,14	RF CUD RX +12V (mon)	volts
14	39,40	IF REC/MOD +12V (mon)	volts
15	15,16	IF REC/MOD +15V	volts
16	41,42	Temp, circulator #1	°C

Digital signals to be monitored include phase-lock alarms on the IF frequency phase-locked oscillators (PLO's). A course of action based on these conditions will be chosen and implemented. For example, the radar transmitter might be automatically turned off if there is a PLO failure.

Software from the UPS manufacturer will be used to monitor the incoming line power. In the event of a power failure, the Radar Monitor process will turn off the radar, radiometer, and computers in the proper sequence, before UPS power is depleted. When power is restored, the entire system will be restarted automatically and resume normal operations.

Radar and radiometer calibrations will be performed both manually and automatically. Full calibrations will be done manually at an appropriate frequency (about once per year, based on our many years' experience with such systems), or whenever failure of components dictates a recalibration. An automated verification of calibration stability will be performed daily. For this verification, two measurements will be made. First, the noise level of the receiver channel will be measured under conditions of zero transmitter power. Also, a known level of white noise will be injected into the radar receiver to produce an output near the middle of the receiver's dynamic range. Both noise levels will be recorded and compared with recent and historical values. If both values remain stable, it can be reasonably assumed that the overall receiver calibration is unchanged. To make this daily check, a digital I/O IP will be used to drive the necessary digital control signals, switching circulators and attenuators into the correct state and turning on the calibration noise diode.

3.5 Communication

GRIDS uses an Internet connection to send data from the on-site GRIDS computers to an off-site Web server and to receive RUC data. It uses a Local Area Network (LAN) to communicate between the various on-site GRIDS computers.

3.5.1 Internet

GRIDS should have a broadband Internet connection for best performance, although use of telephone lines is probably acceptable for experimental purposes. An Internet connection is essential for receiving the RUC data and for providing real-time data to off-site users.

RIPS will send a Graphical Interchange Format (GIF) file of the most recent icing hazard display via Secure Copy Program (SCP) or HTTP to the Boulder Web server for display on the Web. Typically, these files will be updated and sent once per minute.

RIPS will also archive radar, radiometer, RUC, surface meteorological and icing data via SCP to the archival system in Boulder, typically once per hour.

On the AUX system, the Radar Monitor process will download RUC temperature profile data from the Web as data sets become available. Typically, these data sets are updated once per hour.

RIPS will be use the HTTP to transfer data to the home Web server. Several of the components of RIPS working with the HTTP server will serve displays similar to the ones seen in the radar on the Web where they can be viewed with a browser.

A Linux firewall computer will protect the internal GRADS (and other) systems local area network (LAN) from the external network by providing centralized network security.

3.5.2 Local Area Network (LAN)

The LAN has two components: a dedicated 1 Gbit/sec link between the DIFRS computer and the RC+ computer, and a 100 Mbit/sec Ethernet link that connects the RC+ computer to the rest of the GRIDS computers (Figure 15 and Figure 17).

The following describes the primary information flow between the computers.

1) DIFRS sends raw radar data to RC+ over a dedicated 1 Gbit/sec Ethernet link.

2) RC+ sends radar control commands to the Radar Monitor process on AUX and receives radar status (health) messages from it. These commands are used to turn the radar transmitter on and off, initiate receiver calibration sequences, etc. The radar status messages are passed along to RIPS. RC+ also processes the raw radar data and produces meteorological fields that are passed along to RIPS.
3) RIPS integrates all the data streams: radar fields, RUC data, surface met data and radiometer data. It then displays and archives the data locally. As mentioned previously, RIPS also sends the data across the Internet to the off-site computers where it is served to the Internet at large.
4) RIPS will send the Radar Monitor process on the AUX computer commands to start and stop the RUC data acquisition. The Radar Monitor process uses the local area network to send RUC data, surface met data, and system health data to RIPS.
5) The AUX system will send radar system status and error messages to RC+ via a TCP socket. Typical messages might notify the RC+ that the radar has been successfully turned on, or that a hardware failure has been detected and that XRADS should stop data acquisition.
6) UPS software will run on the GRADS, AUX, and the Radiometer PCs to monitor the UPS over a network connection. When a power failure occurs, this software will direct all five of the operating systems to shut down gracefully. This software will also be used to send an automatic e-mail to notify selected recipients of the problem.

3.5.3 IEEE-488 Bus

The AUX system will communicate with the TWTA and the Pulse Controller via the IEEE-488 bus. The Radar Monitor process will be used to send commands to the TWTA and the Pulse Controller and monitor their status.

3.6 Container

The GRIDS prototype will be built into a dedicated, transportable container, so that it can be constructed in one location and demonstrated in other locations. Because of common practice in the transportation and shipping industry, a standard ISO shipping container (seatainer) will be used for this purpose, with nominal dimensions of 20'L x 8'W x 8'H. This rugged steel-shelled container will also serve as a rigid mount for the GRIDS antenna and radiometer. It will be fitted with insulated walls, environmental controls, and an extensive electrical distribution system, thus providing laboratory-like conditions in which to operate. Although this system will be unattended when it is fully developed, there is still a need to make it roomy and pleasant for both visitors and project or operations staff. Below we show the floor plan for the GRIDS container (Figure 19), and an external side view depicting the antenna and radiometer mounted to the container (Figure 20).

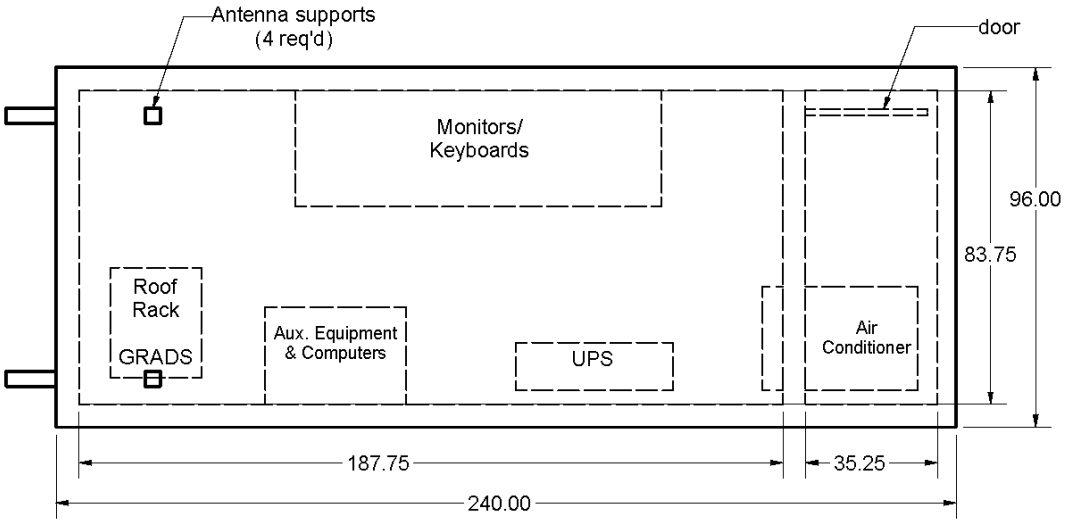

Figure 19. Plan view of GRIDS container showing location of key equipment. Note vestibule entry on the right.

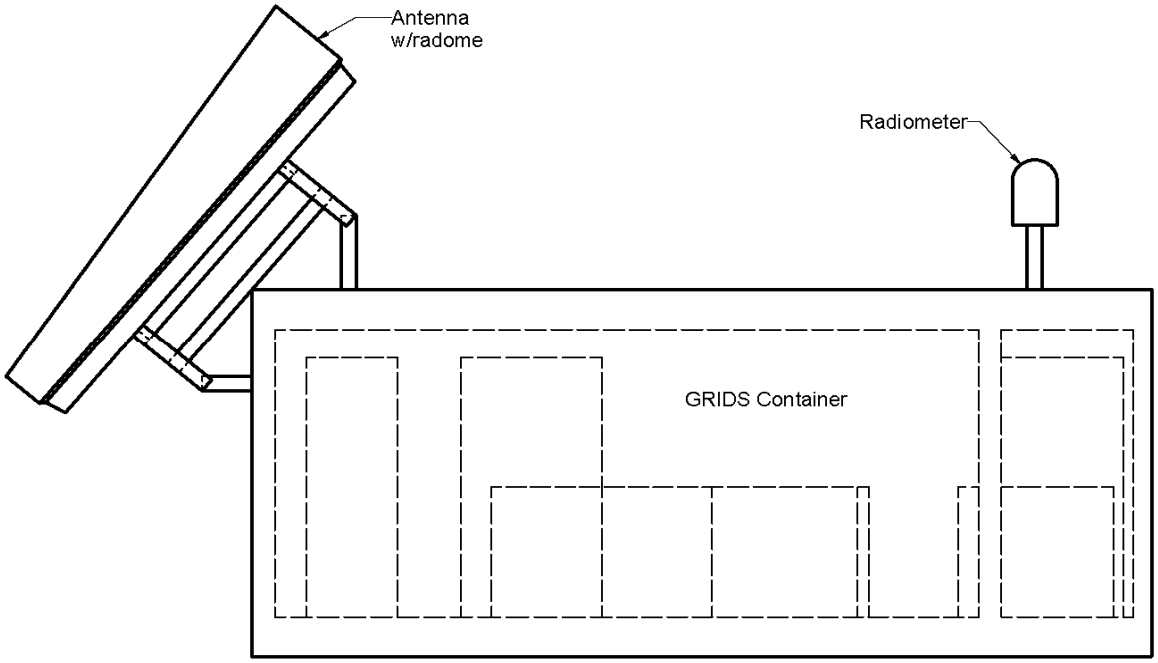

Figure 20. Side view of container showing 3-m antenna with radome pointing at 40º elevation angle, and mailbox radiometer mounted on an opposing side.

Future versions of the GRIDS container could be made considerably smaller, since they will not need to accommodate development staff.

3.7 Off-Site Computer Systems

As previously mentioned, certain products created by RIPS, as well as raw data from the sensors, are shipped from the RIPS machine to a Web server machine in Boulder for Web browser-accessible displays and archival in close to real time. Scripts can be used to send data and images back periodically, but to allow for real-time updating and viewing of data, a more sophisticated architecture is necessary. This part of the GRIDS is described below.

3.7.1 Software Architecture

The off-site software architecture consists of one centralized server called DataRexx, at least one reformatter for each data source, a relay (or fan-out box) for each data source, and various data viewers and archivers, as shown in Figure 21. Briefly, DataRexx is a software product licensed from Bear Peak Software, Inc., that allows multiple remote data producer clients to "post" data to it via HTTP. Data consumer clients can then "get" data from DataRexx via HTTP. Data reformatters receive remote raw data and package it into archival format. Data relays each input a single data stream and deliver that data stream to multiple clients. Data viewers allow the user to view and manipulate the data, while archivers write both the archival data and products to disk for playback. Since many of the capabilities available on the on-site computers are also desirable on the off-site computer, reuse of classes and methods and leveraging on-site processes has helped to decrease the time needed for the software development process. For detailed information about the off-site software system, see Appendix G.

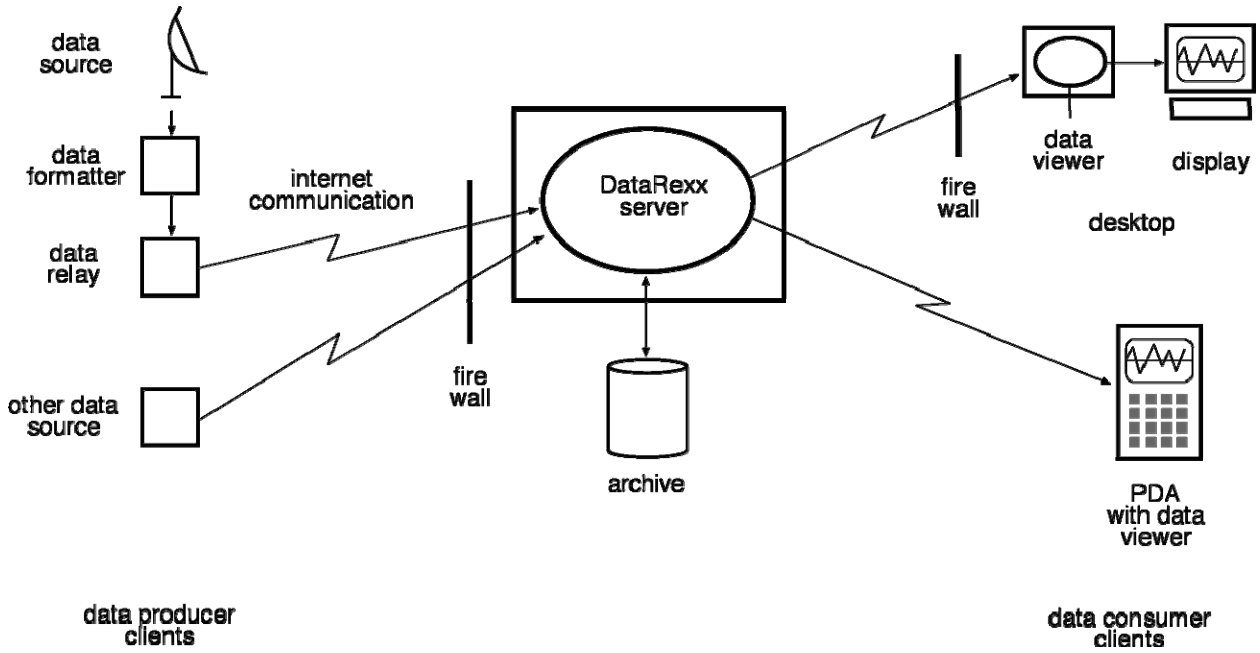

Figure 21. DataRexx server diagram showing data sources, server, and data clients.

3.7.2 Computer Architecture

The Web server machine, located in Boulder, CO, is a Linux-based rack-mount machine with three terabytes of disk space. This allows for multiple large data sets to be archived in close to real time.

4. SUMMARY

In-flight icing annually causes high loss of life and property, and also a high cost for flight delays, cancellations, and re-routings caused by icing concerns that are perhaps needless. Therefore, the nation has a great need to improve its ability to forecast and observe in-flight icing conditions. A preponderance of icing encounters occurs in the vicinity of major airports, where aircraft must fly holding patterns in poor weather before landing. In partnership with the Federal Aviation Administration (FAA), NOAA's Environmental Technology Laboratory (ETL) has for the past two decades conducted research to develop a practical remote sensing system to help improve our ability to detect hazardous icing conditions aloft, and to provide accurate and timely assessment of local icing conditions. We call this system the Ground-based Remote Icing Detection System (GRIDS). This document specifies the scientific basis and the design for this system.

Our research has established that a radar measurement of the polarized scattering properties of clouds can be used to distinguish between two fundamental categories of cloud particles—ice and liquid. It is liquid water particles that present an icing hazard, but they must be super-cooled and have sufficient water content to present a real hazard. GRIDS provides those measurements and is designed for unattended operation. It will observe nearby clouds continuously, measure the amount of liquid water they contain, and determine if hazardous super-cooled droplets are present, *for every portion of the cloud from its base to an altitude of 10 km AGL*. To guarantee that even weak icing conditions high in clouds are detected, GRIDS must employ the most sensitive civilian cloud radar yet built. This is not a fundamental problem because the components are all commercially available.

In summation, through careful design based on new and sound remote sensing theory and field-tested proof of concept, the GRIDS technique has been demonstrated as an effective tool for real-time monitoring of hazardous aircraft icing conditions. It is intended for use within the airspace of major airports, and its continuous output can be linked to enhance, anchor, and verify larger-area forecasts from the now-operational Current Icing Potential model and other icing products.

GRIDS combines information from a "cloud" radar and a microwave radiometer, each developed by ETL, and by ingesting local temperature profiles from a reliable source (National Weather Service). GRIDS is a low-risk endeavor. It is an exercise in optimally configuring existing technology based on proven science, establishing a robust means for unified operation of the sensors, combining measurements with Web-based data automatically, and issuing real-time, easy-to-interpret assessments of icing hazard potential via the Internet. GRIDS will be housed in a transportable container. It requires only power, a broadband Internet connection, and a clear field of view.

Finally, it should be evident at this point that the many radar and radiometric measurements made by the GRIDS multi-sensor system have numerous applications to broader weather

forecasting. With certainty, this will greatly increase the GRIDS benefit-to-cost ratio. Some of the GRIDS by-products—precipitable water, cloud boundaries and thicknesses, multiple ceilings, turbulence from radial velocity variance, essential and specific cloud microphysics well beyond ice vs. liquid, all in continuous data streams suitable for integration into the national network—can support many fundamental aspects of National Weather Service operations if implemented. Assimilation of these data into the network modeling product, and continuous measurement of all these parameters through the depth of the troposphere for the weather and climate assessment databases, provide not-to-be missed opportunities. GRIDS can be employed as a multi-function instrument.

5. ACKNOWLEDGMENTS

The FAA has supported ETL (now integrated with ESRL) in its development of GRIDS, including this design work. The views expressed are those of the authors and do not necessarily represent the official policy or position of the FAA. Much of this report was based on a GRIDS Preliminary Design Review (NOAA ETL Radar Meteorology and Oceanography Division, 2001), which was written by M. J. Post, Roger Reinking, Sergey Matrosov, Carroll Campbell and Janet Gibson, with support from others in the division.

The authors of this report gratefully acknowledge all contributors to that PDR and the very major contributions of the following people to the entire research and development effort: Bruce Bartram, Kurt Clark, Duane Hazen, Robert Kropfli, Sergey Matrosov, Ken Moran, M.J. Post, and Geoff Thompson. These people contributed in diverse ways but this work would not have been possible without their leadership, support, and outstanding expertise.

6. REFERENCES

The following references are in alphabetical order. For a list of ETL references in chronological order, illustrating the history of the development of GRIDS, see Appendix A.

Ashendon, R., and J. D. Marwitz, 1997: Turboprop aircraft performance response to various environmental conditions. *J. Aircraft*, **34**, 278-287.

Ashendon, R., W. Lindberg, J. Marwitz, and B. Hoxie, 1996: Airfoil performance degradation by supercooled cloud, drizzle, and rain drop icing. *J. Aircraft*, **33**, 1040-1046.

Barnes, Stanley L, 1980: Report on a meeting to establish a common Doppler radar data exchange format. *Bull. Amer. Meteor. Soc.*, **61**, 1401-1404.

Benjamin, S.G., G.A. Grell, J.M. Brown, T.G. Smirnova, and R. Bleck, 2004a: Mesoscale weather prediction with the RUC hybrid isentropic / terrain-following coordinate model. *Mon. Wea. Rev.*, **132**, 473-494.

Benjamin, S.G., D. Devenyi, S.S. Weygandt, K.J. Brundage, J.M. Brown, G.A. Grell, D. Kim, B.E. Schwartz, T.G. Smirnova, T.L. Smith, and G.S. Manikin, 2004b: An hourly assimilation/forecast cycle: The RUC. *Mon. Wea. Rev.*, **132**, 495-518.

Bernstein, B.C., and T.L. Schneider, 2004: Two perspectives on a Colorado icing event: GRIDS and CIP. 11th Conf. on Aviation, Range and Aerospace Meteorology, Hyannis MA, 11-14 October. Amer. Meteorol. Soc., Boston. Available on CD from the AMS.

Bernstein, B.C., F. McDonough, M.K. Politovich, B.G. Brown, T.P. Ratvasky, D.R. Miller, C.A. Wolff and G. Cunning, 2004: Current Icing Potential (CIP): Algorithm Description and Comparison with Aircraft Observations. *J. Appl. Meteor.,* **44,** 969-986.

Boudala, F.S., G.A. Isaac, S. G. Cober, and Q. Fu, 2004: Liquid fraction in stratiform mixed-phase clouds from in situ observations. *Quart. J. Roy. Meteor. Soc.,* **130,** 2919-2931.

Campbell, W.C. and J. Gibson, 1997: A programmable real-time data processing and display system for the NOAA/ETL Doppler radars. *Proceedings of the 28th Conf. on Radar Meteorology,* Austin TX, American Meteorology Society, pp 178-179.

Chan, P. W., and C.M. Tam, 2005: Performance and application of a multi-wavelength, ground-based microwave radiometer in rain nowcasting. *Preprints, 9th Symp. Integrated Observing and Assimilation Systems for the Atmosphere, Oceans, and Land Surface*, 9-13 January 2005, San Diego,CA. P1.9, Amer. Meteor. Soc.

Cimini, D., T. J. Hewison, L. Martin, J. Guldner, C. Garrafrd, and F. S. Marzano, 2006: Temperature and humidity profile retrievals from ground-based microwave radometers during TUC. *Meterologische Zeit.,* **15,** 45-56.

Cober, S. G., G. Isaac, and J. W. Strapp, 1995: Aircraft icing measurements in east coast winter storms, *J. Appl. Meteor.,* **34,** 88-100.

Doviak, R.J. and D.S. Zrnic. *Doppler Radar and Weather Observations.* San Diego, CA: Academic Press, 1993.

Federal Aviation Regulations, 1982: Part 25: Airworthiness standards, transport category airplanes (revised edition). Icing FAR's: Parts 25--Appendix C, 91.527, 121.629, 125.221, 135.227. Federal Aviation Administration. U.S. GPO, Wash., D.C.

Frerking, M.E. *Digital Signal Processing in Communication Systems*. Norwell, MA: Kluwer Academic Publishers, 1994.

Frisch, A.S., C.W. Fairall, and J.B. Snider, 1995: Measurement of cloud and drizzle parameters in ASTEX with K_a-band Doppler radar and a microwave radiometer. *J. Atmos. Sci.,* **52**, 2788-2799.

Gibson, J.S., W.C. Campbell, B.E. Martner, 2004: RADS: A radar acquisition and display system for research radars. *NOAA Tech. Report*. OAR ETL-69, NOAA Office of Oceanic and Atmospheric Research, Boulder, CO, 56 pp.

Heggli, M.F., and R.M. Rauber, 1988: The characteristics and evolution of supercooled liquid water in wintertime storms over the Sierra Nevada: A summary of microwave radiometric measurements taken during the Sierra Cooperative Pilot Project. *J. Appl. Meteor.,* **27,** 989-1015.

Hogg, D.C., F.O. Guiraud, J.B. Snider, M.T. Decker, and E.R. Westwater, 1983: A steerable dual-channel microwave radiometer for measurement of water vapor and liquid in the troposphere. *J. Clim. Appl. Meteorol.*, *22,* 789-806.

Klimowski, B.A., R. Becker, E.A. Betterton, R. Bruintjes, T. L. Clark, W.D. Hall, B.W. Orr, R. A. Kropfli, P. Piironen, R.F. Reinking, D. Sundie, and T. Uttal, 1998: The 1995 Arizona Program: Toward a better understanding of winter storm precipitation development in mountainous terrain. *Bull. Amer. Meteor. Soc.,* **79,** 799-813.

Koldaev, A.V., E.N. Kadygrov, A.V. Troitsky, and J.W. Strapp, 1998: Remote sensing of average liquid water content layer height in winter clouds. *Proc. 8th Atmospheric Radiation Measurement (ARM) science team meeting*, U.S. Dept of Energy, 381-385.

Korolev, A.V., G.A. Isaac, S.G. Cober, J.W. Strapp, and J. Hallett, 2003: Microphysical characterization of mixed-phase clouds. *Quart. J. Roy. Meteor. Soc.*, **129,** 39-65.

Kropfli, R.A., and R.D. Kelly, 1996: Meteorological research applications of mm-wave radar. *Meteorol. and Atmos. Phys.,* **59,** 105-121.

Kropfli, R.A., S.Y. Matrosov, T. Uttal, B.W.Orr, A.S. Frisch, K.A. Clark, B.W.Bartram, R.F.Reinking, J.B. Snider, and B.E. Martner, 1995: Cloud physics studies with 8 mm wavelength radar. Special issue on cloud microphysics and applications to global climate change, Atmospheric Research, 35, 299-313.

Lohnert, U., S. Crewell, A. Macke, and C. Simmer, 2001: Profiling cloud liquid water by combining active and passive microwave measurements with cloud statistics. *J. Atmos. Oceanic Tech.*, **18,** 1354-1366.

Martin, L. C. Matzler, T.J. Kewison, and D. Ruffieux, 2006: Intercomparison of integrated water vapor measurements. *Meterologische Zeit.,* **15,** 57-64.

Martner, B.E., and R.A. Kropfli, 1993: Observations of multi-layered clouds using K-band radar. Paper AIAA 93-0394, *Reprints, 31st Aerospace Sciences Mtg.*, Reno, AIAA, 8 pp.

Martner, B.E., R.A. Kropfli, L.E. Ash, and J.B. Snider, 1991: Progress report on analysis of differential attenuation radar data obtained during WISP-91. *NOAA Tech. Memo.*, ERL WPL-215, Boulder, CO, 43 pp.

Martner, B.E., R.A. Kropfli, L.E. Ash, and J.B. Snider, 1993a: Dual-wavelength differential attenuation radar measurements of cloud liquid water content. *Preprints, 26th Intl Conf. on Radar Meteor.*, AMS, Norman, OK, 596-598.

Martner, B.E., R.A. Kropfli, L.E. Ash, and J.B. Snider, 1993b: Cloud liquid water content measurement tests using dual-wavelength radar. *NOAA Tech. Memo.* ERL ETL-235, NOAA Environmental Research Laboratories, Boulder, CO, 47 pp.

Martner, B.E., D.A. Hazen, K.P. Moran, T. Uttal, M.J. Post, and W.B. Madsen, 2002a: NOAA/ETL's vertical-profiling cloud radar and radiometer package. *6th Symp. on Integrated Observing Systems*, Jan 2002, Orlando, FL, Amer. Meteor. Soc.

Martner, B.E., B.W. Bartram, J.S. Gibson, W.C. Campbell, R.F. Reinking, and S.Y. Matrosov, 2002b: An overview of NOAA/ETL's scanning K_a-band cloud radar. *16th Conf. on Hydrology.* Jan 2002, Orlando, FL, Amer. Meteor. Soc.

Matrosov, S. Y., 1991a: Theoretical study of radar polarization parameters obtained from cirrus clouds. *J. Atmos. Sci.,* **48,** 1062-1070.

Matrosov, S. Y., 1991b: Prospects for the measurement of ice cloud particle shape and orientation with elliptically polarized radar signal. *Radio Sci.*, **26**, 847-856.

Matrosov, S.Y., and R.A. Kropfli, 1993: Cirrus cloud studies with elliptically polarized K_a-band radar signals: A suggested approach. *J. Atmos. Oceanic. Tech.*, **10**, 684-692.

Matrosov, S.Y., R.F. Reinking, R.A. Kropfli, and B.W. Bartram, 1995: Identification of ice hydrometeor types with elliptical polarization radar measurements. *Preprints, 27th Conference on Radar Meteorology*, 9-13 October 1995, Vail, CO. Amer. Meteor. Soc., Boston, MA, 539-541.

Matrosov, S.Y., R.F. Reinking, R.A. Kropfli, and B.W. Bartram, 1996a: Estimation of hydrometeor shapes and types from radar polarization measurements. *J. Atmos. Oceanic Tech.*, **13,** 85-96.

Matrosov, S.Y., R.F. Reinking, R.A. Kropfli, B.E. Martner, and B.W. Bartram, 2001: On the use of radar depolarization ratios for estimating shapes of ice hydrometeors in winter clouds. *J. Appl. Meteorol.,* **40,** 479-490.

Matrosov, S.Y., R.F. Reinking, and I.V. Djalalova, 2005: Inferring fall attitudes of pristine dendritic crystals from polarimetric radar data. *J. Atmos. Sci.,* **62,** 241-250.

McDonough, F. and B.C. Bernstein, 1999: Combining satellite, radar, and surface observations with model data to create a better aircraft icing diagnosis. *Preprints, 8th Conference on Aviation*, *Range and Aerospace Meteorology*, Dallas, TX, Amer. Meteor. Soc., 467-471.

Moran, K.P., B.E. Martner, M.J. Post, R.A. Kropfli, D.C. Welsh, and K.B. Widener, 1998: An unattended cloud-profiling radar for use in climate research. *Bull. Amer. Meteor. Soc.*, **79**, 443- 455.

NOAA ETL Radar Meteorology and Oceanography Division, 2001: Preliminary Design, Ground-based Remote Icing Detection System (GRIDS). Report to the FAA Aviation Weather Research Program, In-Flight Icing PDT #4, Task 01.4.3.3, FAA Icing Remote Sensing Testbed, Deliverable 01.4.3.1.E3. 65 pp + appendices.

Paull, G. and E. Hagy, 1999: Historical overview of in-flight icing accidents. TR-9854/01-1 MCR Federal, Inc. Bedford MA 01730. 43 pp.

Politovich, M. K., 1989: Aircraft icing caused by large supercooled droplets. *J. Appl. Meteor.*, **28**, 856-868.

Politovich, M. K, 1996: Response of a research aircraft to icing and evaluation of Severity Indices. *J. Aircraft*, **33**, 291-297.

Politovich, M.K., B.B. Stankov, and B.E. Martner, 1995: Determination of liquid water altitudes using combined remote sensors. *J. Appl. Meteor.*, **35**, 2060-2075.

Popa Fotino, I.A., J.A. Schroeder, and M.T. Decker, 1986: Ground-based detection of aircraft icing conditions using microwave radiometers. *IEEE Trans. Geosci. Remote Sens.,* **GE-24**, 6, 975-982.

Reehorst, A. L., D. J. Brinker, and T. P. Ratvasky, 2005: NASA icing remote sensing system comparisons from AIRSII. AAIA-2005-0253, 10 pp.

Reinking, R.F., 1998: Detection of ice hydrometeors and freezing drizzle with K_a-band dual-polarization radar. *Conf. on Cloud Physics.* 17-21 August 1998, Everett, Washington. Amer. Met. Soc., Boston. pp 249-252.

Reinking, R.F., and R.A. Kropfli, 2000: Breakthroughs in radar polarization technology and related studies. Radar-based Icing Diagnosis Techniques, In-flight Icing PDT Technical Direction FY2000 Year-end Task Progress Report to the FAA, Deliverable 00.4.3.E1. NOAA Environmental Technology Laboratory. 16 pp.

Reinking, R.F., R.Caiazza., R.A. Kropfli, B.W. Orr, B.E. Martner, T.A. Niziol, G.P. Byrd, R.S. Penc, R.J. Zamora, J.B. Snider, R.J. Ballentine, A.J. Stamm, C.D. Bedford, P. Joe, and A.J. Koscielny, 1993a. The Lake Ontario Winter Storms (LOWS) Project. Cover article, *Bull. Amer. Meteor. Soc.*, **74,** 1828-1829.

Reinking, R.F. B.W. Orr, B. Stankov, and C. Davis, 1993b: NOAA K_a-band cloud-sensing radar measurements from WISPIT. *Preprints, 5th Int'l. Conf. on Aviation Weather Systems*, 2-6 August 1993, Vienna, VA. Amer. Meteor. Soc., Boston, MA, 130-134.

Reinking, R.F., S.Y. Matrosov, B.E. Martner, R.A. Kropfli, and B.W. Bartram, 1995a: Hydrometeor identification with millimeter-wave dual-polarization radar. *Conf. on Cloud Physics*, 15-20 January 1995, Dallas, Texas. Amer. Meteor. Soc., Boston, MA, 20-25.

Reinking, R.F., S.Y. Matrosov, R.J. Bruintjes, B.E. Martner, and R.A. Kropfli, 1995b: Further comparison of experimental and theoretical radar polarization signatures due to ice hydrometeor shape. *Preprints, 27th Conference on Radar Meteorology*, 9-13 October 1995, Vail, CO. American Meteorological Society, Boston, MA, 47-49.

Reinking, R.F. S.Y. Matrosov, and R.T. Bruintjes, 1996a: Hydrometeor identification with elliptical polarization radar: Applications for glaciogenic cloud seeding. Cover article, *J. Wea. Modif.*, **28,** 6-18.

Reinking, R.F., S.Y. Matrosov, and R.T. Bruintjes, 1996b: Ice and water hydrometeor identification with elliptical polarization radar: Applications to precipitation enhancement. *Preprints, 13th Conf. on Planned & Inadvertent Weather Modification*, 28 January-2 February, 1996, Atlanta, GA. Amer. Meteor. Soc., Boston, MA, 172-179.

Reinking, R.F., S.Y. Matrosov, B.E. Martner and R.A. Kropfli, 1996c: Differentiation of freezing drizzle from ice hydrometeors and rain with polarization radar. *Pro., FAA International Conference on Aircraft Inflight Icing*. 6-8 May 1996, Springfield, VA, **II,** 331-338. [Available from NTIS, Springfield, VA 22161. DOT/FAA/AR-96/81].

Reinking, R.F., S.Y. Matrosov, B.E. Martner and R.A. Kropfli, 1996d: Differentiation of freezing drizzle from ice hydrometeors with polarization radar. *Pro., 12th International Conference on Clouds and Precipitation.* 19-23 August 1996, Zurich, Switzerland. International Commission on Clouds and Precipitation (ICCP); **I,** 446-449.

Reinking, R.F., S.Y. Matrosov, B.E. Martner, R.A. Kropfli, and B.W. Bartram, 1996e: Hydrometeor identification with millimeter-wave dual-polarization radar. *Proc. ETL/CSU Cloud-related Process Modeling and Measurement Workshop, Boulder, Colorado, 23-25 October 1995.* Environmental Technology Laboratory, U.S. Dept. of Commerce, 209-214.

Reinking, R.F., S.Y. Matrosov, R.T. Bruintjes, and B.E. Martner, 1997a: Identification of hydrometeors with elliptical and linear polarization K_a-band radar. *J. Appl. Meteor.*, **36**, 322-339.

Reinking, R.F., S.Y. Matrosov, B.E. Martner, and R.A. Kropfli, 1997b: Differentiation of freezing drizzle from ice hydrometeors and freezing rain with dual-polarization radar. *J. Aircraft*, **34**, 778-784.

Reinking, R.F., J.B. Snider, and J.L. Coen, 2000a: Influences of storm-embedded orographic gravity waves on cloud liquid water and precipitation. *J. Appl. Meteor.,* **39,** 733-759.

Reinking, R.F., B.W. Orr, L. R. Bissonnette, G. Roy, and A. S. Frisch and S. Y. Matrosov, 2000b: Remote sensing of cloud droplets during MWISP. *Pro., Int'l. Geoscience and Remote Sensing Symposium (IGARSS 2000).* Honolulu, HI, 24-28 July 2000. Pp 187-189. (Available from customer.services@ieee.org).

Reinking, R.F., S.Y. Matrosov, B.W. Bartram, and R.A. Kropfli, 2000c: Evaluation of a slant-45-quasi-linear polarization state for distinguishing among drizzle droplets and quasi-spherical ice particles. *Preprints, Int'l. Conf. on Cloud Physics*, Reno, NV, 14-18 Aug 2000. Pp. 243-246. (Avail. from Desert Research Inst., 2215 Raggio Parkway, Reno, NV.)

Reinking, R.F., R.A. Kropfli, S.Y. Matrosov, W.C. Campbell, M.J. Post, D.A. Hazen, J.S. Gibson, K.P. Moran, and B.E. Martner, 2001a: Concept and Design of a Pilot Demonstration Ground-based Remote Icing Detection System. *Pro. 30th Int'l. Conf. on Radar Meteorology,* 19-24 July, Munich. Amer. Meteor. Soc., Boston, 199-201.

Reinking, R.F., R.A. Kropfli, S.Y. Matrosov, W.C. Campbell, M.J. Post, D.A. Hazen, J.S. Gibson, K.P. Moran, B.E. Martner, and T. Schneider, 2001b: Concept and Design of a Pilot Demonstration Ground-based Remote Icing Detection System. *Proc. Conf. on Battlespace Atmospheric and Cloud Impacts on Military Operations (BACIMO)*. July, Ft. Collins, CO.

Reinking, R.F., S.Y. Matrosov, B.W. Bartram, and R.A. Kropfli, 2002: Evaluation of a 45°-slant quasi-linear radar polarization state for distinguishing drizzle droplets, pristine ice crystals, and less regular ice particles. *J. Atmos. Oceanic Tech.*, **19,** 296-321.

Riley, J., and B. Horn, 1996: Plenary sessions. Proc. FAA Intn'l. Conf. Aircraft Inflight Icing. DOT/FAA/AR-96/81, I, 263 pp. (Available from NTIS, Springfield VA 22161.)

Riley, J.T. and R. McDowall (eds.), 1998: Proc. FAA specialists workshop on mixed-phase and glaciated conditions, 2-3 Dec 1998. FAA Tech. Center, Atlantic City, NJ. 346 pp.

Ryerson, C.C., M.K. Politovich, K.L. Rancourt, G.G. Koenig, R.F. Reinking, and D.R. Miller, 2000: Mt. Washington Icing Sensors Project: Conduct and Preliminary Results. *Paper # AAIA-2000-0488, Preprints, 38th AAIA Aerospace Sciences Meeting and Exhibit*, 10-13 January 1999, Reno, NV, 10 pp.

Sand, W. R., A. Cooper, M. K. Politovich, and D. L. Veal, 1984: Icing conditions encountered by a research aircraft. *J. Clim. Appl. Meteor.*, 1427-1439.

Schneider, T.L. and W.C. Campbell, 2006: A ground-based remote icing detection system (GRIDS) perspective on the November 11, 2003 SLD case during AIRS2. *12th Conf. on Aviation, Range and Aerospace Meteorology,* Atlanta, GA, Amer. Meteorol. Soc., January 2006, 7B.4.

Schneider, T.L., S.Y. Matrosov, M.D. Shupe, B.W. Bartram, W.C. Campbell, J.S. Gibson, D.A. Hazen, and R.F. Reinking, 2004: An overview of ground-based remote sensing during AIRS-2 and WISP-04, using the NOAA GRIDS system. *11th Conf. on Aviation, Range and Aerospace Meteorology*, Hyannis MA, 11-14 October 2004. Amer. Meteorol. Soc., Boston. Available on CD from the AMS.

Schneider, T.L., B.C. Bernstein, and R.F. Reinking, 2005: Forecasting and Ground-based Remote Icing-Detection System (GRIDS) documentation of the transition from a glaciated environment to an SLD icing environment. *43rd Aerospace Sciences Meeting & Exhibit*, 10-13 January 2005, Reno, NV. American Institute of Aeronautics and Astronautics, Washington, D.C.. Paper AIAA 2005-0257, 7 pp.

Schultz, P., and M.K. Politovich, 1992: Toward the improvement of aircraft-icing forecasts for the continental united States. *Wea. Forecast.,* **7,** 491-500.

Stankov, B.B., B.E. Martner, J.A. Schroeder, M.K. Politovich, and J.A. Cole, 1993: Liquid water and water vapor profiling in multi-layered clouds using combined remote sensors. Paper AIAA 93-0395, *Reprints, 31st Aerospace Sciences Mtg.*, Reno, NV, AIAA, 8 pp.

Stankov, B. B., B. E. Martner, and M. K. Politovich, 1995: Moisture profiling of the cloudy winter atmosphere using combined remote sensors. *J. Atmos. Oceanic Tech.,* **12,** 488-510.

Vivekanandan, J., B.E. Martner, M.K. Politovich, and G. Zhang, 1999: Aircraft icing detection using dual-wavelength radar observations. *IEEE Trans. Geosci. Remote Sens.*, 2325-2334.

Westwater, E.R., 1972: Microwave emission from clouds. NOAA TR ERL 219-WPL 18, 43 pp. [Avail. from Supt. of Documents, U.S. Gov't. Printing Office, Washington, DC 20402.]

Westwater, E.R., S. Crewell, and C. Matzler, 2005: Surface-based microwave and millimeter wave radiometric remote sensing of the troposphere: a tutorial. *IEEE Geosci. Remote Sens. Newsletter,* Issue 134, 16-33.

Westwater, E.R., S. Crewell, C. Matzler, and D. Cimini, 2006: Principles of surface-based microwave and millimeter wave radiometeric remote sensing of the troposphere. *Proc. Societa Italiana di Elettromagnetisomo (in press).*

Zawadski, I., W. Szyrmer, and S. Laroche, 2000: Diagnostic of supercooled clouds from single-Doppler observations in regions of radar-detectable snow. *J. Appl. Meteor.,* **39,** 1041-1058.

Zrnic, D.S., and A.V. Ryzhkov, 1999: Polarimetry for weather surveillance radars. *Bull. Amer. Meteor. Soc.*, **80,** 389-406.

Appendix A

History of Icing Hazards Research at NOAA/ETL

Table 1. NOAA/ETL History of instrument development for detection of icing hazards.

Instruments	Started	Use, Tests, Key References
Microwave Radiometer	1983	Measure vertically integrated liquid water path; correlate with icing pireps and aircraft incidents (e.g., Popa Fotino et al. 1986; Stankov et al. 1993)[1].
Cloud Radar	1991	Determine cloud layer altitudes and internal structure with high resolution (e.g., Martner and Kropfli 1993).
Microwave Radiometer + Cloud Radar	1993	Estimate vertical profile of liquid within cloud layers; compare with aircraft soundings of liquid (Politovich et al. 1995; Frisch et al. 1995).
Unattended, Zenith-pointing Cloud Radar	1996	Continuous monitoring of altitudes and internal structure of clouds overhead (Moran et al. 1998; Martner et al. 2002a).
Dual-wavelength Radar	1991	Measure liquid water content of clouds and map it in 3-D; comparisons with liquid path of steerable microwave radiometer (Martner et al. 1991, 1993a,b).
Dual-polarization Cloud Radar	1991	Identify hydrometeor types; comparison with scattering theory and in situ particle sampling (e.g., Matrosov 1991a,b; Matrosov et al. 1996; Reinking et al. 1997a,b; Matrosov et al. 2001; Reinking and Kropfli 2000, Reinking et al. 2002; Martner et al. 2002b; Matrosov et al. 2005)

ETL's earliest icing research used ground-based dual-frequency (near 20- or 23-GHz and 31- GHz) microwave radiometers to monitor the liquid water path overhead and correlated those measurements with nearby pilot reports (Westwater 1972; Hogg et al. 1983; Popa Fotino et al. 1986; Stankov et al. 1993). A few years later, ETL developed a scanning millimeter-wave Doppler cloud radar (35-GHz, K_a-band) which has evolved into a powerful research tool (Kropfli et al. 1995; Kropfli and Kelly 1996). This radar uses a much shorter wavelength (8.66 mm) than conventional weather surveillance radars (typically 5 or 10 cm), to more readily detect tiny cloud droplets and ice crystals, in addition to the larger raindrops and snowflakes. Thus clouds themselves, and not just precipitation, are observed.

Vertically pointing cloud radar delineates cloud layer boundaries and internal reflectivity and velocity structure with remarkable detail, accurately defining cloudy and cloud-free (hence, icing-free) altitudes aloft (Martner and Kropfli 1993). A logical step was to combine the radiometer's path-integrated liquid measurements with the cloud radar's range-resolved observations of cloud structure and boundaries, to allow vertical profiles of liquid within cloud layers to be estimated (Politovich et al. 1995; Frisch et al. 1995).

Unattended, continuous monitoring of cloud layer heights and structure became available in 1996 with ETL's development of a vertically pointing version of the scanning radar (Moran et al. 1998; Martner et al. 2002a). That Millimeter-wave Cloud Radar (MMCR), as well as other remote sensing systems, gave ETL experience in building unattended, nearly operational

[1] Note that references in this and all Appendices refer to the Reference section in the main report, and not to the chronological Bibliography in this Appendix.

systems. The MMCR now provides 24/7/365 measurements at several DOE CART (Clouds and Radiation Testbed) sites worldwide.

In 1991 and 1999 NOAA/ETL attempted to combine data from a second radar (X-band, 9.3 GHz or 3.1 cm) with its K_a-band radar data to test a dual-wavelength differential-attenuation method for measuring the three-dimensional distribution of liquid water content in clouds. The shorter wavelength K_a-band signal is more strongly attenuated than the longer wavelength, and in theory the wavelength attenuation difference is directly related to the cloud liquid water content. Tests, however, revealed that practical problems (e.g., antenna sidelobes and ground clutter in the X-band) and natural cloud conditions (e.g., variations in hydrometeor size distribution) disrupt this relationship and make the liquid content estimation dubious under many circumstances (Martner et al. 1991, 1993a,b; Vivekanandan et al. 1999). Hence ETL abandoned the dual-wavelength approach to icing detection because it appeared to have too many practical problems, including the need to precisely match radar sensing volumes while maintaining sufficient sensitivity at useful ranges.

In 1991 NOAA/ETL also began to explore the utility of dual-polarization methods, both theoretically and with its K_a-band radar. The theoretical work focused on various observational techniques to distinguish the many types of ice particles in clouds, beginning with cirrus observations for climate studies. A key advance was the prediction, and subsequent confirmation, that the depolarization ratio of different ice and water hydrometeors in clouds varies markedly with elevation angle (Matrosov 1991a,b; Matrosov and Kropfli 1993). During a series of Winter Icing and Storms Projects (WISP), it was shown that measurements of depolarization by various types of ice particles could be used to identify them. In fact, hydrometeor evolution could be followed in winter storms (Reinking et al. 1993b, 1995a,b, 1996a; Matrosov et al. 1995; Matrosov et al. 1996a). Whereas drizzle-sized droplets were initially used only for calibration, it was quickly realized that the depolarization measurements could be used to distinguish all spherical (liquid) cloud droplets, including SLD, from ice crystals (Reinking et al. 1996b-e, 1997a,b).

Henceforth, ETL's most important ongoing task for the FAA became the development of a dual-polarization K_a-band radar to detect clouds of hazardous SLD, and to distinguish them from clouds with non-hazardous ice particles. Supporting theory was improved (Matrosov et al. 1996a, 2000, 2001; Reinking et al. 1997a, 2002), and in a long series of intensive tests culminating with the Mount Washington Icing Sensors Project (MWISP), ETL was able to demonstrate a remote-sensing capability for deterministic hydrometeor identification using the pattern of depolarization-ratio vs. elevation-angle. These remotely-sensed radar results were corroborated by direct detection of cloud particles and precipitation by other means (e.g., aircraft and mountain-top in situ sensors). (Matrosov et al. 1996a, 2001; Reinking et al. 1997a,b, 1998, 2000a-c, 2002).

This *excellent and repeatable* agreement between theory, measurement, and independent validation thus pointed the way to the design for an operational system of integrated sensors for detecting icing conditions aloft, which is GRIDS (Reinking and Kropfli 2000; Reinking et al. 2001a,b). GRIDS is designed to be an operational system providing 24/7/365 measurements.

A Bibliography of NOAA/ETL Publications Establishing the Foundation of GRIDS, in chronological order.[2]

Westwater, E.R., 1972: Microwave emission from clouds. NOAA TR ERL 219-WPL 18, 43 pp. [Avail. from Supt. of Documents, U.S. Gov't. Printing Office, Washington, DC 20402.]

Hogg, D.C., F.O. Guiraud, J.B. Snider, M.T. Decker, and E.R. Westwater, 1983: A steerable dual-channel microwave radiometer for measurement of water vapor and liquid in the troposphere. *J. Clim. Appl. Meteorol.*, *22,* 789-806.

Popa Fotino, I.A., J.A. Schroeder, and M.T. Decker, 1986: Ground-based detection of aircraft icing conditions using microwave radiometers. *IEEE Trans. Geosci. Remote Sens.*, **GE-24**, 6, 975-982.

Martner, B.E., R.A. Kropfli, L.E. Ash, and J.B. Snider, 1991: Progress report on analysis of differential attenuation radar data obtained during WISP-91. *NOAA Tech. Memo.*, ERL WPL-215, Boulder, CO, 43 pp.

Matrosov, S. Y., 1991: Theoretical study of radar polarization parameters obtained from cirrus clouds. *J. Atmos. Sci.,* **48,** 1062-1070.

Matrosov, S. Y., 1991: Prospects for the measurement of ice cloud particle shape and orientation with elliptically polarized radar signal. *Radio Sci.,* **26**, 847-856.

Politovich, M.K., B.B. Stankov, and B.E. Martner, 1992: Use of combined remote sensors for determination of aircraft icing altitudes. *Preprints, 11th Int'l. Conf. on Clouds & Precip.*, Montreal, Canada, ICCP, 979-982.

Rasmussen, R.M. Politovich, J. Marwitz, W. Sand, J. McGinley, J. Smart, R. Pielke, S. Rutledge, D. Wesley, G. Stossmeister, B. Bernstein, K. Elmore, N. Powell, E. Weswater, B. Stankov, and D. Burrows, 1992: Winter Icing and Storms Project (WISP), *Bull. Amer. Meteorol. Soc.,* **73,** 951-974.

Matrosov, S.Y., and R.A. Kropfli, 1993: Cirrus cloud studies with elliptically polarized K_a-band radar signals: A suggested approach. *J. Atmos. and Oceanic Tech.*, **10**, 684-692.

Stankov, B.B., B.E. Martner, J.A. Schroeder, M.K. Politovich, and J.A. Cole, 1993: Liquid water and water vapor profiling in multi-layered clouds using combined remote sensors. Paper AIAA 93-0395, *Reprints, 31st Aerospace Sciences Mtg.*, Reno, NV, AIAA, 8 pp.

Martner, B.E., and R.A. Kropfli, 1993: Observations of multi-layered clouds using K-band radar. Paper AIAA 93-0394, *Reprints, 31st Aerospace Sciences Mtg.*, Reno, AIAA, 8 pp.

Martner, B.E., R.A. Kropfli, L.E. Ash, and J.B. Snider, 1993: Dual-wavelength differential attenuation radar measurements of cloud liquid water content. *Preprints, 26th Intl Conf. on Radar Meteor.*, AMS, Norman, OK, 596-598.

Martner, B.E., R.A. Kropfli, L.E. Ash, and J.B. Snider, 1993: Cloud liquid water content measurement tests using dual-wavelength radar. *NOAA Tech. Memo.* ERL ETL-235, NOAA Environmental Research Laboratories, Boulder, CO, 47 pp.

[2] Some of these publications are listed only in this bibliography and are not referenced elsewhere in the text of this report.

Reinking, R.F. B.W. Orr, B. Stankov, and C. Davis, 1993: NOAA K_a-band cloud-sensing radar measurements from WISPIT. *Preprints, 5th Int'l. Conf. on Aviation Weather Systems*, 2-6 August 1993, Vienna, VA. Amer. Meteor. Soc., Boston, MA, 130-134.

Reinking, R.F., R.Caiazza., R.A. Kropfli, B.W. Orr, B.E. Martner, T.A. Niziol, G.P. Byrd, R.S. Penc, R.J. Zamora, J.B. Snider, R.J. Ballentine, A.J. Stamm, C.D. Bedford, P. Joe, and A.J. Koscielny, 1993. The Lake Ontario Winter Storms (LOWS) Project. Cover article, *Bull. Amer. Meteor. Soc.,* **74,** 1828-1829.

Frisch, A.S., C.W. Fairall, and J.B. Snider, 1995: Measurement of cloud and drizzle parameters in ASTEX with Ka-band Doppler radar and a microwave radiometer. *J. Atmos. Sci.,* **52**, 2788-2799.

Orr, B.W., and B.E. Martner, 1995: Detection of weakly precipitating winter clouds by a NOAA 404 MHz wind profiler. *J. Atmos. Oceanic Tech.,* **13**, 570-580.

Politovich, M.K., B.B. Stankov, and B.E. Martner, 1995: Determination of liquid water altitudes using combined remote sensors. *J. Appl. Meteor.,* **35**, 2060-2075.

Stankov, B. B., B. E. Martner, and M. K. Politovich, 1995: Moisture profiling of the cloudy winter atmosphere using combined remote sensors. *J. Atmos. Oceanic Tech.,* **12,** 488-510.

Kropfli, R.A., S.Y. Matrosov, T. Uttal, B.W.Orr, A.S. Frisch, K.A. Clark, B.W.Bartram, R.F.Reinking, J.B. Snider, and B.E. Martner, 1995: Cloud physics studies with 8 mm wavelength radar. Special issue on cloud microphysics and applications to global climate change, *Atmospheric Research,* **35,** 299-313.

Gibson, J.S., and B.E. Martner, 1995: Interactive auxiliary real-time data system for NOAA/ETL Doppler radars. *Preprints, 11th Intl. Conf. on Interactive Info. Processing Systems for Meteor., Ocean., and Hydrology*, Dallas, AMS, 304-309.

Matrosov, S.Y., R.F. Reinking, R.A. Kropfli, and B.W. Bartram, 1995: Identification of ice hydrometeor types with elliptical polarization radar measurements. *Preprints, 27th Conference on Radar Meteorology,* 9-13 October 1995, Vail, CO. Amer. Meteor. Soc., Boston, MA, 539-541.

Reinking, R.F., S.Y. Matrosov, B.E. Martner, R.A. Kropfli, and B.W. Bartram, 1995: Hydrometeor identification with millimeter-wave dual-polarization radar. *Conf. on Cloud Physics*, 15-20 January 1995, Dallas, Texas. Amer. Meteor. Soc., Boston, MA, 20-25.

Reinking, R.F., S.Y. Matrosov, R.J. Bruintjes, B.E. Martner, and R.A. Kropfli, 1995: Further comparison of experimental and theoretical radar polarization signatures due to ice hydrometeor shape. *Preprints, 27th Conference on Radar Meteorology*, 9-13 October 1995, Vail, CO. American Meteorological Society, Boston, MA, 47-49.

Kropfli, R.A., and R.D. Kelly, 1996: Meteorological research applications of mm-wave radar. *Meteorol. and Atmos. Phys.,* **59,** 105-121.

Matrosov, S.Y., R.F. Reinking, R.A. Kropfli, and B.W. Bartram, 1996: Estimation of hydrometeor shapes and types from radar polarization measurements. *J. Atmos. Oceanic Tech.,* **13,** 85-96.

Reinking, R.F., S.Y. Matrosov, and R.T. Bruintjes, 1996: Ice and water hydrometeor identification with elliptical polarization radar: Applications to precipitation enhancement.

Preprints, 13th Conf. on Planned & Inadvertent Weather Modification, 28 January-2 February, 1996, Atlanta, GA. Amer. Meteor. Soc., Boston, MA, 172-179.

Reinking, R.F. S.Y. Matrosov, and R.T. Bruintjes, 1996: Hydrometeor identification with elliptical polarization radar: Applications for glaciogenic cloud seeding. Cover article, *J. Wea. Modif.*, **28,** 6-18.

Reinking, R.F., S.Y. Matrosov, B.E. Martner and R.A. Kropfli, 1996: Differentiation of freezing drizzle from ice hydrometeors and rain with polarization radar. *Pro., FAA International Conference on Aircraft Inflight Icing.* 6-8 May 1996, Springfield, VA, **II,** 331-338. [Available from NTIS, Springfield, VA 22161. DOT/FAA/AR-96/81].

Reinking, R.F., S.Y. Matrosov, B.E. Martner and R.A. Kropfli, 1996: Differentiation of freezing drizzle from ice hydrometeors with polarization radar. *Pro., 12th International Conference on Clouds and Precipitation.* 19-23 August 1996, Zurich, Switzerland. International Commission on Clouds and Precipitation (ICCP); **I,** 446-449.

Reinking, R.F., S.Y. Matrosov, B.E. Martner, R.A. Kropfli, and B.W. Bartram, 1996: Hydrometeor identification with millimeter-wave dual-polarization radar. *Proc. ETL/CSU Cloud-related Process Modeling and Measurement Workshop, Boulder, Colorado, 23-25 October 1995.* Environmental Technology Laboratory, U.S. Dept. of Commerce, 209-214.

Reinking, R.F., S.Y. Matrosov, R.J. Bruintjes, B.E. Martner, and R.A. Kropfli, 1996: Further comparison of experimental and theoretical radar polarization signatures due to ice hydrometeor shape. *Proc. ETL/CSU Cloud-related Process Modeling and Measurement Workshop,* Boulder, Colorado, 23-25 October 1995. Environmental Technology Laboratory, U.S. Dept. of Commerce, 215-218.

Reinking, R.F., S.Y. Matrosov, R.T. Bruintjes, and B.E. Martner, 1997: Identification of hydrometeors with elliptical and linear polarization K_a-band radar. *J. Appl. Meteor.*, **36**, 322-339.

Reinking, R.F., S.Y. Matrosov, B.E. Martner, and R.A. Kropfli, 1997: Differentiation of freezing drizzle from ice hydrometeors and freezing rain with dual-polarization radar. *J. Aircraft*, **34**, 778-784.

Reinking, R.F., 1997: Hydrometeor and dispersion measurements with 3-cm and 8-mm dual-polarization radar. *Pro., WMO Workshop on Cloud Properties for Forecasts of Weather and Climate*. 23-27 June 1997. Mexico City, Mexico. WMO TD No. 852, 255-269.

Campbell, W.C. and J. Gibson, 1997: A programmable real-time data processing and display system for the NOAA/ETL Doppler radars. *Proceedings of the 28th Conference on Radar Meteorology,* Austin TX, American Meteorology Society, pp 178-179.

Reinking, R.F., 1998: Detection of ice hydrometeors and freezing drizzle with K_a-band dual-polarization radar. *Conf. on Cloud Physics.* 17-21 August 1998, Everett, Washington. Amer. Met. Soc., Boston. pp 249-252.

Klimowski, B.A., R. Becker, E.A. Betterton, R. Bruintjes, T. L. Clark, W.D. Hall, B.W. Orr, R. A. Kropfli, P. Piironen, R.F. Reinking, D. Sundie, and T. Uttal, 1998: The 1995 Arizona Program: Toward a better understanding of winter storm precipitation development in mountainous terrain. *Bull. Amer. Meteor. Soc.*, **79,** 799-813.

Matrosov, S.Y., A.J. Heymsfield, R.A. Kropfli, B.E. Martner, R.F. Reinking, J.B. Snider, P.Piironen, and E.W. Eloranta, 1998: Comparisons of ice cloud parameters obtained by combined remote sensor retrievals and direct methods. *J. Atmos. Oceanic Tech.*, **15,** 184-196.

Kropfli, R.A., B.E. Martner, S.Y. Matorsov, R.F. Reinking, A.S. Frisch, and T. Uttal, 1998: Radar and radiometer measurements of the physical parameters of clouds and precipitation at the NOAA Environmental Technology Laboratory. *Proc. Conf. on Battlespace Atmospheric and Cloud Impacts on Military Operations (BACIMO)*. Hanscom AFB, MA, 1-3 Dec 1998, 125-132.

Moran, K.P., B.E. Martner, M.J. Post, R.A. Kropfli, D.C. Welsh, and K.B. Widener, 1998: An unattended cloud-profiling radar for use in climate research. *Bull. Amer. Meteor. Soc.*, **79**, 443- 455.

Reinking, R.F., S.Y. Matrosov, B. E. Martner, B.W. Orr, R.A. Kropfli, and B.W. Bartram, 1999: Slant-linear polarization applied to detection of supercooled drizzle. *Preprints, 29th Conf. on Radar Meteorology*, Montreal, Canada, 285-288.

Reinking, R.F., 1999: Influence of ice particles on remote detection and assessment of atmospheric supercooled liquid water. Proceedings, FAA Specialists' Workshop on Mixed-phase and Glaciated Icing Conditions, 2-3 December 1998, Atlantic City, NJ, Editors, James T. Riley and Rosemarie McDowall. FAA Technical Center, Atlantic City, pp. 303-304.

Vivekanandan, J., B.E. Martner, M.K. Politovich, and G. Zhang, 1999: Aircraft icing detection using dual-wavelength radar observations. *IEEE Trans. Geosci. & Remote Sensing*, 2325-2334.

Frisch, A.S., B.E. Martner, I. Djalalova, and M.R. Poellot, 2000: Comparison of radar/radiometer retrievals of stratus cloud liquid water content profiles with in-situ measurements by aircraft. *J. Geophys. Res.*, **105**, 15361-15364.

Moran, K.P., B.E. Martner, and H.A. Winston, 2000: Dual-polarization and processor efficiency enhancements of the DOE's millimeter-wavelength cloud radars (MMCR). *Reprints, TECO-2000, WMO Tech. Conf. on Meteor. & Environ. Instruments and Methods of Observation*, Beijing, China, 4 pp.

Reinking, Roger F., Jack B. Snider, and Janice L. Coen, 2000: Influences of storm-embedded orographic gravity waves on cloud liquid water and precipitation. *J. Appl. Meteor.*, **39,** 733-759.

Ryerson, Charles C., Marica K. Politovich, Kenneth L. Rancourt, George G. Koenig, Roger F. Reinking, and Dean R. Miller, 2000: Mt. Washington Icing Sensors Project: Conduct and Preliminary Results. *Paper # AAIA-2000-0488, Preprints, 38th AAIA Aerospace Sciences Meeting and Exhibit*, 10-13 January 1999, Reno, Nevada, 10 pp.

Reinking, R.F., B.W. Orr, L. R. Bissonnette, G. Roy, and A. S. Frisch and S. Y. Matrosov, 2000: Remote sensing of cloud droplets during MWISP. *Proceedings, Intn'l. Geoscience and Remote Sensing Symposium (IGARSS 2000).* Honolulu, HI, 24-28 July 2000. Pp 187-189. (Available from customer.services@ieee.org).

Matrosov, S.Y., R.F. Reinking, R.A. Kropfli, B.E. Martner, and B.W. Bartram, 2000: Inferring hydrometeor shapes using different polarization states of radar signals. Proceedings Intn'l. Geoscience and Remote Sensing Symposium (IGARSS 2000). Honolulu, HI, 24-28 July 2000. Pp. 1577-1579. (Available from customer.services@ieee.org.)

Reinking, R.F., S.Y. Matrosov, B.W. Bartram, and R.A. Kropfli, 2000: Evaluation of a slant-45-quasi-linear polarization state for distinguishing among drizzle droplets and quasi-spherical ice particles. *Preprints, International Conference on Cloud Physics*, Reno, NV, 14-18 Aug 2000. Pp. 243-246. (Avail. from Desert Research Inst., 2215 Raggio Parkway, Reno, NV.)

Reinking, R.F., S.Y. Matrosov, C.C. Ryerson, R.A. Kropfli, and B.W. Bartram, 2000: Verified detection of supercooled large droplets with dual-polarized, millimeter-wave radar. *Ninth Conf. on Aviation, Range, and Aerospace Meteorology*, 11-15 Sept. 2000, Orlando Fla. Amer. Meteor. Soc., Boston. 537-542.

Reinking, R.F., and R.A. Kropfli, 2000: Breakthroughs in radar polarization technology and related studies. Radar-based Icing Diagnosis Techniques, In-flight Icing PDT Technical Direction FY2000 Year-end Task Progress Report to the FAA, Deliverable 00.4.3.E1. NOAA Environmental Technology Laboratory. 16 pp.

Matrosov, S.Y., R.F. Reinking, R.A. Kropfli, B.E. Martner, and B.W. Bartram, 2001: On the use of radar depolarization ratios for estimating shapes of ice hydrometeors in winter clouds. *J. Appl. Meteorol.*, **40,** 479-490.

NOAA ETL Radar Meteorology and Oceanography Division, 2001: Preliminary Design, Ground-based Remote Icing Detection System (GRIDS). Report to the FAA Aviation Weather Research Program, In-Flight Icing PDT #4, Task 01.4.3.3, FAA Icing Remote Sensing Testbed, Deliverable 01.4.3.1.E3. 65 pp + appendices.

Reinking, R.F., R.A. Kropfli, S.Y. Matrosov, W.C. Campbell, M.J. Post, D.A. Hazen, J.S. Gibson, K.P. Moran, and B.E. Martner, 2001: Concept and Design of a Pilot Demonstration Ground-based Remote Icing Detection System. *Proceeding 30th International Conference on Radar Meteorology*, 19-24 July, Munich. Amer. Meteor. Soc., Boston, 199-201.

Reinking, R.F., R.A. Kropfli, S.Y. Matrosov, W.C. Campbell, M.J. Post, D.A. Hazen, J.S. Gibson, K.P. Moran, B.E. Martner, and T. Schneider, 2001: Concept and Design of a Pilot Demonstration Ground-based Remote Icing Detection System. *Proc. Conf. on Battlespace Atmospheric and Cloud impacts on military operations (BACIMO)*. July, Ft. Collins, CO.

Reinking, R.F., S.Y. Matrosov, B.W. Bartram, and R.A. Kropfli, 2002: Evaluation of a 45E-slant quasi-linear radar polarization state for distinguishing drizzle droplets, pristine ice crystals, and less regular ice particles. *Journal of Atmospheric and Oceanic Technology*, **19,** 296-321.

Martner, B.E., B.W. Bartram, J.S. Gibson, W.C. Campbell, R.F. Reinking, and S.Y. Matrosov, 2002: An overview of NOAA/ETL's scanning K_a-band cloud radar. *16th Conf. on Hydrology*. Jan 2002, Orlando, Fla. Amer. Meteor. Soc.

Martner, B.E., D.A. Hazen, K.P. Moran, T. Uttal, M.J. Post, and W.B. Madsen, 2002: NOAAETL's vertical-profiling cloud radar and radiometer package. *6th Symp. on Integrated Observing Systems*, Jan 2002, Orlando, FL, Amer. Meteor. Soc.

Gibson, J.S., W.C. Campbell, B.E. Martner, 2004: RADS: A radar acquisition and display system for research radars. *NOAA Tech. Report*. OAR ETL-69, NOAA Office of Oceanic and Atmospheric Research, Boulder, CO, 56 pp.

Reinking, R. F., and Sergey Y. Matrosov, 2004: Fall attitudes of pristine snow crystals estimated from radar depolarization measurements. *Proceedings, 14th International Conference on Clouds and Precipitation*, 18-23 July 2004, Bologna, Italy. II: 912-915 (Available from Inst. Atmos. Sci. and Climate (ISAC), National Research Council, Via Gobetti 101, 40129 Bologna, Italy).

Schneider, T.L., S.Y. Matrosov, M.D. Shupe, B.W. Bartram, W.C. Campbell, J.S. Gibson, D.A. Hazen, and R.F. Reinking, 2004: An overview of ground-based remote sensing during AIRS-2 and WISP-04, using the NOAA GRIDS system. 11th Conf. on Aviation, Range and Aerospace Meteorology, Hyannis MA, 11-14 October. Amer. Meteorol. Soc., Boston. Available on CD from the AMS.

Bernstein, B.C., and T.L. Schneider, 2004: Two perspectives on a Colorado icing event: GRIDS and CIP. 11th Conf. on Aviation, Range and Aerospace Meteorology, Hyannis MA, 11-14 October. Amer. Meteorol. Soc., Boston. Available on CD from the AMS.

Schneider, Timothy L., Ben C. Bernstein, and Roger F. Reinking, 2005: Forecasting and Ground-based Remote Icing-Detection System (GRIDS) documentation of the transition from a glaciated environment to an SLD icing environment. 43rd Aerospace Sciences Meeting & Exhibit, 10-13 January 2005, Reno, NV. American Institute of Aeronautics and Astronautics, Washington, D.C.. Paper AIAA 2005-0257, 7 pp.

Matrosov, S.Y., R.F. Reinking, and I.V. Djalalova, 2005: Inferring fall attitudes of pristine dendritic crystals from polarimetric radar data. *J. Atmos. Sci.,* **62,** 241-250.

Westwater, E.R., S. Crewell, and C. Matzler, 2005: Surface-based microwave and millimeter wave radiometric remote sensing of the troposphere: a tutorial. *IEEE Geosci. and Remote Sensing Newsletter,* Issue 134, 16-33.

Westwater, E.R., S. Crewell, C. Matzler, and D. Cimini, 2006: Principles of surface-based microwave and millimeter wave radiometeric remote sensing of the troposphere. *Proc. Societa Italiana di Elettromagnetisomo (in press).*

Appendix B

Enhancements to Core Icing Algorithm for GRIDS

1. INTRODUCTION

The core icing algorithm, as described in the main text, has been tested and will provide an effective starting point for icing detection. However we can already envision enhancements to it that will improve its performance. Most of these enhancements require only software improvements, but a few do extend the hardware capability of the radar by adding elevation scanning. As with any new system, operational experience will surely lead to further enhancements not contemplated here.

2. LW ENHANCEMENT

The value of the path-integrated liquid water (LW) sensed by the microwave radiometer can be distributed throughout those cloud layers that have liquid water, to estimate LWC (g m^{-3}) in each liquid layer and hence the potential severity of the icing hazard. LW of 1 mm equates to an average LWC of 1 g m^{-3} in a cloud 1 km deep. In FAR Appendix C, the minimum LWC threshold for moderate icing is at the point (LWC, D_e, T) = (0.06 g m^{-3}, 40 μm, 20º C), where D_e is the droplet size.

Here is an outline of how it will work in GRIDS:

We assign liquid only to clouds for which Z_e > -23 dBZ, and assume that any part of a cloud with a lower reflectivity has minimal LWC.

(a) If *Condition Red* (Table 2, Sec. 3.3) is met over the entire cloud path: Determine this path length from radar measurements and normalize the liquid water path (LWP) to it. If LWC < 0.06 g m^{-3}, the potential icing hazard is minimal. If 0.06 g m^{-3} < LWC < 0.1 g m^{-3} light to moderate icing is possible. If LWC > 0.1 g m^{-3}, severe icing is possible. These "break point" values are the most conservative (smallest) within FAR Appendix C envelopes. Experience with GRIDS may show that the break point values should be adjusted.

(b) If *Condition Red* is met over only part of the cloud where Z_e > -23 dBZ, and the rest of the cloud is *Condition Yellow* or warm *(Condition Green)*, two options are available:

(1) Allocate all liquid to that depth of the cloud where *Condition Red* is met. This is the most conservative approach, yielding maximum value of LWC and likely overestimating the potential icing severity. This approach excludes allocating any liquid to additional parts of clouds that may be mixed phase (*Condition Yellow)* or to any warm cloud (*Condition Green*).

(2) Assign equal LWC to liquid (or potentially liquid) cloud paths of all three conditions. This is the less conservative approach that may underestimate the potential icing hazard.

(c) If *Condition Yellow* is met and there is no cloud along the path rated *Condition Red*: Assign LWC by either of the two options in (b) above.

The table below classifies potential icing hazard according to LWC. A Condition Red carries more weight than a Condition Yellow with the same LWC, because the ice particles in the Condition Yellow will tend to consume the liquid by vapor deposition or riming.

Table 1. Icing hazard rating and LWC.

Condition	**LWC** (g m^{-3})	**Hazard Rating**
Red	LWC ≥ 0.1	Red-1
	0.06 ≤ LWC < 0.1	Red-2
	LWC < 0.06	Red-3
Yellow	LWC ≥ 0.1	Yellow-1
	0.06 ≤ LWC < 0.1	Yellow-2
	LWC < 0.06	Yellow-3
Green	LWC (any value)	Green

As noted in Section 3.3.2, it may be possible in the near future to estimate the LW profile with reasonable accuracy from continuous radiometric and radar measurements, to which the above classifications could be applied.

3. TEMPERATURE ENHANCEMENTS

Several measures of the cloud temperatures and the altitude of the freezing/melting level can be provided by GRIDS. The RUC model temperature profile is central to the GRIDS algorithm, but like all other measures is subject to some error, particularly at times quite apart from the 12-hr radiosondes that anchor the RUC forecasts. Therefore, the GRIDS estimates of cloud temperature and the altitudes of hazardous, supercooled liquid would best be served by establishing a hierarchy of priorities and cross-checks in applying radiometric profiling measurements, the radiometric layer-mean temperature estimate, the bright band measurements, and the RUC. Additional enhancements using icing temperature statistics and employing measures of instability that creates SLW can readily be introduced.

3.1 Radiometric Temperature Profiling Enhancements

The 30 and 90 GHz dual channel radiometric data can be manipulated to estimate a layer-mean temperature of the cloud LW. GRIDS software is readily adaptable to include this estimate. The GRIDS design also includes a third, ~55GHz, radiometer channel, which provides estimates of the temperature profile. Since it is part of the hardware design, this option has been discussed in more detail in the main body of the text. As noted there, the temperature profiling radiometer is limited in measuring detail and is best in the lowest few kilometers of the troposphere. It generally overestimates temperature in the upper reaches of inversions, and underestimates in the lower regions, but it can provide a good smoothed temperature profile, *continuously* with temporal resolution of seconds, to verify and compare to the RUC output. This cross-check on the RUC will be particularly important in situations with frontal activity where the 1-hour resolution and time-interpolation of the RUC may become too coarse. These radiometric temperature data are not included in the GRIDS core algorithm, but its inclusion as an enhancement, is recommended.

3.2 Temperature Instability Enhancement

The tropospheric profile of dew point temperature as well as the profile of temperature can be downloaded from the RUC model output. Therefore, by applying an appropriate (in)stability index, such as either the Showalter or Lifted Index, the potential for cloudy convection can be estimated quantitatively. This can be integrated with the core algorithm decision points to additionally estimate the potential for enhanced condensation and LW by convection, which if supercooled can increase the icing potential. Particularly, the degree of correlation between the instability and enhanced LW should be established through field tests. The instability indicator will be valid only if increased production of LW is observed, and only then can the warning level be upgraded. The simplest approach would be to make a yes or no determination as to whether any part of the cloud depth is unstable. The degree of instability could add further detail.

3.3 Temperature Classification Enhancement

Further refinement of the potential icing hazard is possible via temperature classification. A statistical study (Schultz and Politovich 1992) estimated that approximately 90% of icing incidents occur in the temperature range of 0º C to -20 º C, and 70% occur when -15º C < T < -2º C. Icing potential increases with temperature because warmer air can hold more vapor and thus produce more condensed liquid. A temperature classification such that T ≤ 20º C means minimal risk, -20º C < T ≤ -10º C means moderate risk, -10º C < T < 0º C means highest risk, and T > 0º C means no risk could be applied alone, or in combination with the LWC stratification. In mixed phase clouds, which are readily detected by the radiometer-radar combination, allowance can be made for consumption of LW by the ice crystals, which is temperature dependent. This consumption is maximized, and the icing potential is *diminished* primarily near -15º C and secondarily near -5º C. Also, since temperature and LWC are not truly independent, applying an additional temperature classification becomes somewhat redundant and adds complication. Still, from each point (LWC, T) in the cloud profile, it may be possible to estimate not only the icing severity, but also the *droplet size (D_e)* that is contributing to the hazard. After a sufficient set of GRIDS data are acquired and analyzed, it will be possible to study such an enhancement.

3.4 Bright band (melting level) enhancement

Obviously, supercooled cloud liquid can occur only at altitudes where T < 0°C. These altitudes will begin slightly above the melting level if one occurs. The melting level is detected with radars as the bright band. Freezing drizzle and rain can occur at the surface when falling snowflakes melt, and the droplets they create fall into colder, sub-cooled air nearer the surface. The first indicator of falling drizzle or rain is the appearance of a bright band, the signature of which is much more defined in the depolarization measurement than the reflectivity measurement. It is lucidly depicted by the GRIDS radar as a line of extremely high depolarization (DR approaching 0 dB, the level for complete depolarization), clearly separated from much lower DRs immediately above and below the melting level. GRIDS will also show the minimal signature value of DR in freezing drizzle, but may show a DR that decreases with range in freezing rain due to non-Rayleigh scattering (Reinking et al. 1997b). Any effects of rain attenuation on reflectivity at Ka band will be much reduced at the 40º antenna elevation from that measured at much lower elevations commonly used with scanning radars. Also, a Z_e > -15 dBZ in all range gates between the surface and the bright band will show that this hazardous

precipitation is reaching the surface. The GRIDS surface temperature and/or the ingested temperature profile will indicate if the necessary supercooling is occurring below the melting level. Algorithms for detecting freezing drizzle and rain by measuring the vertical DR gradient to isolate the bright band have been developed for other applications and can be adapted to GRIDS.

4. VERTICALLY-POINTING ENHANCEMENT (DEPOLARIZATION AND VERTICAL MOTION MEASUREMENTS)

In mixed-phase rather than liquid-only clouds, cloud physics principles dictate that ice particles will rapidly consume liquid droplets, so the LW component in mixed-phase clouds can present a lasting icing hazard only if the dynamics support continued condensation that outpaces the consumption by ice. The GRIDS radar includes Doppler measurements, so estimates of the beam-radial velocity, V_e, of reflecting hydrometeors and the variance of V_e are routinely measured. Without modification to GRIDS, the velocity variance measured in cloud along the 40° slant-path can be taken directly as an estimate of in-cloud turbulence. The degree of turbulence can in turn serve as an indicator of heightened potential for icing, because shear zones and convection tend to produce relatively large and dangerous SLDs. Additional gains in icing hazard detection can be made by modifying the radar to alternate between pointing to the 40° elevation and then to the vertical.

The GRIDS radar is designed with options to replace pulse-pair processing with spectral processing, and to add a zenith-pointing capability. Pointing to zenith and 40º elevation in alternating 5 min periods would provide superior ice particle identification in DR, as well as measurements of Doppler vertical velocity and vertical velocity variance. The pointing angle of the microwave radiometer would alternate in synchronization with that of the radar. Spectral processing could add sensitivity to the radar, and if implemented with the zenith-pointing option, would provide spectral measurements of the vertical velocity (Schneider et al. 2004, 2005). Formulations of specific algorithm enhancements from these additional measurements offer considerable promise.

The identification of the different ice particles in itself can add another level of confidence to detection of an icing condition, especially in those clouds of mixed-phase. Ice crystal families can be identified and differentiated from droplets with a high level of confidence in the 40º elevation DR measurement alone. However, the specific type of ice particle and changes in particle type are best established by measuring DR as a function of a full range of elevation angles, or at a minimum of two elevation angles including zenith. This has been thoroughly demonstrated (see e.g., Matrosov et al. 2001 for the theory and Reinking et al. 2002 for the field demonstration). Ice types are more specific indicators of the microphysical processes that are active in a cloud, and hence of the likely rate of consumption of hazardous liquid by ice. For example, the presence of pristine ice crystals indicates minimal riming of the crystals by cloud droplet collection, and thus a minimal icing hazard. However, the presence of graupel is normally indicative of liquid-producing convection; it shows that considerable liquid-consuming riming has occurred, and warns that liquid build-up may occur in successive convective elements.

Doppler velocity parameters can be used to estimate both vertical air motion and the falling speed of hydrometeors when the radar is pointed to zenith. Mixed-phase clouds can produce

droplets of sufficient size and LWC to be an icing hazard only if upward air motion is sufficient to condense liquid faster than the ice can consume it. Strong upward air motion can be liquid-producing when it exceeds the terminal velocity of ice particles (hail excluded). Vertical velocity spectra might help decide if the cloud is of single or mixed phase, and they can be used to estimate the *effective size* of any droplets from *differences* in ice particle and cloud droplet fall speed (Zawadski et al., 2000).

The GRIDS radar can operate in a vertically-pointing, time series mode that provides measurements of the full Doppler spectra, which is the distribution of returned power as a function of the velocity of the targets within a given range gate. In effect, the Doppler spectrum is a convolution of hydrometeor fall speeds and air turbulence combined with mean air motions. Under minimal turbulence, Doppler spectra from single-phase (all ice or all liquid) clouds are relatively narrow. The presence of turbulence, multiple phases of particle habits, and /or vertical wind shear can lead to relatively broad and possibly multi-modal Doppler spectra. These Doppler spectra features may provide information that is useful for identifying and quantifying potential aircraft icing conditions. A demonstration of this is as follows (from Schneider et al. 2004). Figure 1 shows three Doppler moments (reflectivity, velocity, spectral width) measured with the NOAA-K (GRIDS demonstration) radar during AIRSII. A spiral descent by NASA research aircraft confirmed the supercooled liquid near the top and the additional complex nature of this cloud.

Twin Otter:
Icing near cloud top
LWC ~0.5g/m^3

NASA radiometer:
LWP ~210-280 g/m^2

17:00 Z sounding:
T<0 C above 2.2 km

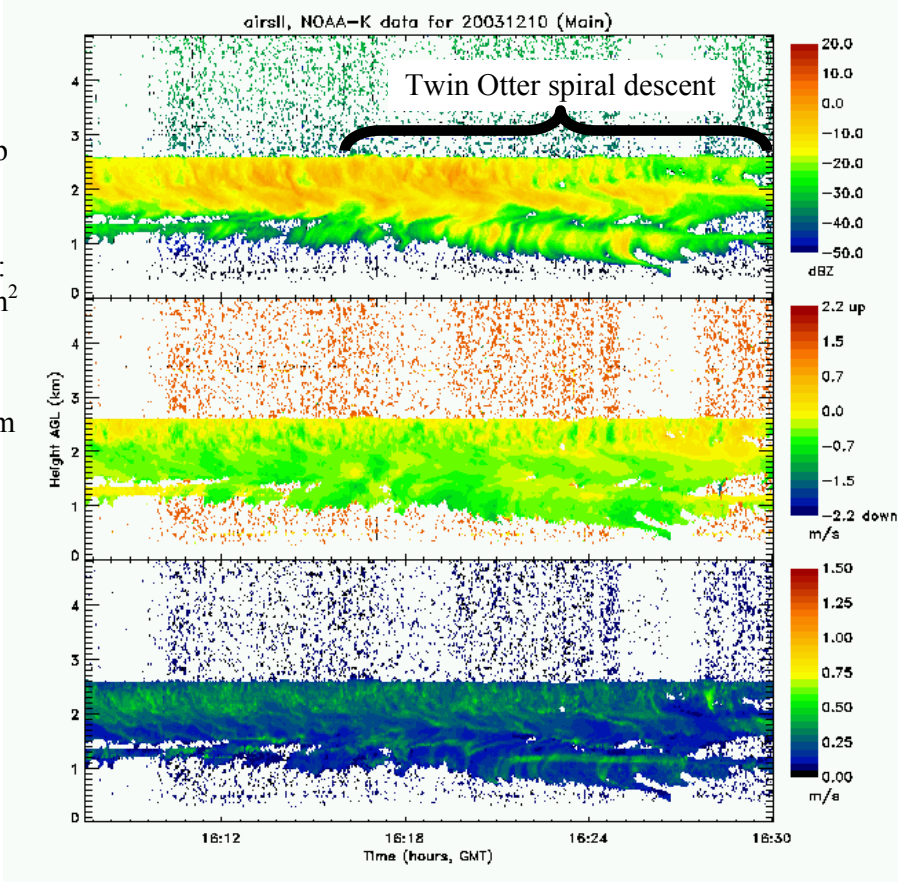

Figure 1. Doppler moments of reflectivity, velocity, and spectral width measured during AIRSII.

A spectrograph that depicts the evolution of the Doppler spectra with height during this case is shown in Figure 2. Horizontal slices of this contour plot represent individual Doppler Spectra. Both above and below the melting level (~2.2 km), bi-modal spectra suggest that multiple phases and crystal growth habits may have been present. Above 2.2 km, bi-modal spectra (e.g., inset panel) may indicate the presence of supercooled liquid droplets at negligible fall speeds and ice particles at fall speeds near 0.5 m s^{-1}. At 2.0 and 1.1 km there are indications of liquid cloud layers near 0 m s^{-1} that produce drizzle at higher fall speeds. The DR measurement with GRIDS combined with the path LW from the microwave radiometer will readily show the all-liquid versus mixed phase clouds, but the altitudes of the LW is not determined. This type of spectral information, combined with temperature profiles, may provide a means for identifying the distribution of mixed-phase cloud regions with supercooled liquid. In some cases, the microphysical properties of both liquid and ice components can be derived from these spectra.

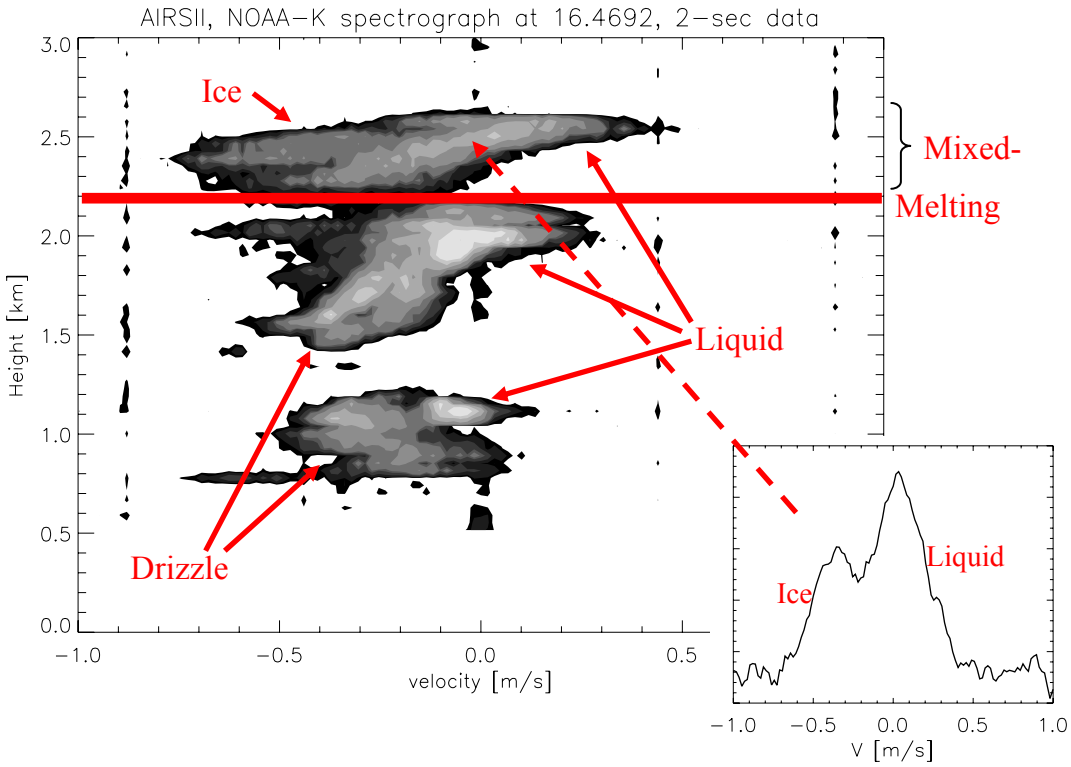

Figure 2. Spectrograph of the evolution of Doppler velocity spectra with altitude.

5. RAIN RECOGNITION ENHANCEMENTS

The recognition of degradation of signals caused by rainfall, and definition of appropriate decision-path alterations are important parts of the GRIDS algorithm. This is mentioned last in this list of specific potential enhancements only because some of the possible approaches to rain-recognition depend on some of the aforementioned enhancements.

As noted before, rain could degrade the signal received by the microwave radiometers. The core icing hazards algorithm does not incorporate rainfall directly because the commercially available microwave radiometers integrate a blower system to dry a microwave penetrating window that protects the antenna. However, experiments by NASA with these drying devices

during the 2nd Alliance Icing Research Study (AIRSII, 2003) indicate that unreasonably high values of LW are obtained during significant rain. Drizzle is unlikely to induce false readings (Reinking et al. 2000a), but at this writing a rain-rate threshold above which the dryers fail has not yet been established.

To address this issue, one reasonably direct solution to this problem is to use the surface rain-rate sensor incorporated with GRIDS and apply a sensible, conservative threshold to the measurement. Thus, for example, if RR > N mm/hr (where N is yet to be determined), and other algorithm thresholds are met at some altitudes, a yellow warning would be issued for those flight levels. This simple rain-no rain decision would indicate that there is uncertainty in the reliability of the radiometer measurement, but icing is possible.

This can be upgraded further by directly sorting reliable from potentially unreliable LW measurements by evaluating the values and variance of the radiometer's LW signature. The yellow warning would then be issued only if the rain-rate threshold is met, the other parameters meet their criteria for a hazard, *and* the LW signal is erratic (large variance) with high value spikes commonly well in excess of 2 mm.

Alternatively or additionally, the radar itself is a well-established instrument for detecting and estimating rain rate via the standard reflectivity-rain rate (Z-R) relationships. Algorithm enhancements that use the radar rather than the rain-rate sensor to identify rain will be only slightly more complicated but are certainly achievable and can more readily deal with distinguishing snowfall (which will not degrade the radiometer or radar measurements) from rainfall, by also using bright-band detection and the depolarization measurements.

Further use of the radar can be made if the vertically-pointing option is implemented. Then the measurement of the vertical velocity within the clouds above can be incorporated to identify updrafts that are likely to produce regions of elevated LW vs. benign motion that is non-productive. This option would be particularly useful to refine the warning of icing potential during rain to an estimate that is more quantitative than simply "yellow." Additionally, or alternatively, estimates of vertical motion from the RUC model could be used for the same purpose, although they would be filtered by the larger scale they represent.

The Ka-band radar's attenuation due to rain should also be noted. It can be expressed as

$$\text{Attenuation (dB)} = 0.56 * \text{rain rate (mm/hr)} * \text{range (km)}.$$

Thus a 5mm/hr rain measured at 3 km range would cause ~8.4 dB attenuation. Due to the low altitude of the bright band in (winter) icing conditions, and the high pointing angle of GRIDS, the propagation path through rain falling between the bright band and the radar is normally quite short, such that only heavy rain will seriously attenuate the radar reflectivity (and the radiometer measurements as well) and render the GRIDS icing algorithm unusable. Under such circumstances of uncertainly, only a yellow warning can be issued. We further note, however, that when heavy rain is being produced by stratiform clouds, the ice processes removing the SLW are very active, so these situations are likely not a prime time for icing events. Note that attenuation is rarely sufficient to impede the vertical motion and Doppler spectra measurements, so algorithms should be adjusted to focus on those. If the clouds are severely convective, aircraft would be warned away by on-board radars or NEXRAD, regardless of the icing conditions, so that is not a situation that GRIDS needs to address.

6. GRIDS-CIP SYNERGY

The noted enhancements to the GRIDS algorithm begin a list that will add to the power of GRIDS. As new developments in instrumentation, measurements, and modeling that could support GRIDS come on line, they would logically be examined and incorporated as appropriate. Integration of the Current Icing Product (CIP, McDonough and Bernstein 1999, Bernstein and Schneider 2004) could be one such strong addition. The CIP integrates several network data products to produce mapped estimates of icing and SLD potential on a 0.0-10 scale and icing severity on a 0-8 scale. The integrated network products include satellite and NEXRAD data, surface observations (ceiling, precipitation,, type), lightning, pilot reports of icing, RUC temperature, relative humidity, vertical motion, and SLW profiles.

Figure 3 contains a schematic of these data ingests and a flow diagram that shows how the CIP data are translated into icing potential. The analyses that are part of the GRIDS Operational Experience (Section 2.5 of this report) illustrate the potential synergy between real-time measurements with GRIDS and application of the CIP. Each is a stand-alone system, but together the power for identifying the real icing potential can be greatly enhanced. Comparison of the GRIDS and CIP estimates of icing potential would serve to substantiate and refine both systems. The GRIDS local area measurements would anchor the CIP estimates, and the CIP estimates would extrapolate the GRIDS verification to the larger area.

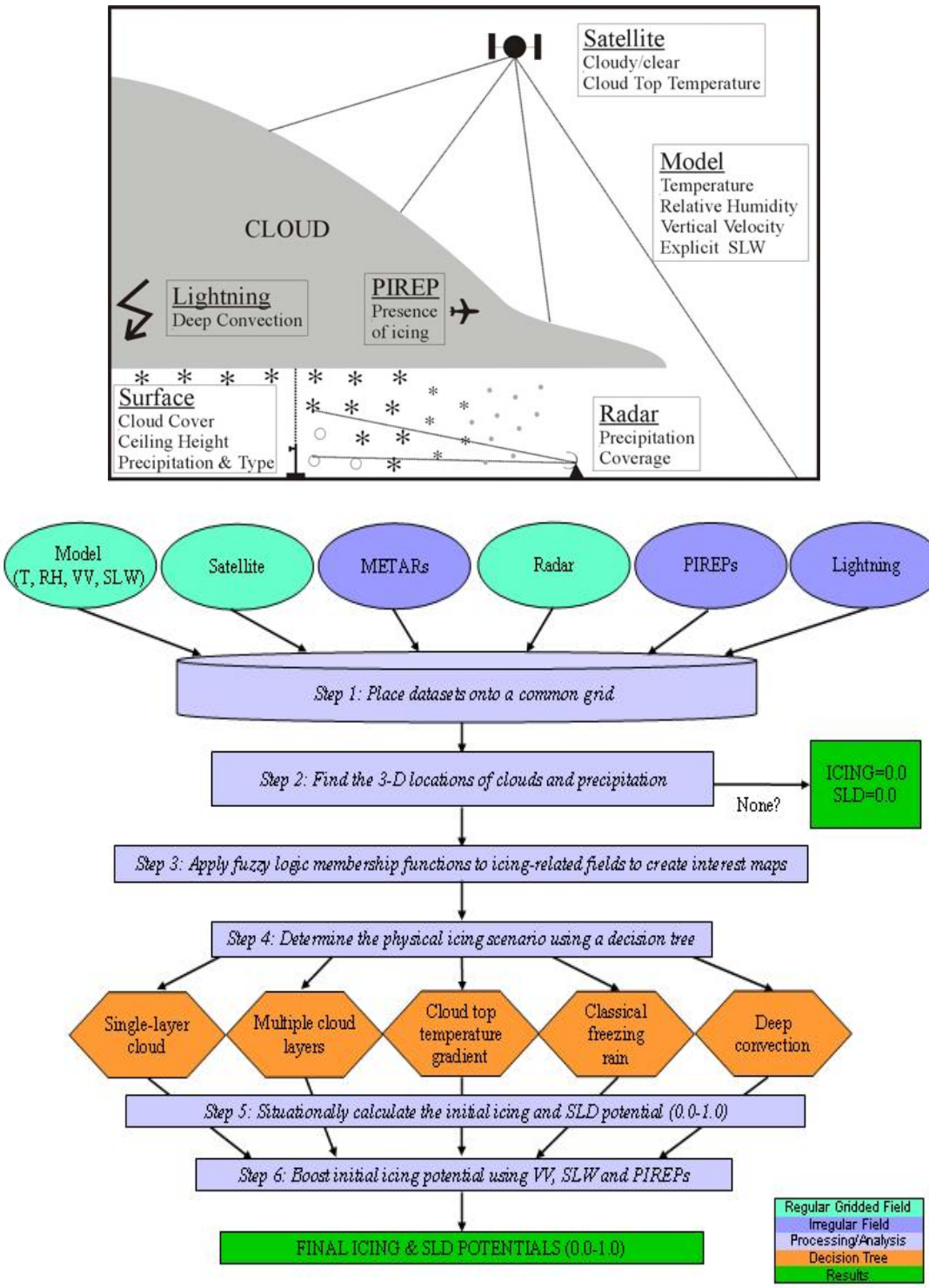

Figure 3. The Current Icing Potential Product (CIP) in its current state of development.

Appendix C

GRIDS Requirements

1. DESCRIPTION

The GRIDS (Ground-based Remote Icing Detection System) is an autonomous and reliable pilot demonstration radar/radiometer system whose purpose is to detect, from the ground, icing conditions that are hazardous to aircraft. To accomplish this, it utilizes a K_a-band radar transmitting a circularly polarized signal (the co-polarized signal) and receiving a co-polarized and cross-polarized signal simultaneously, using a fixed pointing angle of about 40 degrees. Icing conditions are detected using an algorithm that utilizes the depolarization ratio between the co-polarized and cross-polarized channels, the absolute reflectivity from the co-polarized channel, liquid water information from 23.8 GHz and 31.6 GHz radiometers, local surface temperature and humidity, and temperature profiles retrieved from a 55 GHz radiometer and from the RUC (Rapid Update Cycle) model, which is obtained via the Internet. GRIDS will run continuously while unattended and transmit data over the Internet for archival at ETL. A display indicating the possibility of aircraft icing will be served over the Internet and will be accessible with common Web browser software.

Functionally, GRIDS consists of a container system (a seatainer), a radar system, three radiometer systems, a surface meteorological system and a data processing system. An Internet link is needed to ingest model temperature data and to communicate warnings, data and system health information to the outside world. The radar system consists of the radar transmitter, radar receiver and antenna. The radiometer systems consist of a dual-channel, liquid/vapor microwave radiometer and a 55 GHz temperature-profiling radiometer. The radiometers are mounted in a PSR scanhead that retracts into the container for calibration.

2. CONTAINER AND ENVIRONMENTAL REQUIREMENTS

2.1 The GRIDS shall be housed in a seatainer of dimensions 8’6” H x 8’ W x 20’ L.
2.2 The GRIDS shall be capable of being transported by flat bed semi-trailer (min. 30 ft long, oversized load due to the antenna).
2.3 The GRIDS shall operate on single-phase, 240 VAC power, center-tapped, at 60 Hz.
2.4 The GRIDS shall operate over an ambient temperature range of -20 deg C to +40 deg C.

3. RADAR REQUIREMENTS

3.1 The radar shall operate in the Ka band at about 35 GHz.
3.2 The radar shall transmit a single circular polarization and receive simultaneously that polarization (co-polarization) and the orthogonal polarization (cross-polarization).
3.3 The radar transmitter shall use a TWTA.
3.4 The radar receiver shall receive simultaneously the co-polar and cross-polar channel, and provide these signals at a 60 MHz IF frequency for use in a digital receiver.

3.5 The radar receiver shall provide a 20 MHz reference signal synchronous with the 60 MHz IF frequency.
3.6 The radar shall meet the performance requirements indicated in Table 1.
3.7 The antenna shall be manually adjustable, in less than one day, from at least 30 to 90 degrees. The nominal pointing angle is 40.2 degrees. The design shall allow for easy upgrade to a motor drive that will slew between 40.0 degrees and 90.0 degrees in less than 1 minute.
3.8 It is a design goal that it will be easy to add system health capability as used in the MMCR.

Table 1. Radar specifications.

Parameter	**Min**	**Nominal**	**Max**	**Units**	**Comment**
Transmit frequency	34.5	34.86	35.5	GHz	
Transmit tube lifetime		20000		hours	
Pulse repetition period	50		150	μsecs	
Peak transmit power		1000		watts	
Duty cycle			15%		
Transmit pulse width	0.05	2.0	10	μsecs	
Receiver noise floor		-105	-100	dBm	
Antenna diameter		3		meters	
Antenna elevation	30	40.2	90	degrees	mechanically adjustable
Antenna elevation	30		90	degrees	scanning option
Antenna beamwidth		0.2		degrees	circular beam
Antenna cross-polar isolation	30			dB	as measured on antenna range
Antenna gain	57			dB	

4. RADIOMETER SYSTEM REQUIREMENTS

4.1 The radiometer system shall consist of a dual-channel, liquid/vapor microwave radiometer meeting the specifications shown in Table 2 and a temperature-profiling 55 GHz radiometer.
4.2 The radiometer shall be capable of being adjusted to selected fixed elevations, or scanned in elevation to match the positioning options for the radar.
4.3 The microwave radiometers shall perform auto-calibrations at regular intervals.

Table 2. Liquid/vapor radiometer specifications.

Parameter	Min	Nominal	Max	Units	Comment
Frequencies		23.8 31.6		GHz	
Bandwidth		400		MHz	
Antenna beam width		5.7		degrees	
Accuracy		0.5		degrees K	
Operating temperature	-20		+50	C	

4.4 The temperature-profiling radiometer system shall provide a profile of temperature suitable for use in the icing algorithm.
4.5 The temperature-profiling radiometer shall have several channels around 55 GHz.
4.6 The radiometer system shall process the raw radiometer data to produce brightness temperatures, integrated liquid water, integrated ice and a temperature profile.
4.7 The radiometer computer shall transmit the radiometer data to the GRADS via Ethernet.

5. GRIDS RADAR ACQUISITION AND DATA SYSTEM (RADS) REQUIREMENTS

5.1 GRADS shall support unattended operation by executing operator-defined queues of operating parameters, and by allowing remote (via Internet) monitoring of its operation.
5.2 GRADS shall process radar data in real-time in a covariance (pulse-pair) and spectral mode, and calculate, as a minimum, the fields shown in Table 3. DC correction shall be applied.
5.3 GRADS shall be capable of performing spectral processing of time series data.
5.4 GRADS shall be capable of displaying data fields from the covariance and spectral processing methods in a time-range (A-scope) format.
5.5 GRADS shall be capable of saving covariance and spectral data to disk.
5.6 GRADS shall ingest temperature profile data from external sources via the Internet for the purpose of determining the freezing level. The system will be able to obtain temperature data accurate to one degree Celsius from ground level to ten km in altitude, once per hour for a point within 40 km radius with a vertical resolution between 100 and 300 meters.

Table 3. Moment data fields.

Field	From co-polar channel	From cross-polar channel	From both channels	Units	Purpose
Velocity	Vc	Vx		m/s	research
Width	Wc	Wx		m^2/s^2	research
Correlation (covariance mode only)	Cc	Cx		None	diagnostic
Intensity (power at receiver output)	Ic	Ix		dBm	diagnostic
Power received (at antenna terminals)	Pc	Px		dBm	diagnostic
Reflectivity	Zc	Zx		dBZ	algorithm
Depolarization ratio			DR	dB	algorithm

5.7 GRADS shall ingest liquid-water and temperature-profiling radiometer data.

5.8 The data processing system shall run unattended with no local operator intervention except for maintenance.

5.9 GRADS shall integrate radar, radiometer, and temperature data and execute an icing detection algorithm in real time.

5.10 GRADS shall provide an easy-to-interpret time-height display of icing conditions within clouds, possibly based on a green-yellow-red color scheme. The current icing condition display shall be served on the Internet and be accessible to interested parties through a standard Web browser, in near real-time. Displays will be updated every 60 seconds and will have a maximum delay of no more than three minutes.

5.11 Moment data shall be sent over the Internet and archived remotely. Because of the possibility of Internet outages, data shall be buffered locally until it has been sent. Sufficient local storage shall be provided to buffer data for 48 hours without loss of data.

5.12 GRADS shall meet the requirements specified in Table 4.

Table 4. GRADS performance specifications.

Parameter	Min	Nominal	Max	Units	Comment
A/D converter, channels	2				two parallel channels at IF
A/D sampling rate		80	100	MHz	
A/D bits	14			Bits	
A/D dynamic range	71			dB	S/(N + D)
Pulse repetition period (PRP)	50		1000	μsecs	
Resolution of PRP			1	μsecs	
Number of range gates	4		72		may vary based on other parameters

6. OPTIONS

6.1 Improved cloud particle information

6.1.1 Dual angle beam positioning antenna

This option would allow the radar to alternate between a low pointing angle to a vertically pointing configuration, using limit switches, in no longer than one minute. The azimuth will be unchanged. This feature would be controlled automatically. The two limits can be mechanically changed within the range 30 and 90 degrees. The radiometer antennas would move with the radar antenna.

7. TESTING AND DEMONSTRATION

7.1 Testing

The radar shall pass the following tests before being deployed for demonstration:

7.2 Basic radar function test.

Transmit power and signal sensitivity will be tested and evaluated.

7.3 Radar calibration test.

GRIDS will be operated close to another Ka-band radar. Echo strength from atmospheric targets will be compared.

7.4 Local data archiving test. (with scheduling)

Typical operating modes will be scheduled and the data will be recorded in the radar for a period of at least one week. The data taken and the operation of the radar will be monitored

to insure that the radar has operated continuously with no manual intervention. This test may be run concurrently with 7.5.

7.5 Remote data archiving test. (with scheduling)

Typical operating modes will be scheduled and the data will be archived remotely for a period of at least two weeks. The data taken and the operation of the radar will be monitored to insure that the radar has operated continuously with no manual intervention. This test may be run concurrently with 7.4.

8. TYPICAL OPERATING MODES AND SENSITIVITY

The following table shows the independent radar parameters for typical operating modes. Parameters below the double line are independent parameters that may be altered in software. Parameters below the triple line are dependent parameters. A dual-channel receiver is assumed. Note that the dwell time and vertical range resolution are held constant in the table.

Table 5. GRIDS operating modes

mode	40 deg slant	40 deg slant	vertical	vertical
radar wavelength	8.6 mm	8.6 mm	8.6 mm	8.6 mm
antenna diameter	3.0 m	3.0 m	3.0 m	3.0 m
peak transmitter power	1000 watts	1000 watts	1000 watts	1000 watts
elevation angle	40.2 degrees	40.2 degrees	90 degrees	90 degrees
pulse repetition period	110 μsecs	110 μsecs	71 μsecs	71 μsecs
pulse width	1.55 μsecs	1.55 μsecs	1.00 μsecs	1.00 μsecs
number of time-domain averages	1	1	1	10
number of FFT points	64 points	256 points	256 points	256 points
dwell time	60 secs	60 secs	60 secs	60 secs
range gate spacing	1.55 μsecs	1.55 μsecs	1.00 μsecs	1.00 μsecs
number of range gates	69	69	67	67
receiver bandwidth	0.645 MHz	0.645 MHz	1.0 MHz	1.0 MHz
unambiguous radar range	16.49 km	16.49 km	10.64 km	10.64 km
minimum height	68 m	68 m	105 m	105 m
maximum usable height	10.2 km	10.2 km	10.0 km	10.0 km
maximum unambiguous radial velocity	±19.55 m/s	±19.55 m/s	±30.28 m/s	±3.03 m/s
maximum unambiguous horizontal velocity	±25.60 m/s	±25.60 m/s	NA	NA
time available for one spectrum computation	51 μsecs	204 μsecs	135.6 μsecs	1356 μsecs
number of spectrum averaged per gate per dwell time	8523	2131	3301	330
duty cycle	1.41%	1.41%	1.41%	1.41%
average power	14.1 watts	14.1 watts	14.1 watts	14.1 watts
range resolution	232.3 meters	232.3 meters	150 meters	150 meters
height resolution	150.0 meters	150.0 meters	150 meters	150 meters
radial velocity resolution	0.611 m/s	0.153 m/s	0.237 m/s	2.366 m/s
Estimated sensitivity at 5 km AGL using spectral processing	-69.4 dBZe	-66.4 dBZe	-73.1 dBZe	-78.1 dBZe
Estimated sensitivity at 6 km AGL using spectral processing	-67.8 dBZe	-64.8 dBZe	-71.5 dBZe	-76.5 dBZe
Estimated sensitivity at 10 km AGL using spectral processing	-63.4 dBZe	-60.4 dBZe	-67.0 dBZe	-72.0 dBZe

Appendix D

GRIDS Block Diagram and Parts List

Table 1 shows the parts referenced in the block diagram and gives details on parts that have been specified. COTS refers to commercial-off-the-shelf components.

Description	Manufacturer	Model	Comment
Traveling wave tube amplifier			Specifications req'd
IF Modulator/Receiver			Build in-house
Coherent Up/Down Converter (CUDC)			Specifications req'd
Low-noise amplifiers			May be incorporated in CUDC
Circulator assembly			
Orthomode transducer			COTS
Polarizer			COTS
Antenna			Specifications req'd
Oscilloscope			Used as "A-scope"
Linux rack-mountable PC	Technoland		DIFRS computer
Frequency synthesizer card	Echotek	ECSG-1R3ADC-PMC	Part of DIFRS
Digital receiver card	Interactive Circuits & Systems	ICS-554B-2-MN	Part of DIFRS
Radar Timing Generator card	Acromag	IP1K110-2412	Part of DIFRS
Noise diodes			
Circulator drivers			
Pulse controller	Vaisala		
Linux rack-mountable PC	Technoland		RC+ computer
GPS card	Symmetricom	BC6371PCI	Part of RC+
Surface meteorological instruments			
Windows PC			GRIDS-AUX computer
A/D card			Part of GRIDS-AUX
Digital I/O card			Part of GRIDS-AUX
IEEE-488 card			Part of GRIDS-AUX
Three-channel radiometer	ETL GSR or Radiometrics TP/WVP-3000		
Radiometer computer			
Linux rack-mountable PC	Technoland		RIPS computer
Ethernet switch	generic		
Linux rack-mountable PC	Technoland		Firewall computer
Uninterruptible power supply			

Table 1. Partial parts list.

GRIDS Block Diagram

Notes:
1)RF frequency is 34.86 GHz.
1) IF frequency is 60 MHz.
2) Displays & keyboards for computers are not shown.
3) LNAs may be incorporated in CUD.

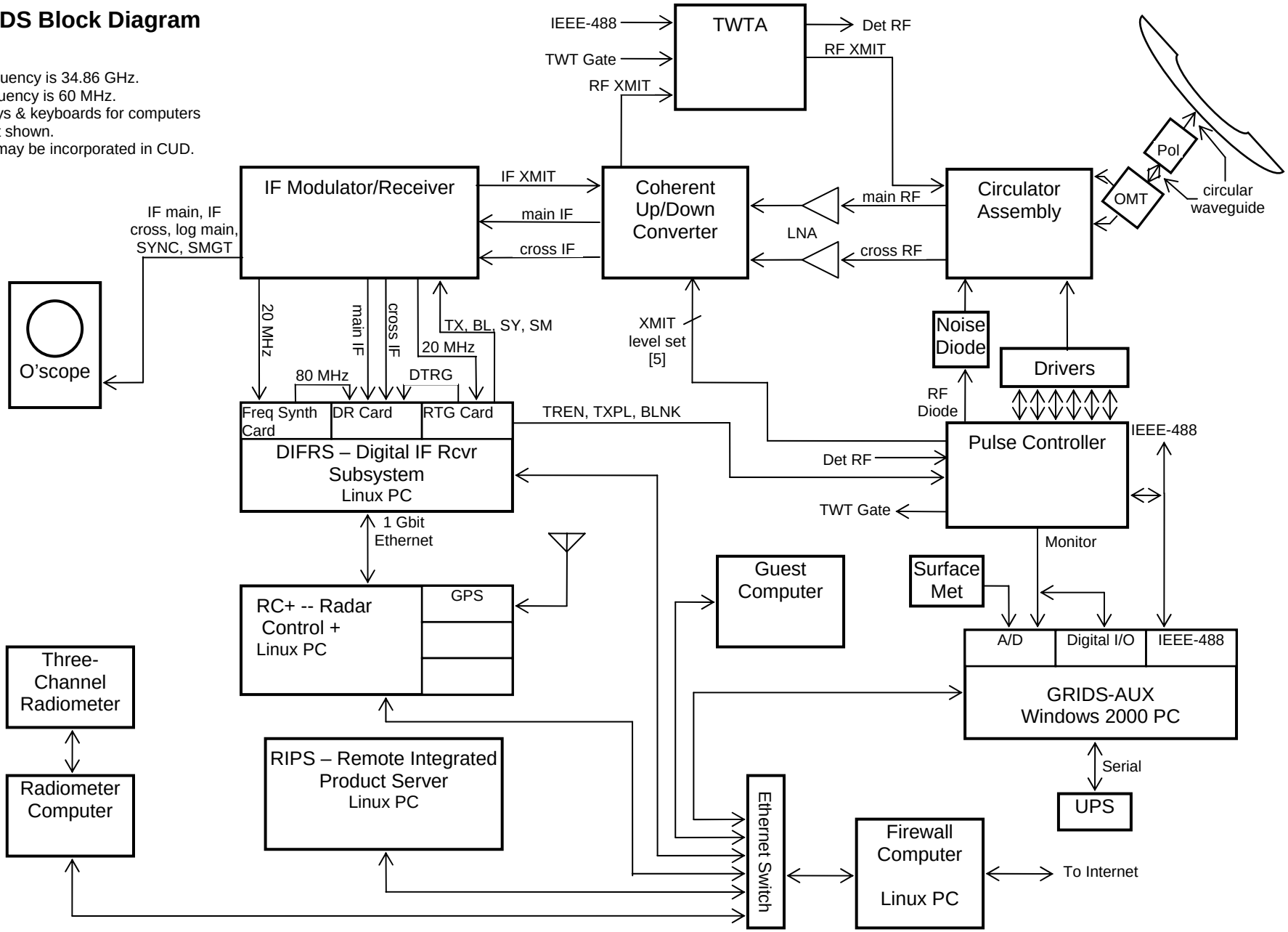

Appendix E

GRIDS Features and Benefits

Feature	Benefit	Comment
TWTA (traveling wave tube amplifier) transmitter	Longer lifetime than magnetron tube. Allows for higher transmit power, if necessary.	Higher power would require a longer pulse, which means pulse coding would have to be implemented.
MMCR-based radar design	Mature design that has performed well in the several deployed MMCRs.	
RADS-based computer design	RADS was developed by current staff and has performed well in ETL's research radars. Allows for complete visibility of all data in real time.	
Housed in seatainer	Allows for easy, inexpensive shipping. Inexpensive, rugged container. Strong enough to serve as a mounting point for the antenna.	Works especially well for transport by ship or barge.
Icing data served by remote server	Allows for many simultaneous accesses to icing data without compromising the performance of GRIDS.	
Data archived remotely	Eliminates the need for local operators.	
System UPS	Protects system from intermittent power outages. Allows for complete unattended recovery from a power outage.	

Monitoring and notification of system health	Allows the system to work without constant attention of a technician.	
Firewall computer	Protects other computers from computer vandals. Simplifies computer security.	Most security updates need only be implemented on the firewall computer. This enhances the stability of the other computer systems.
Spectral processing	Improves performance in conditions of low signal.	
Moveable antenna (slant and vertical operation)	In conjunction with spectral processing, differentiates ice vs. droplet fall velocities to enhance icing algorithm in mixed phase clouds.	
Dual receiver	Improves performance in conditions of low signal by 3 dB.	
Spares	Improves mean time to repair, dramatically so in the case of a failure of a radar component	Some radar components have delivery times of many months.
Complete system	Designed to be close to an operational prototype. Would allow systems to be put into production quickly.	

Appendix F

Software Catalog

1. INTRODUCTION

This Appendix is intended to provide a brief overview of the software that was developed for GRIDS. Because the project was terminated before completion, some of the software is incomplete. The software is divided into two categories: utility programs and programs that run on the Digital IF Receiver Subsystem (DIFRS) computer; and programs that run on the Radar Control Plus (RC+) and Remote Integrated Product Server (RIPS) computers. This software was written by two different people, and is largely uncoupled, so it is convenient to divide it in this way.

Many of the data structures used in the software are based on legacy formats, and so a brief review of these structures is given here.

1.1 Universal Format

Universal Format (UF) was developed at a meeting of meteorological radar researchers (Barnes 1980) to serve as a common format for recording data from Doppler radars. It was based on the current technology at the time, namely 16-bit minicomputers and 9-track magnetic tape. This was later extended to recording data on disk through the use of the "4-record-4" format.

1.2 4-Record-4 format

4-record-4 format was developed to create a virtual magnetic tape on a single disk file. Magnetic tapes have records, end-of-file (EOF) marks, and an end-of-tape (EOT) mark, and this needed to be simulated within a disk file. The encoding to do this is called 4-record-4 format, because four bytes containing the record length in bytes are written before the record; then the record itself is written; and then four bytes containing that same record length are written following the record. The record length written does not include the "4" information, and is always written in big-endian format. EOF marks are simulated by writing a zero-length record, which is eight bytes of zeroes. The EOT mark is represented by two EOF marks in a row, or 16 bytes of zeroes.

1.3 Extended Format

UF uses 16-bit integer data, and so must be extended for floating-point data. In the Extended Format (EF), the first two bytes contain ASCII 'EF' instead of 'UF.' And the data (non-header) fields contain 32-bit IEEE floating-point data.

1.4 Radar Parameters

The Radar Parameters, which contains all the parameters necessary to specify the operation of the radar, are represented in a Radar_Params structure consisting of several data types. This is defined in Gibson et al 2004.

2. DIFRS AND UTILITY SOFTWARE

2.1 Introduction

Except for drex.cpp, all these programs are utility programs that may be run on any machine. drex.cpp, however, is designed to work with the Digital Receiver card to ingest data, and so will only run on the DIFRS computer. At project termination, all of these programs were functional, but drex.cpp had some limitations as discussed below. What is missing from this set of programs is one that runs both the Digital Receiver and the Radar Timing Generator, and sends the data via Ethernet to the RC+ computer. To complete the functionality of DIFRS, drex.cpp can be used as a basis for creating this program.

All the programs, libraries and classes in this section are written in C or C++, and run with the Linux operating system.

2.2 Standalone Programs

2.2.1 diff_hdr_dump.cpp

diff_hdr_dump is a program that reads radar data records recorded with “extended format” UF headers, and dumps header information to the screen. Only parameters whose value has changed from the previous header are dumped, making it easy to trace parameter changes through the data set.

2.2.2 drex.cpp

drex is the Digital Receiver EXerciser program. It allows an operator to input commands and parameters from the console and record data from the ICS-554 Digital Receiver. Data from the Digital Receiver may also be dumped to the screen. This program needs to be extended to deal with amplitude scaling of the incoming data.

2.2.3 raw2rawNC.cpp

raw2rawNC reads raw radar files from RADS and produces a netCDF file with the same data content. No changes are made to the data at all, but some of the header information is dropped as being not relevant.

2.2.4 rpInit.cpp

rpInit is used to maintain Radar Parameter sets. It is typically used before experiments to create the parameters that will be used during the experiment.

2.3 Libraries

2.3.1 complex.c

complex is a library program that contains various functions for processing complex numbers.

2.3.2 sio_.c

sio_ is the Sequential I/O package for tape and disk and is a library program that supports 4-record-4 format. Its purpose is to create an I/O abstraction layer whereby calling routines utilize the same functions calls independently of whether the I/O is to tape or to disk. To accomplish this, data within disk files is encoded to simulate tape records in the 4-record-4 format.

2.4 Classes

2.4.1 Sockets

Class Sockets is used to implement Berkeley socket connections between processes on the same or different computers using Internet Protocol. A socket connection enables the two processes to exchange information. Sockets consists of three classes and an abstract base class, Socket, which provides basic services to the other classes. ServerSocket is used on the server side to listen for clients trying to connect. When one tries to connect, Connection is used to accept the connection. On the client side, ClientSocket is used to connect to a server.

The classes communicate by sending packets of data. An 8-byte header is added during a write, and stripped off on read. The header has two words: the first is a "magic" number flagging the beginning of a packet, and the second is the length of the packet, including the header. Thus a null packet has a length of eight.

2.4.2 RadConfig

RadConfig is used to configure radar programs (or any program) at runtime by extracting parameter values from a text file. The text file has entries such as

NTRG = 256 # parameter NTRG is the number of triggers

MNEL = 1.5 # parameter MNEL is the minimum elevation angle

and is created with a text editor. Methods in RadConfig allow you to extract a parameter's value by name. The parameter value may be a float, int or char variable.

2.4.3 PrmtrList

PrmtrList is useful for maintaining parameter lists that contain different types of parameters. Information about the parameter, such as name and type (float, int, etc.), is stored along with the actual value of the parameter. This makes it possible to process parameters as a group, with methods being provided to list all parameters to the terminal, and update the parameter value from the keyboard by entering its name and value.

2.4.4 Rp2ef

Rp2ef reads a Radar_Params block, and creates an EF (Extended Format) header from it. Only one field is created, the "RD" or "raw data" field. This implementation will put padding between the different sub-headers in the UF specification, which could possibly cause a problem with some programs that do not (correctly) read the pointers in the sub-headers, and follow them to find other sub-headers, or the actual data.

2.4.5 RadParms

The purpose of RadParms is to provide a means for client programs to access the Radar_Params structure without having to know which version of Radar_Params they are accessing (by using polymorphism). Currently the Radar_Params exist in versions 0 and 1, and so are represented by derived classes RadParms0 and RadParms1 which are not seen by the client program. Methods exist for all the common operations one would do on a parameter list, such as getting and setting parameters, verifying the validity of a parameter block, checking all the parameters, reading a parameter value from the keyboard, printing, etc. Minor revisions (which do not change parameter displacements) are handled by incorporating them into the latest version. A major revision would necessitate the creation of a new derived class: RadParms2.

2.4.6 RpBeam

RpBeam is used to read and manipulate data in RP format, which is the Radar_Params structure concatenated with the raw data received from the Digital Receiver. RpBeam uses the RadParms class, and so makes available all the parameter manipulation that RadParms provides.

2.4.7 Thread, Mutex and ConditionVariable

These three classes are used to make working with pthreads easier and to provide some additional error checking.

3. RC+ AND RIPS SOFTWARE

3.1 Introduction

The RC+ code consists of five separate C++ processes; radarReformatter, radarRelay, reformatter, writeDisk and xDisplay. DIFS sends the RC+ unit radar data. That data is then reformatted, distributed, written to disk, displayed and sent to the RIPS. The RIPS consists of 20 separate processes that ingest four data streams, calculate the icing product, provide viewers to allow display of the products locally and remotely. It also includes a web server that allows viewing of data remotely via internet browsers. Throughout both systems, reformatters extract or reformat the data and relays act as software fan-out boxes distributing data streams to multiple consumers simultaneously. All of the code is C++ or Java. The C++ code runs on either Solaris or Linux and the Java code runs under Windows.

3.2 RC+

3.2.1 Programs

The RC+ subsystem consists of the following processes: radarReformatter, radarRelay, reformatter, writeDisk and xDisplay.

3.2.1.1 radarReformatter

radarReformatter ingests two radar data streams from the DIFRS; raw data and calculated field data for display. This process adds the EF header information and then sends the data to radarRelay for distribution. It also includes a control window graphical user interface for

debugging and testing purposes. It interfaces with Motif libraries and allows the user to control the data ingest from the four data sources and to set various parameters.

3.2.1.2 radarRelay

radarRelay is analogous to a software fan-out box that allows the data to be sent to multiple processes simultaneously in pseudo-real-time using shared memory technology. It ingests the display data from the radarReformatter process and sends it to the viewer process, xDisplay and the reformatter process. radarRelay also sends the raw data to the writeDisk process.

3.2.1.3 xDisplay

The xDisplay process displays the field data in close to real-time as either marching time-range displays, ppi displays or rhi images. It offers the user an interface for changing color scales, fields, thresholding and zooming. It uses Xlib and Xview libraries.

3.2.1.4 Reformatter

The reformatter program receives display data from the radarRelay process and extracts the reflectivity and depolarization data and sends them to the RIPS. These quantities are needed for calculating the icing product and for viewing on the RIPS. It also writes the reformatted data to disk.

3.2.1.5 writeDisk

writeDisk writes raw EF files, field EF files and/or netcdf files to disk.

3.2.2 Classes

Although there are numerous classes used in these programs, the following are shared among the programs.

3.2.2.1 Config

Config calls RadConfig and specifies the variables needed for the particular configuration file being read, depending upon the program.

3.2.2.2 RadConfig

Same as above.

3.2.2.3 RadParms

Same as above

3.2.3 Libraries

3.2.3.1 Gdb

Gdb is a global data base that allows the multiple processes to share information through shared memory.

3.2.3.2 Xpm

Xpm is a library that stores and retrieves images to and from XPM format and is available on the Web.

3.2.3.3 Xlib
Xlib is the X11R6 library for graphical display calls and is available on the Web.

3.2.3.4 Xview
Xview is a wrapper for Xlib calls and is available on the Web.

3.2.3.5 Gd1_2
Gd1_2 is a gd library that creates GIF images and is available on the Web.

3.3 RIPS

3.3.1 Programs
RIPS is composed of five relay processes, four RMI servers, an icing algorithm process, two viewer processes and four writer processes. Relay processes always relay data from one source to one or multiple destinations. RIPS uses three different protocols to relay data: RMI, HTTP and TCP/IP socketing. There are two versions of the viewers; one which receives RMI objects and one that "gets" HTTP objects.

3.3.1.1 radarRelay
Although radarRelay is capable of serving data to multiple clients, it currently only sends radar data to the radarRMIServer.

3.3.1.2 radarRMIServer
radarRMIServer is an RMI server that serves radar RMI objects to the writeRadar, icingViewer, and icingAlg processes.

3.3.1.3 icingAlg
icingAlg ingests the data streams from the four instruments and calculates the icing product. The icing algorithm is performed on every beam of radar data at every range gate. It uses reflectivity and depolarization data from the radar, liquid water from the radiometer and temperature from the RUC to calculate an icing product. It sends icing RMI objects to the icingViewer, writeIce and to iceRelay.

3.3.1.4 iceRelay
iceRelay distributes the icing product from the icingAlg to DataRexx for Web service.

3.3.1.5 writeRadar
writeRadar receives RMI radar objects from radarRMIServer and writes raw data files to disk for archival.

3.3.1.6 icingViewer
There are actually two versions of the icingViewer. One is used on-site and the other off-site. The on-site icingViewer process ingests the icing products that are served via RMI by the icingAlg. The off-site version of the icingViewer ingests icing products via DataRexx using HTTP. Each version consist of three tabbed panes; one for the icing hazard product, one for reflectivity and one for depolarization. The process allows the user to select how often the

automatic snapshots should be captured, where they should be written, when to perform a special snapshot, which fields to view and what values to use for scaling the fields.

3.3.1.7 writeIce

writeIce receives the icing product from the icingAlg process and writes the icing product, reflectivity and polarization data to disk for archival

3.3.1.8 radiomRelay

radiomRelay is the fan-out box for the radiometer data; it ingests the radiometer data stream and serves it to both the radiometerRMIServer and DataRexx.

3.3.1.9 radiomRMIServer

radiomRMIServer serves radiometer RMI objects to the writeRadiom, radSurfViewer and icingAlg processes.

3.3.1.10 writeRadiom

writeRadiom writes the radiometer RMI objects to disk for archival.

3.3.1.11 radSurfViewer

There are two versions of the radSurfViewer processe. One is used for on-site and one is used for off-site. The on-site version receives and displays the radiometer data and the surface meteorological data as RMI objects. The off-site version receives radiometer data and surface meteorological data using HTTP from DataRexx. Both versions consist of three separate windows. Two display radiometer data as Marching Time Displays, and one displays surface meteorological data as a Marching Time Display. The newest data comes in on the left side of the screen and the older data moves off to the right. Six radiometer variables are available and are plotted against time. These are: liquid water, vapor, temperature, and brightness temperature from each of the three channels. The surface meteorological variables available are: humidity, pressure, and temperature. The user can select from the available variables and change scale values for each variable. GIF or JPEG images can be captured automatically or through operator initiation.

3.3.1.12 RUCRelay

RUCRelay ingests RUC data and serves it to the RUCRMIServer and DataRexx. This part of the system has not been implemented.

3.3.1.13 RUCRMIServer

RUCRMIServer receives RUC data from RUCRelay and serves RUC RMI objects to the radSurfViewer, writeRUC, and icingAlg processes. This has not been completed.

3.3.1.14 writeRUC

writeRUC receives RUC RMI objects from RUCRMIServer and writes RUC data to disk for archival. This has not been implemented.

3.3.1.15 surfaceMetRelay

surfaceMetRelay sends surface meteorological data to the surfaceMetRMIServer and to DataRexx.

3.3.1.16 surfaceMetRMIServer

surfaceMetRMIServer ingests surface data from surfaceMetRelay and sends surface meteorological RMI objects to the writeSurf, icingAlg and radSurfViewer processes.

3.3.1.17 writeSurf

writeSurf ingests surface meteorological RMI objects from the surfaceMetRMIServer and writes the surface meteorological data to disk for archival.

3.3.1.18 DataRexx

DataRexx is a third party product which acts as a real-time data hub. It collects, serves and archives data using HTTP. Since DataRexx works across the internet and through firewalls, multiple remote clients are able to access the data in near real-time. DataRexx allows multiple remote data producer clients to post data to it via HTTP. Currently iceRelay, radiomRelay, and surfaceMetRelay post data to DataRexx. RUCRelay will do the same. Data consumer clients such as radSurfViewer and icingViewer can then get data from DataRexx via HTTP.

Appendix G

GRADS Software Capabilities

1. INTRODUCTION

This document outlines and specifies the essential software components required for the GRIDS RADS, or GRADS. The GRADS is a multi-level distributed software architecture that has been designed for the GRIDS. Its design allows for significant changes in hardware and operating systems and its modularity lends itself to functional software changes as needed. Several distributed processes comprise the GRADS. They not only acquire four separate data streams, but also perform integration, archival and display of the data in real-time. The structure easily lends itself to additional data streams as required. The system produces data files as well as graphical products in real-time. The four data streams in this application are Ka-band radar, radiometer, surface meteorological (surface met), and RUC files.

Included are descriptions of the four major software subsystems that complete the GRADS: the Digital IF Receiver Subsystem (DIFRS), the Radar Control Plus (RC+) subsystem, the Remote Integrated Product Server (RIPS) and the Radar Monitor. These modules constitute the "on-site" (at-the-radar) system. The DIFRS and Radar Monitor software are discussed only as they relate to the RC+ and RIPS software. The DIFRS software is discussed in a separate document (Appendix H). The majority of this document is devoted to describing the RC+ and the RIPS. The long proven RADS (Radar Acquisition and Display System) and POP (Profiler On-line Program) software systems were studied, and their desired features have been included in the GRADS software design. A description of the "off-site" Web server system and viewers is also included.

2. GRADS

2.1 Data Flow

Figure 1 is a graphical overview of the GRADS data flow for the four instruments needed to calculate the icing hazard product for the GRIDS and the processes associated with each data stream. The radiometer, RUC and surface meteorological data streams utilize TCP/IP socket architecture to transmit their data records to the RIPS for Web service and viewing. RIPS uses remote method invocation or RMI to share objects among its multiple processes. RMI is a means of distributing objects across machines and between processes, and works well as long as it does not have to scale firewalls. The radar data stream also uses TCP/IP to transmit data to the RC+ processes. The RC+ processes employ RMI architecture and shared memory technology to share objects between multiple processes and the RIPS. Relay processes, which are found throughout the system, are software fan-out boxes and serve the data to one or multiple client processes simultaneously. RMI server processes also act as fan-out boxes as they serve RMI objects simultaneously to various other RMI processes.

In order to share objects beyond the firewalls, hypertext transfer protocol or HTTP has been shown to work well. In order to accommodate both HTTP and RMI protocols,

two versions of the RIPS capitalize on the modular design. Each has a different front-end and protocol scheme, yet share multiple classes. The on-site version of the code uses RMI communication and the off-site version uses HTTP. (See Section 2.3.)

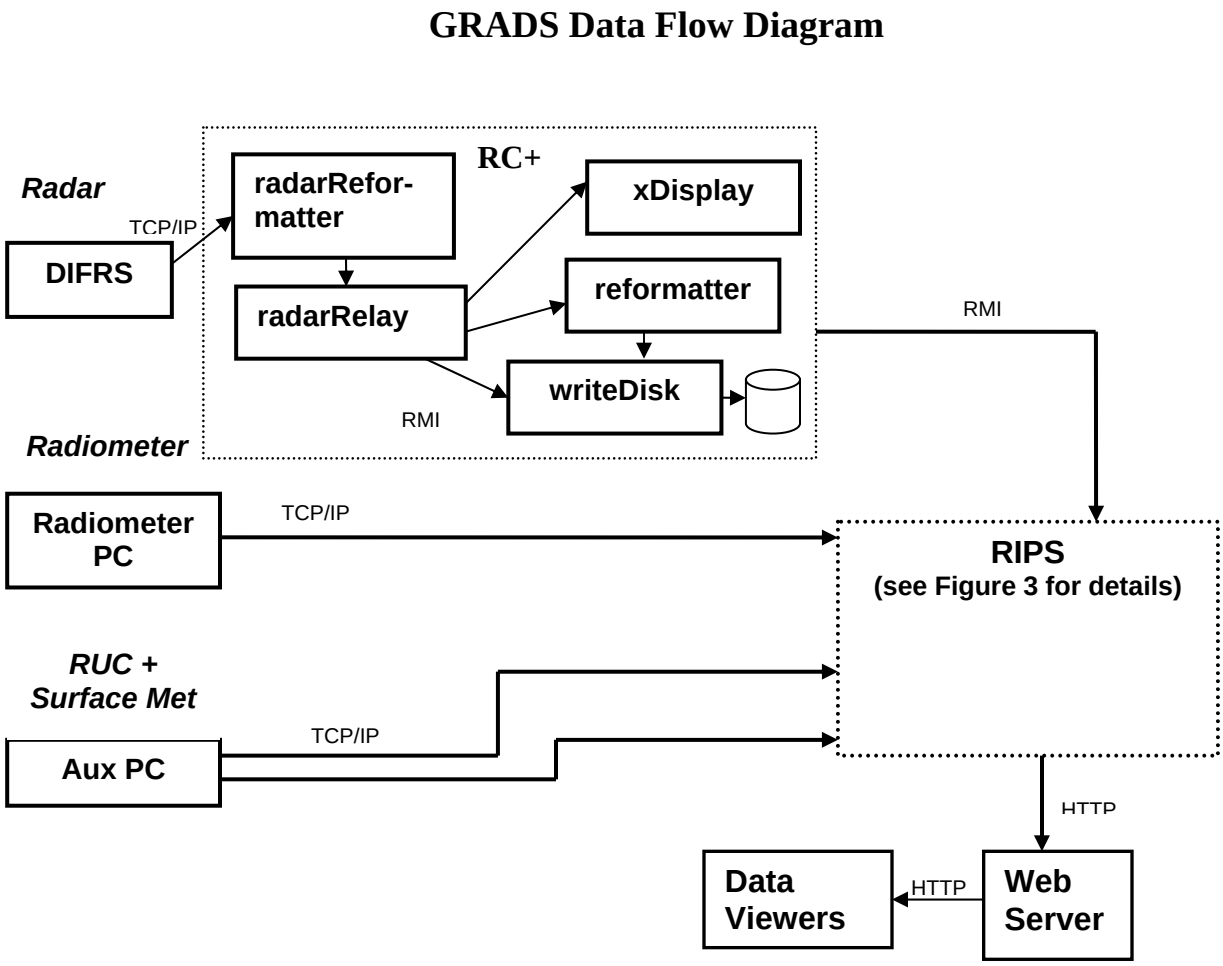

Figure 1. Software architecture diagram of GRADS data flow. The architecture implements TCP/IP, RMI, and HTTP.

2.2 On-Site Computers

The on-site computers, which are physically connected with a Local Area Network (LAN), are the DIFRS PC, the Radar Monitor Aux PC, the RC+ PC, the RIPS PC and the Firewall PC. Figure 2 shows the data and control flow between these five machines, as well as the high level software architecture design. This document will not discuss the Firewall PC, as it serves as a gateway to the Internet for the LAN and provides standard system security for the LAN.

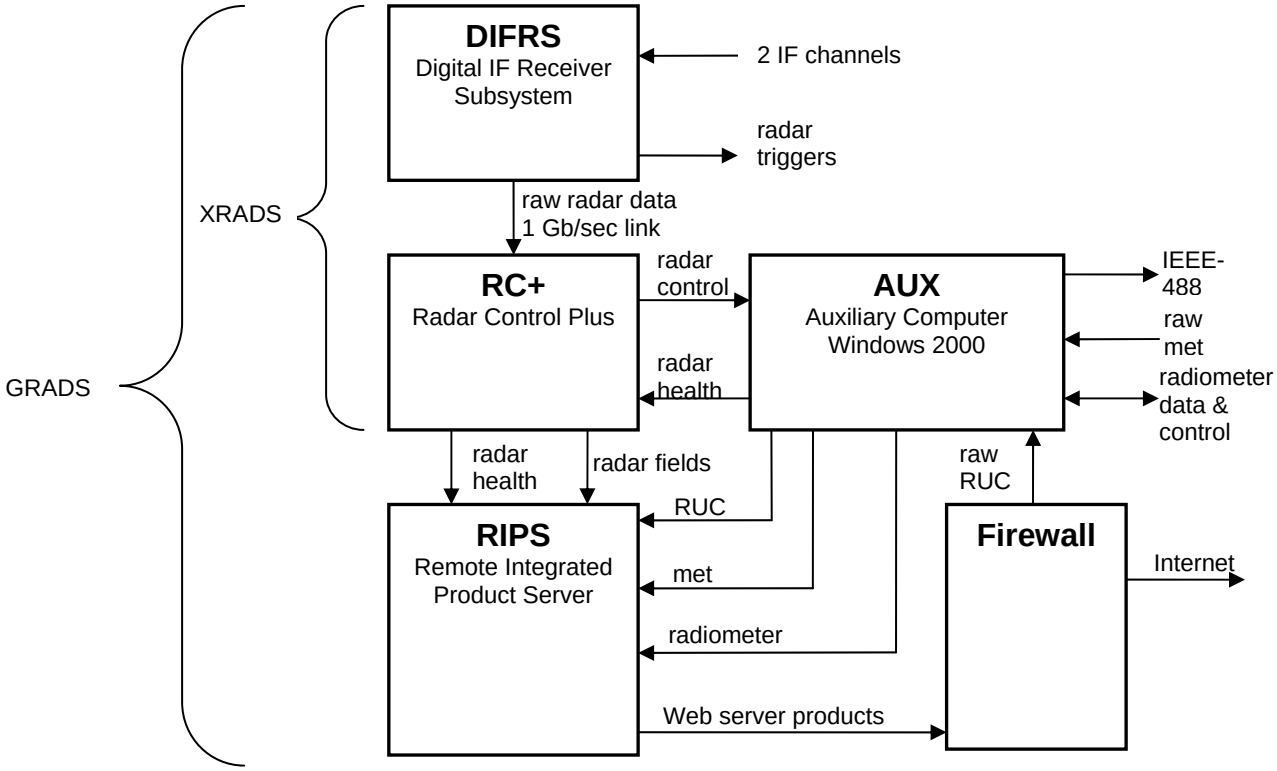

Figure 2. System architecture diagram showing control and data flow. Each block represents a different computer.

2.2.1 Data ingest

In order to calculate the icing hazard product, the four data sources must be ingested. The design calls for four separate but simultaneous processes to each ingest one data stream and communicate with the icing algorithm. The data are available asynchronously and in various formats. They all ultimately flow into the RIPS which calculates the icing hazard product and displays the icing product and the raw data products in close to real-time. The four data streams are described in detail below.

As mentioned earlier, the GRADS ingests these data streams via TCP/IP sockets, RMI or HTTP. The communication protocol depends upon the remote sensor's hardware configuration, where it is located, how it communicates and where the RIPS is executing. The RIPS allows for the input protocols to be configured and thus can dynamically interface with changing input streams. The RIPS executes on-site in the radar, ingesting remote sensor data streams via TCP/IP. In the radar, RIPS uses RMI to share objects among its internal processes. RC+ uses RMI and shared memory to share its objects among its internal processes.

Since RIPS also runs off-site as a Web application (and thus needs to be able to penetrate firewalls), in that configuration it not only ingests remote data via HTTP, but the internal processes communicate via HTTP as well. See Section 2.3.

Figure 3 details the data flow of the RIPS and the processes which compose the RIPS subsystem. It not only illustrates the data flow within RIPS, but the software architecture employed as well. The data flow and several of the associated processes are discussed below. Further details regarding the RIPS and its processes are found in Section 2.2.3.2.

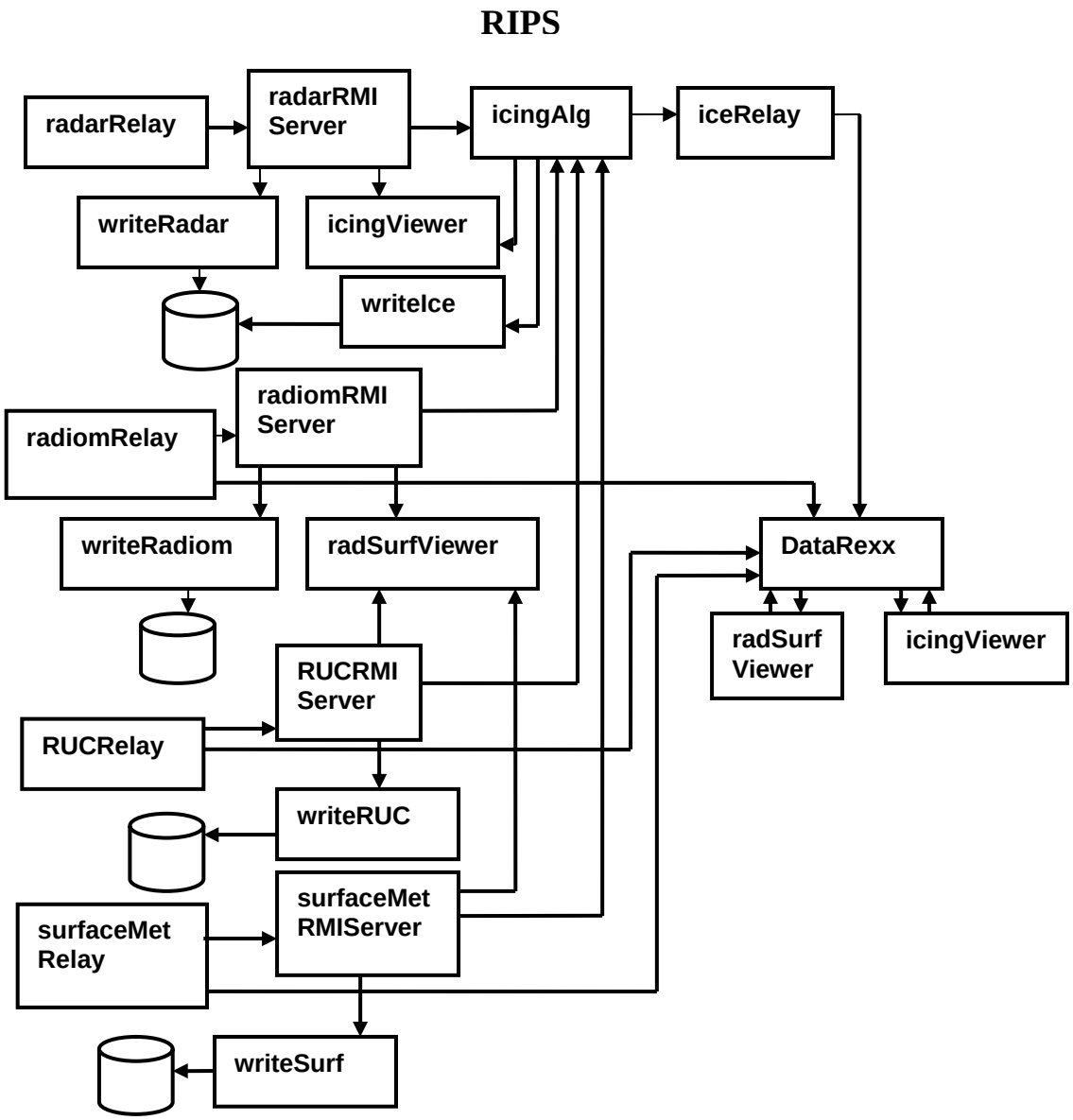

Figure 3. RIPS data flow and software architecture. Every arrow going into or out of DataRexx is an HTTP connection. All connections out of the RMIServers are RMI and all other connections are TCP/IP sockets.

2.2.1.1 Radar data

The DIFRS sends covariance data to the RC+ subsystem via TCP/IP sockets. Covariance data is defined in the *GRIDS Covariance Algorithms* (Appendix I) document. The modular software design easily allows for future additional modes such as spectra.

These modes are selectable by the user. GRADS reads and writes Radar Parameters version 1.2, as outlined in Gibson et al (2004).

Range gate limits are operator enabled. Four to 100 range gates are available in the covariance mode. The number of range gates in the usual operating mode is 69. The maximum number of triggers is 1,000,000, with a standard operating number of 545,454 triggers for a 60-second dwell. Typically the data rate will be one beam every 60 to 62.5 seconds. If time series data is sent from DIFRS for recording and viewing, the data rate is approximately 10 Mbytes/sec.

As in the RADS design, the radarReformatter process (see Figure 1) in RC+ ingests two different kinds of data: raw data and display data. Raw data is archived; display data is calculated from raw data and is displayed in the radar for the operator. radarReformatter sends the display data to the process radarRelay which acts like a software fan-out box, which in turn sends the display data simultaneously to both the viewer process, called xDisplay, and the reformatter process which extracts and forwards reflectivity and depolarization data. At the same time, radarRelay also sends raw data to the writeDisk process for archival on disk. The reformatter then sends the reformatted data to the RIPS where it is input to the icing algorithm process, icingAlg, and displayed. The reformatter also sends the reformatted data to writeDisk for archival, if required. File naming conventions include the year, month, day, hour and minute in the file name.

2.2.1.2 Radiometer data

Time stamped radiometer data is sent to RIPS from the Radiometer PC every minute via a TCP/IP socket. Since the radiometer generates a point every 15-17 seconds, the software on the Radiometer PC averages the last four data samples before sending them to the RIPS' process radiometerRelay every minute. The variables sent include integrated liquid (which is needed for the icing algorithm), integrated vapor, and brightness temperature from each channel. The process writeRadiom in RIPS appends radiometer data into hourly files. The size of these files is typically between 30-50 Kbytes per hour. File naming conventions include the year, month, day, hour and minute. The RIPS' process radiometerRelay also sends the data to the radSurfViewer process for display, and the icingAlg process via TCP/IP sockets, RMI and/or HTTP, as explained earlier. The radiometer displays are updated as soon as the radSurfViewer process receives the data.

2.2.1.3 RUC data

RUC model output is served to RIPS from the Radar Monitor process on the AUX computer approximately every hour, or as the data becomes available. The timing is driven by the update of RUC data on the Web site. Data becomes available on the RIPS machine as a file via a TCP/IP socket. Format and filenames of these files must include the time and date. A RIPS' process, RUCRelay, reads RUC data as it becomes available and will interpolate the data in space. It then sends the height and temperature data to icingAlg via RMI, if on-site, or HTTP if off-site. RUCRelay simultaneously sends the RUC data to the radSurfViewer process for viewing and to the writeRUC process which archives the data into hourly disk files.

2.2.1.4 Surface meteorological data

Every minute a surface meteorological data record is served to RIPS from the Radar Monitor process on the AUX computer via a TCP/IP socket. This data includes temperature, humidity and pressure. A process called surfaceMetRelay listens for these packets, does some reformatting and sends the packets to multiple processes. SurfaceMetRelay can send the minute radiometer data to the icingAlg process via a TCP/IP socket or RMI. surfaceMetRelay also sends the surface meteorological data to the radSurfViewer for display via RMI, TCP/IP sockets and/or HTTP depending upon the implementation writeSurf also receives the data via RMI and archives the data to disk. It creates a time stamped file every hour and appends the minute surface meteorological data record as it receives it. The format and filenames include the time and date.

2.2.2 Control Window Graphical user interface

Although the GRIDS was designed to be run primarily without an operator through pre-configured files that are read at startup, the RC+ system process radarReformatter includes a graphical user interface (GUI) for debugging and testing purposes. This GUI, as shown in Figure 4, is written in C++ with calls to Motif and allows an operator to control the data ingest from all four data sources and to set various parameters. Some of the functions of the RC+ include turning on and off the various data streams, turning on and off the instruments, and positioning the instruments.

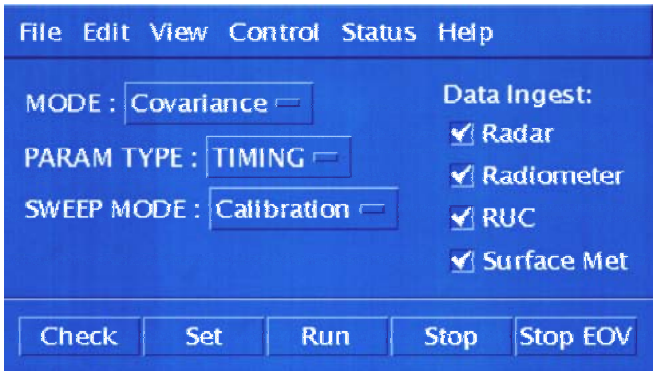

Figure 4 RC+ GUI user interface

2.2.2.1 Data Ingest control

As described previously, there are four data streams that need to be ingested by RIPS in order to calculate the icing algorithm. The user is able to turn these data streams on and off individually by selecting the check boxes on the right hand side of the above menu. The icing algorithm is only calculated when all four of the data streams are turned on, which is the default.

2.2.2.2 Data Archival

A separate archival function has been made available to the user. This switch allows the user to turn on and off the archival capabilities. When the archival switch has been turned on (which is the default) the four ingested data streams will be archived along with

the generated icing, radar and radiometer GIF files and the results of the icing algorithm. If the switch is turned off, no files will be written.

2.2.2.3 Instrument Control

The user is able to run the radar in continuous scan mode or in a queuing mode. The queuing mode allows the user to run various scan control tables consecutively while continuous mode runs the same scan control table repeatedly. The user can also pause the system. Extensive instrument control, including positioning, and starting and stopping the radar and the radiometer, is available. The user can exit RC+ from the "File Exit" menu bar option in the RC+GUI.

2.2.2.4 Radar Parameters

The user can edit, store, load, list, view and check different individual scan control tables, through drop-down menus from the "Edit" and "View" menu bar options. The user is able to list the names of the existing scan control tables. These tables allow users to indicate which mode they wish to run and to select which parameters to change (e.g., housekeeping) and view. The user can select between covariance and spectral modes. The user is able to create, edit, store, load, list and run individual queues (lists of scan control tables), as well.

2.2.3 Viewers

There are three data viewers available in the GRIDS: xDisplay, icingViewer and radSurfViewer. They allow users to manipulate and view the data. This section describes the numerous options available to the user for creating a custom look at the data. The data displays themselves are described in Section 2.2.4. The xDisplay process is part of RC+ and allows the user to view radar data in real-time. The icingViewer and radSurfViewer are part of the RIPS, and display the icing product, some radar products, radiometer products and surface meteorological products in close to real-time.

2.2.3.1 RC+ Data Viewer

There is a separate RC+ process called xDisplay that ingests data for graphical display and updates in real-time. The xDisplay process is a C++ process which calls XLib library functions to display the radar data in real-time on-site. It has its own GUI to allow the user to control the viewing of radar data.

The xDisplay GUI includes options for selecting display type (i.e., Marching Time-Range or A-scope) and field to be viewed. Any field or variable can be displayed on either the A-scope or Marching Range-Time display simultaneously. It also allows the user to change the minimum and maximum scale for each field, and the maximum range and threshold on correlation. It has both an erase, and a GIF or JPEG capture capability. There is no exit button in the xDisplay GUI. It communicates with the other processes through shared memory and TCP/IP sockets.

2.2.3.2 RIPS (Remote Integrated Products Server) Data Viewers

The on-site Remote Integrated Products Server (RIPS) is a Java based system consisting of several processes which communicate via remote method invocation (RMI).

See Figure 3 for the RIPS data flow diagram. One of its processes, the rmiregistry, is the name service for the RMI processes and does not appear in the figure. Some of the relay processes, which need to be able to scale firewalls in order to serve data off-site, also communicate via HTTP. This is discussed further in Section 2.3.

RIPS is composed of five relay processes: one for each of the four data streams ingested and another one for the derived icing hazard product. It is also composed of four RMI servers: one for each of the four data streams ingested. Additionally, it includes an icingAlg process which performs the icing algorithm and produces the icing product. RIPS includes two viewer processes: radSurfViewer and icingViewer. These viewers not only run in the radar van, but can also run through a browser over the Internet. They each include a GUI that allows the person viewing the data to change the scales, the foreground and background colors, and the variables or fields plotted. They allow the user to take snapshots, and to change the periodicity of automatic snapshots.

2.2.3.2.1 radSurfViewer

The radSurfViewer ingests radiometer and surface meteorological remote objects from the radiometerRelay and the surfaceMetRelay processes. It receives these via RMI and TCP/IP sockets if executing on-site, and HTTP if running off-site. It displays them in real-time in three panels, updating shortly after the beginning of every minute. The first panel includes liquid water, vapor and liquid water temperature. The second panel includes brightness temperatures from all available channels, and the third panel displays humidity, pressure and temperature from the surface met device.

All of the variables may be selected and scaled. Figure 5 shows the user interface for selecting and scaling variables. The user selects which variables are to be viewed and then specifies the minimum and maximum values for the y-axis. The user can also select the number of minutes between automatic JPEG or GIF snapshots (or turn the feature off) and can select special snapshots. Background colors and line colors may be selected by the user. This process reads a previously configured file upon startup. The configuration file defines default scales, how many channels, minutes between automatic snapshots, fields to be displayed, and the rest of the features offered in the user interface.

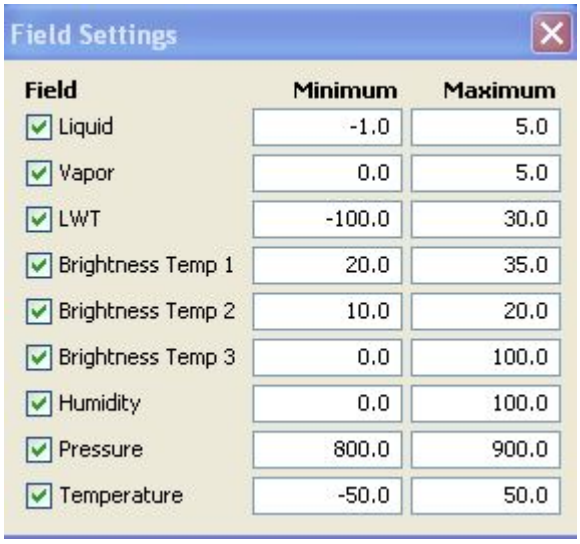

Figure 5. The GUI panel in RIPS' radSurfViewer allows the user to select fields and scale them for display.

2.2.3.2.2 icingViewer

The icingViewer process ingests the derived icing products that are served by the icingRelay process. It consists of three tabbed panes: one for the icing hazard product, one for reflectivity (ZShD), and one for depolarization (ZdrD). The viewer allows the user to select how often the automatic snapshots should be captured, when to perform a special snapshot, which fields to view and what values to use for scaling the fields. At start-up it reads the same configuration file as the radSurfViewer.

2.2.4 Data Displays

As discussed above, the viewers allow the user to manipulate the data as shown on the screen. The different types of displays available are described in this section. When discussing displays, it is necessary to differentiate between variables and fields. A variable is a function only of time (e.g., integrated liquid water). Variables like this are plotted as the y-coordinate versus time (x-coordinate). A field is a function of range and time, such as radar reflectivity. Here the magnitude of the field is indicated by a color on a plot of range (y-coordinate) vs. time (x-coordinate).

There are four types of display available for selection: Marching Time-Range (formerly called BSCAN), Time-Range or A-scope (including RUC model output), Marching Time-Icing Displays and Marching Time-Radiometer Displays.

2.2.4.1 RC+

2.2.4.1.1 Radar Data Displays

For radar data, the nineteen possible fields are available one at a time for the Marching Range-Time and A-scope displays in the RC+ process xDisplay. The displays are updated in real-time as the radar data is ingested. The user can change fields and the scales corresponding to each field. The user can also adjust the height or range of the image. Updates to the displays are made in real-time.

Marching Range-Time displays present a maximum of 600 beams or ten hours of radar data, with the oldest data scrolling off the left-hand side of the display. A-scope displays are not normalized as seen in current RADS displays. The user can change the scale of x for spectra and A-scopes, and max range (or y) in Marching Time-Range displays and A-scope displays.

Figure 6 is an example of data from the AIRSII project. This Marching Range-Time display is as seen on the RC+ machine in the radar van. The field displayed is reflectivity or ZShD. The x-axis is time and the y-axis is height in kilometers. The color identifies the reflectivity in dBZ.

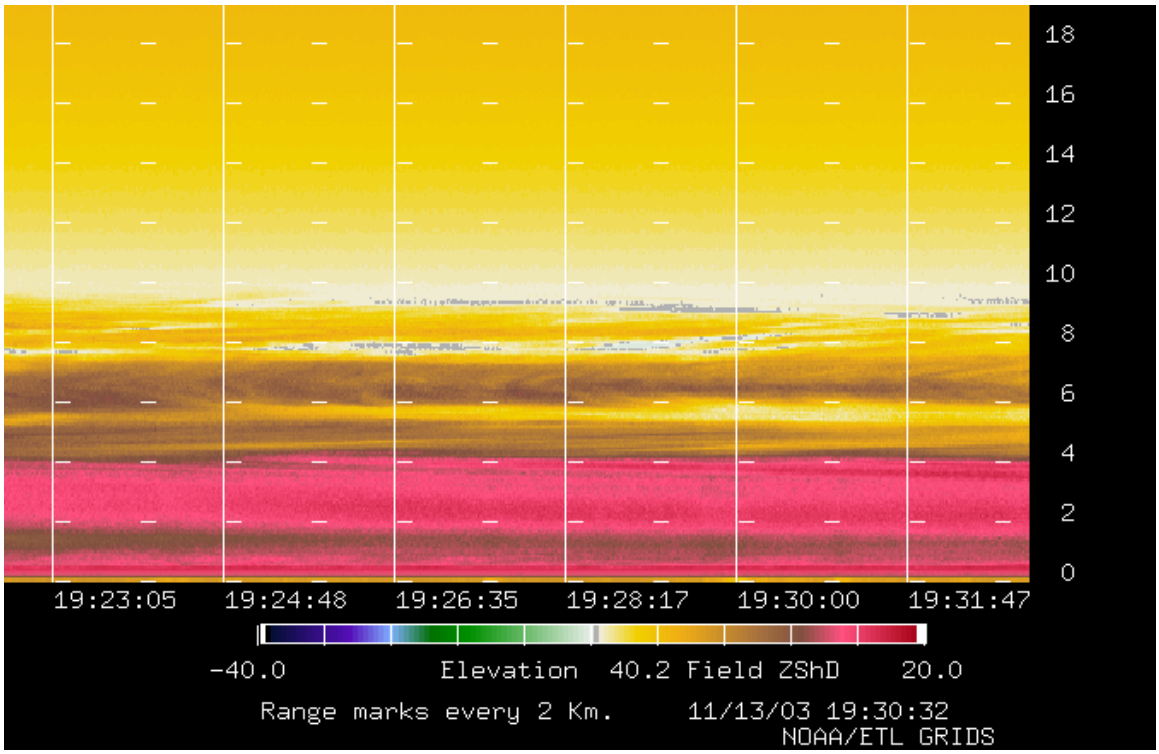

Figure 6. Example of the RC+ radar data Marching Time-Range Display of reflectivity, ZShD. Time is on the x axis (hh:mm:ss), height or range in kilometers is on the y axis.

Figure 7 is an example of an AScope display as it would be seen in the radar van. The x-axis is range in kilometers and the y-axis is uncorrected correlation. The transmitted polarization of the radar was slant and the correlation was derived from data received in the horizontal channel

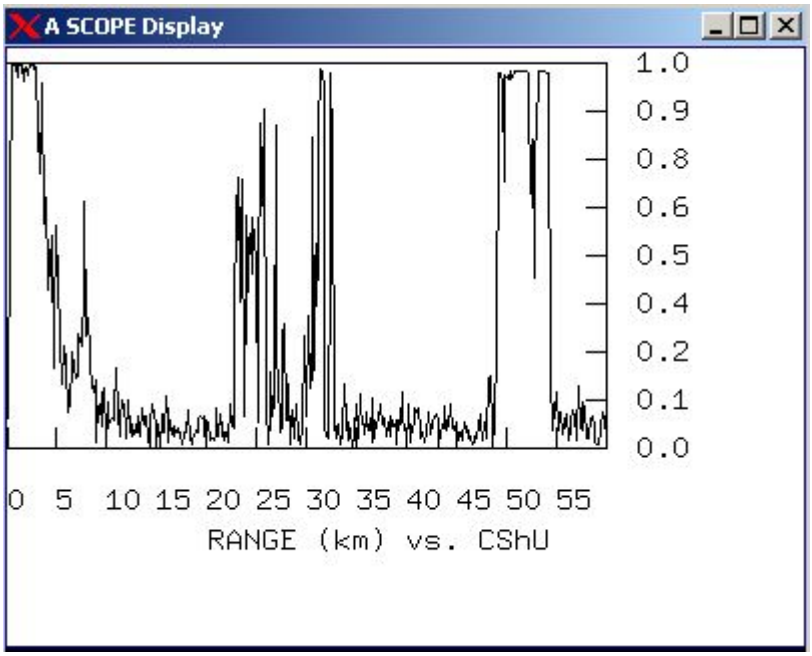

Figure 7. Example of an AScope display showing range in km on the x-axis vs uncorrected correlation from transmitting slant polarization and received on the h channel.

2.2.4.2 RIPS

There are two processes in the RIPS which allow the user to view and manipulate three types of displays: radSurfViewer and icingViewer. The display types are Range-Time Displays of RUC model output, Marching Icing Displays, and Marching Radiometer Displays. These processes can ingest data using RMI from the on-site RIPS system or HTTP data as served by the DataRexx web server off-site. DataRexx is discussed in more detail in Section 2.3.

The display types can be viewed simultaneously, but there can only be one field of each type viewed at any one time. Although the Icing Display has the same appearance as the Marching Range-Time display, it is designed to be displayed on a dedicated console to avoid congestion on the screen. The GRADS is designed to show another Marching Range-Time display of a user selected variable on another monitor simultaneously.

2.2.4.2.1 Radar Data Displays and Icing Hazard Displays

In the on-site RIPS, the icingViewer process displays radar and icing hazard data. Three fields are available to the Marching Icing Displays: reflectivity, icing hazard and depolarization. These are updated every minute or whenever data is received. JPEG or GIF snapshots can be captured automatically or through user initiation.

The icing hazard data is viewed as a Marching Range-Time display that is updated every minute. It displays up to ten hours of data, with the oldest data scrolling off the left-hand side of the panel. One local copy is served on the console and one to another dedicated monitor. Changing the scale of the icing field will only affect the local copy of the image. A GIF or JPEG file of the current icing display on the dedicated monitor is sent to the home office or operations center, in our case Boulder, every minute to be served over the Web no longer than three minutes behind real-time. Since a copy of the data is also sent over the internet to the PSD Web server, similar displays which are updated in close to real-time, are available at the PSD GRIDS website as well. See Section 2.3 for further details on the Web server used for GRIDS. The icing product currently has three values (and thus three colors) available to it. No hazard is shown in green, possible hazard is shown as yellow and hazard is red.

Each of the two radar fields and the icing hazard field may be selected and the scale may be changed for each. Figure 8, below, is an example of the reflectivity field, ZShD, from the AIRSII experiment (Schneider et al 2004) as displayed by the icingViewer. The x-axis is time, the y-axis is height in kilometers, and the colors indicate reflectivity in dBZ. The blank vertical bars occurred when the prototype radar was running a non-vertical mode for testing.

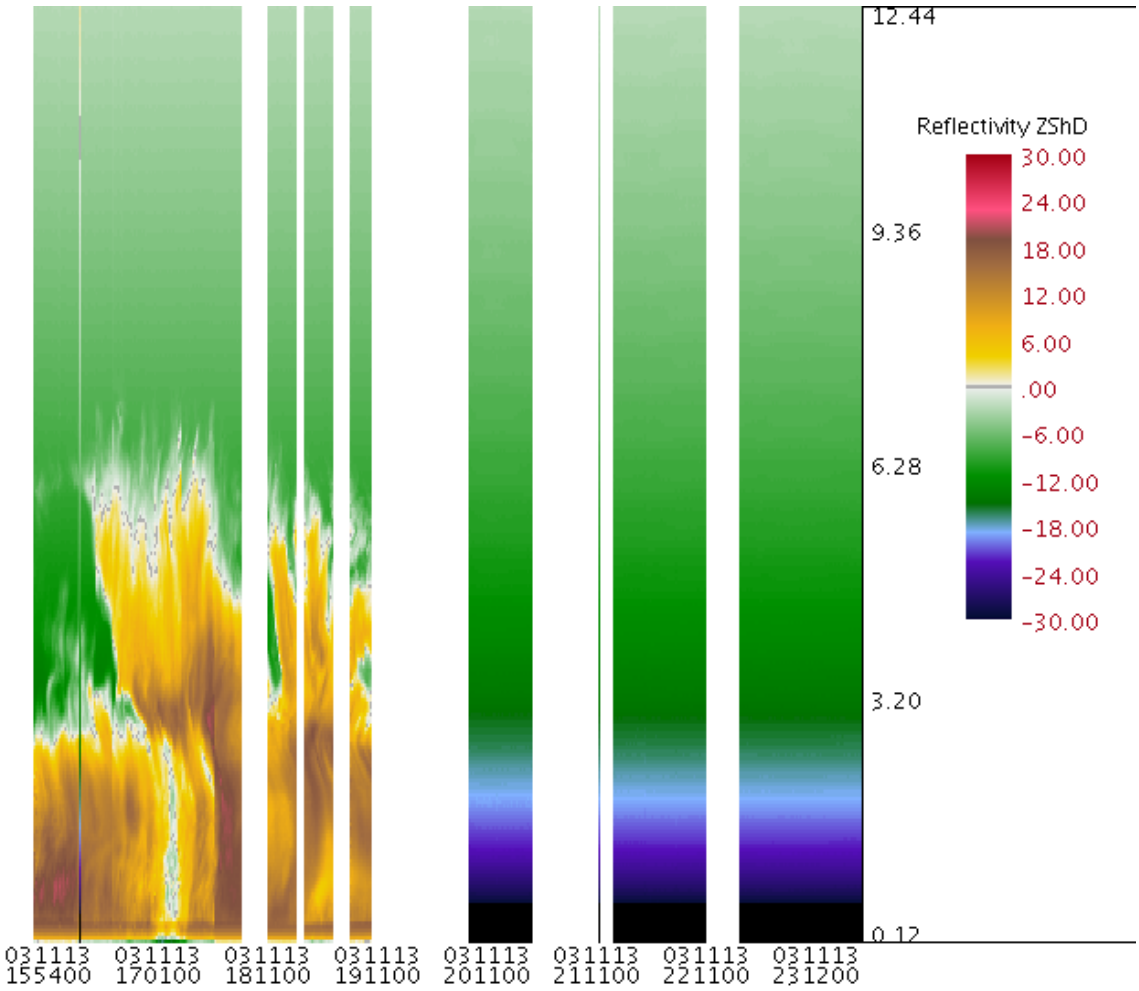

Figure 8. Example of the RIPS Radar Data Marching Range-Time Displays. Reflectivity, ZShD, in dBZ is shown. X is time, with about eight hours shown, and Y is height or range in kilometers.

2.2.4.2.2 Radiometer Data Displays

Radiometer data is viewed as Marching Time-Radiometer Displays through the RIPS process radSurfViewer. Six variables are available to the Marching Time-Radiometer Displays. These are liquid water, water vapor, liquid water temperature, and the brightness temperature from each of the three channels. The user is able to select from the available variables and change scale values for each variable.

Plots are x-y displays of integrated liquid water, integrated water vapor and liquid water temperature overlaid on one panel and the three brightness temperatures overlaid on another panel. These variables are plotted against eight hours of time (on the x-axis). The six variables are plotted in different colors, configurable by the user before start-up or during data collection. This display type operates like the other display types in that the user is allowed to select the six radiometer variables from the select field menu bar option. Corresponding scales and ranges for those variables can be selected as well. The displays are updated every minute or as new radiometer data is ingested. GIF or JPEG images can be captured automatically or through operator initiation.

Figure 9 is an example of the radiometer display types and the surface meteorological data display types generated by the radSurfViewer in RIPS. The three separate panels are displayed together in one window. This example is for illustration purposes only and contains simulated data.

Figure 9. Example of the RIPS Radiometer and Surface Meteorological Marching Time Data Displays

2.2.4.2.3 Surface Meteorological Data Display

The radSurfViewer process also displays the surface meteorological data. Three variables are available to the Marching Time-Surface Met Displays: humidity, pressure

and temperature. The surface meteorological panel is updated every minute with new data and contains eight hours of data. The time between two vertical bars is one hour. The oldest data scrolls off the left-hand side of the display. The user is again able to select from the three available variables and can change the scale for each. GIF or JPEG images can be captured automatically or through operator initiation. In Figure 9 the surface meteorology data display is the bottom panel and illustrates the concept with simulated data.

2.2.4.2.4 RUC Model Display

The RUC model displays are profiles of temperature vs. height. They are shown in an x-y plot. The user is able to change the scale for this variable. The displays are updated every hour or whenever new RUC data is ingested by the AUX Radar Monitor subsystem.

2.2.4.3 Perform the icing algorithm every minute and update the icing displays

A separate process in the RIPS called icingAlg, performs the icing algorithm every minute using the most recent data from the RUC mode, the radar, the radiometer and surface meteorological input. The icing displays are updated every minute with the latest icing product as described in Section 2.2.4.2.1 above. The icing algorithm is performed on every beam of radar data, at every range gate. It uses reflectivity and depolarization data from the radar, liquid water from the radiometer and temperature from the RUC. The surface meteorological data are used as a diagnostic tool to aid the operator, but are not used in the icing product calculation.

2.2.4.4 Automatically capture the icing displays

Every minute the most recent icing display is automatically captured as a GIF or JPEG image and sent to a Web server in Boulder that makes them available on the Web. These are updated every minute and are less than three minutes behind real-time. Also, the icing data is sent to the PSD Web server to be displayed in close to real-time through a browser for remote access.

2.2.4.5 Write data to disk

RC+ stores raw radar data in EF (Extended UF; Gibson et al 2004) disk files. The SWTM parameter (sweep time) determines the size and length of time of the radar file. Covariance radar files require 56 bytes per range gate. With 69 gates and 60-second beams, the files are 291,840 bytes/hour (with a 1000-byte header on each beam). All file names conform to a standard that indicates type, location (radar parameter RDID) and time. It also archives GIF and JPEG snapshot files of the radar fields automatically. This feature, including which fields and how often to automatically capture the image, is configured by the user before run time.

RIPS stores radiometer data, icing model output, snapshot files of radar, icing hazard, radiometer, surface met and RUC marching displays, RUC input files, and surface meteorological data as separate files. File names include time and date. A problem with all of these files arriving asynchronously is determining which files were

used in a particular icing model calculation. Therefore the icing model filename must include the creation time of the input files as well.

The RIPS process writeRadiom saves radiometer data to a separate file. It appends a radiometer data record onto this file every minute, when data is available. At the end of the hour the file will be closed and sent to the archival system. The data rate generation for these files has been shown to be 30-50 Kbytes per hour.

Surface meteorological data is handled in the same way as radiometer data, with a RIPS process called writeSurf. Data can be ingested via either RMI or a TCP/IP socket every minute and appended to an hourly file.

Typically a new GIF or JPEG file of the icing display is generated every minute and is sent to the Web server at that time. Once an hour, the half hour GIF or JPEG files for the previous hour are served to the archival system. These files are about 110 Kbytes each.

RUC files are archived as they come into the RIPS system. Real-time automatic capture of RUC images is currently not available.

RIPS stores all the data for up to 48 hours, in case the link to the archival system is unavailable.

2.2.4.6 Archive the data

There is a script that uses Secure Copy (SCP) to copy the icing, radar, radiometer, RUC, GIF images and surface meteorological data to the archival system once an hour, unless the Internet link is down. Once the files have been archived, they are moved to another part of the disk for playback purposes.

Although a GIF or JPEG file of the icing display can be sent to the server every minute, only two of the half hour GIF or JPEG files are archived each hour.

2.2.4.7 Monitor disk usage and take appropriate action

Since a month's worth of data takes less than a gigabyte of storage space, the disk scrubbing process only deletes files after they are at least four weeks old.

2.3 Off-Site Computers

2.3.1 Web Service of icing displays

Each of the relay processes in the RIPS can ship data through the firewall and to the DataRexx server via HTTP. DataRexx is a third party product written and distributed by Bear Peak Software, Inc. DataRexx acts as a real-time data hub that collects, serves and archives data using HTTP. Since DataRexx works across the Internet and through firewalls, multiple remote clients are able to access the GRIDS data in near real-time. DataRexx allows multiple remote data producer clients to "post" data to it via HTTP. Data consumer clients can then "get" data from DataRexx via HTTP.

Figure 10 is the system overview of the DataRexx system. The data formatter takes raw data and packages it into archive format. Data relays "post" data through HTTP to

the server. Clients are Java applications for viewing and archival. The RIPS system supplies all of these modules. Versions of radSurfViewer and icingViewer running on end-user desktop machines ingest data via HTTP from the DataRexx server. They display radiometer, surface met, radar, RUC and icing hazard data, making this data remotely accessible in near real-time. Once the viewer clients are started, the marching time displays are updated every minute or whenever data is available.

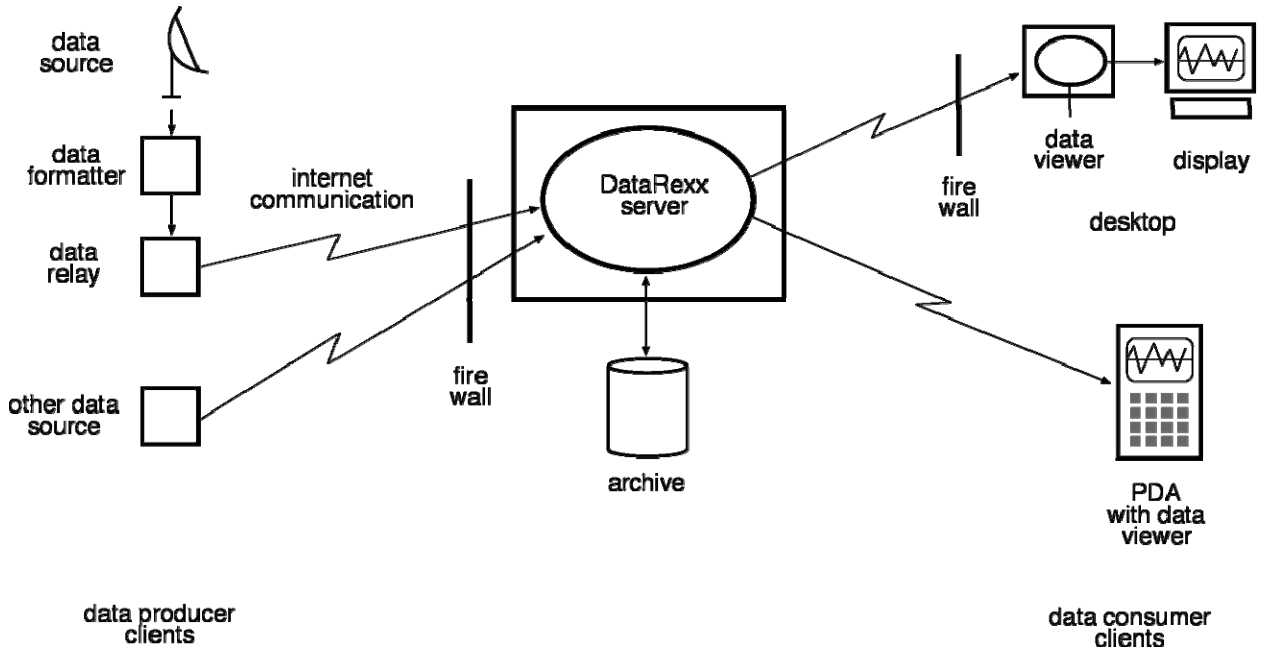

Figure 10. System Overview of the DataRexx server.

2.3.2 Web Archival of data

DataRexx archives all of the data streams that it receives. Another script archives the GIF or JPEG files as they are produced or sent from the on-site computers once an hour, unless the network link is down. Once the files have been archived, they will be moved to another part of the disk for playback purposes.

Although a GIF or JPEG file of the icing display will be sent to the server every minute, only two of the files will be archived each hour; one at the hour and one at the half-hour.

3. ADDITIONAL FEATURES

3.1 Playback capabilities

The system is able to run in playback mode as well as in real-time mode. Playback is able to read from local data files that were previously archived. It displays the data, much as it does in real-time. Since it does not need to be a VME system, or to have any specialized hardware, it can run on the AUX system, or another Linux system at the same time as the GRADS, or on a stand-alone Linux system. The icing images, radiometer displays and variables, RUC displays, surface data and displays, plus the nineteen radar display fields and images need to be made available in playback mode, thus allowing the archived RUC data, radar data, radiometer data, surface meteorological data and icing model data to be ingested by the playback machine.

3.2 On-line help

On-line help in the form of an on-line manual is available.

3.3 Reacting to system health messages

Reacting to system health messages includes power failure recovery and the ability to resume scheduled activities without operator intervention. Other items to be considered include how often health messages should be sent and in what format. Trouble messages come over to RC+ from the Radar Monitor with an error code. A tabular structure might be used to categorize responses for each trouble message. For every kind of message there might be several possible actions that can be defined (note that several actions could be selected for each problem although some are mutually exclusive) including ignore, print message on console, e-mail message, stop and restart, permanently stop, execute a special routine and continue, execute a special routine and restart, *etc*. GRADS runs autonomously and remote monitoring is available via a Web interface.

3.4 Spectral processing and displays

This mode has not been defined yet and will have its own associated parameters, including windowing, number of spectral points, spectral averaging, and DC filtering. For display purposes, it will be its own display type, and will include a cascade or waterfall window as well as displays for user selected ranges. The user will need to be able to change the color scale, but may not change ranges.

3.5 Radar/radiometer control

This includes pause/start, position and shutdown. The Radar Monitor process on the AUX system does the actual shutdown of the radar, which can be initiated by either UPS software or by RC+. Computer shutdown is independent of shutdown of the instruments.

Appendix H

Implementation of the Digital Receiver System

1. INTRODUCTION

The digital receiver system takes two channels of IF (co-polarized and cross-polarized channels), digitizes them, digitally mixes them to baseband, runs the signals through several stages of digital filtering, and then transfers them to the host computer. The data transferred is the standard I (in-phase) and Q (quadrature-phase) signals that would be output by an analog receiver. All of this is performed on one PCI card in the host computer.

There are several advantages to the digital approach, including elimination of much of the hardware in the receiver, flexibility in bandwidth, elimination of several receiver calibration steps, and improved performance. The chief performance enhancements are elimination of the spectral image and an increased dynamic range.

2. OVERVIEW

The digital receiver system will take a 60 MHz IF and digitize it at an 80 MHz rate (sampling at less than the Nyquist rate is called harmonic sampling). These frequencies allow the use of a common IF frequency and minimize the effects of aliasing. (See equation 7.51 in Frerking 1994, where N = 1.) The digitizing process translates the IF frequency to 20 MHz in the digital domain. The digital mixer in the digital receiver chip is then used to mix the signal down to baseband.

3. DIGITAL RECEIVER CARD

The digital receiver is a PCI card contained in the DIFRS computer chassis. This card is the model ICS-554B-2-MN from Interactive Circuits and Systems and contains two A/D channels and four digital receiver integrated circuits. The digital receiver ICs are the model GC4016 from Graychip and each of them contains four receiver channels, which yields a total of 16 receiver channels on the ICS-554B. The reader should refer to both manufacturers' literature for complete detail, but to facilitate the following discussion Figure 1 reproduces a diagram of a single receiver channel in the GC4016.

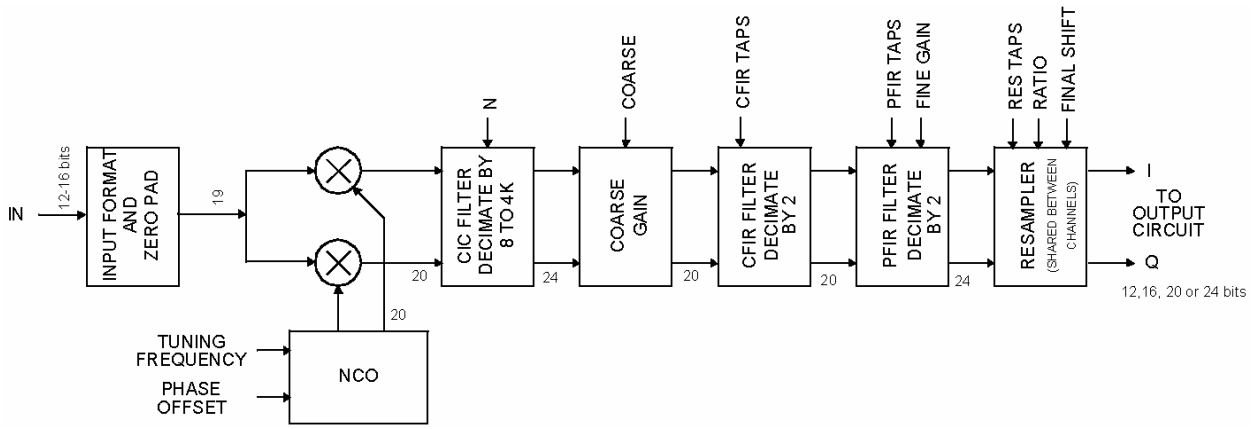

Figure 1. A single receiver channel in the Graychip 4016.

Note that a single channel is capable of taking an IF signal and complex demodulating it to baseband using a Numerically Controlled Oscillator. The complex demodulation process generates two channels (In-phase and Quadrature) that feed the digital filters, which are capable of processing I and Q in parallel. Looking at the minimum decimation values of the digital filters, we see that the minimum total decimation is 32. With an 80 MHz sampling rate, this means that the maximum data rate at the output is 2.5 MHz, which may not be fast enough for some radar work. However channels on the chip can be combined to increase the data rate.

Split-I/Q mode accomplishes this by using one channel to process the real half of the complex data, and a second channel to process the imaginary half. Since only half as much data is going through a single channel, the filters can run twice as fast and so the minimum value of the CIC filter decimation becomes four, rather than eight. (Although the diagram suggests that there are two parallel channels in each filter, there is actually one channel that is time-multiplexed to appear as two.) This gives an output data rate of 5 MHz.

Still more throughput can be achieved by sharing the data flow with the two unused channels on the chip. (This is called the wideband downconvert mode.) These extra two channels operate in Split-I/Q mode also, but now one pair of channels processes the even-numbered samples and the other pair processes the odd-numbered samples. These samples are combined in the output circuit so it is as if the PFIR decimate-by-two doesn't exist. Now the minimum decimation of the data becomes eight and so, with an 80 MHz sampling rate, the maximum output data rate is 10 MHz, which means an IF bandwidth of 5 MHz is possible. This is the mode that is implemented in the software.

4. GRIDS DIGITAL RECEIVER SYSTEM

4.1 Digital Filtering Strategy

Because of the wide bandwidth typically required in pulsed radars as compared to usual communications systems, care must be taken to provide adequate bandwidth in the digital receiver system which was primarily designed for narrowband use. This means keeping the decimation values as small as possible using the means discussed in the previous section. Once

this has been achieved, it is a simple matter to narrow the bandwidth when required for long pulses.

The other radar requirement imposed on the receiver system is the matched filter, which means that the shape of the filter response should approximate a Gaussian curve (Doviak and Zrnic 1993) whose width is a function of the transmitted pulse width. This Gaussian response is performed in the CFIR where the signal has been decimated as little as possible.

At this point, all the necessary filtering has been done and so the PFIR filter is essentially bypassed by programming the appropriate coefficients to just pass the data through. The Resampler is now used only to decimate the data to get to the desired range gate spacing.

4.2 Radar Timing Generator

The digital receiver card will operate in conjunction with a Radar Timing Generator (RTG) card and a frequency synthesizer card which will be housed in the same chassis. Figure 2 shows a diagram of the digital receiver system and the IF Modulator/Receiver. The frequency synthesizer card (Echotek ECSG-1R3ADC-PMC) is used to synthesize an 80 MHz sampling signal needed by the digital receiver card from a 20 MHz signal generated in the IF Modulator/Receiver. This same 20 MHz signal drives the RTG and is used to synthesize other required timing signals in the system.

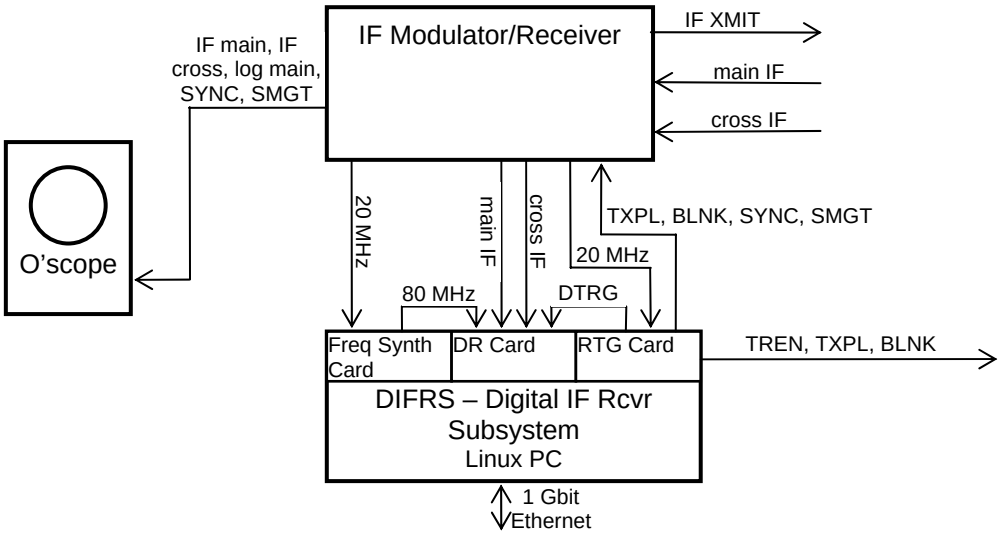

Figure 2. Digital receiver system.

Table 1 shows all the timing signals generated by the RTG. The names of the signals are similar to the ones used in the MMCR. In fact, truncating the names to the first two letters yields the MMCR nomenclature. Some of the signals are not needed in the current configuration, such as RPOL, which was to switch receive channels in a single receiver configuration.

The RTG was implemented on a VME board in an earlier configuration of GRIDS using three Altera EPLDs. The new RTG will use a single Altera part on a PMC card (Acromag IP1K110-2412).

Table 1. External signal list for Radar Timing Generator

#	**Short Signal Name**	**Full Signal Name**	**Function**	**Used By**	**Controlling Parameters** (50 ns resolution unless indicated)	**Comment**
1	SYNC	Sync	Oscilloscope trigger	Display only	PRPR (1 us), NSYC	MMCR used absence of this to indicate cross-channel receive. Now done by RPOL. SYNC may occur every TXPL, every other TXPL, or every 4th TXPL to maintain MMCR compatibility.
2	TREN	Transmit-Receive Envelope	Brackets transmit pulse	Pulse controller	TRDL, TRWD	
3	BLNK	Blank	Receiver blanking	IF Mod/Rcvr, Pulse Controller	BLDL , BLWD	
4	TMEN	Transmit Envelope	Brackets transmit pulse	Pulse Controller	TMDL, TMWD	Not used in MMCR
5	TXPL	Transmit Pulse	Transmit pulse	IF Mod/Rcvr, Pulse Controller	TXDL, TXWD	
6	SMGT	Sample	Sampling gates	Display only	DLAY (1 us), SPAC, NGAT	GRIDS digitizer only uses DTRG & DCLK
7	RPOL	Received Polarization	Indicates whether to receive on co- or cross-channel	Pulse controller	RPDL, RPOL[0:7]	Eight-bit shift register controls RPOL
8	PHAS	Phase	Pulse-coding phase modulation within radar trigger	IF Mod/Rcvr	PHWD, NCBT	Possible future
9	SCYC	Start Cycle	O'scope trigger. Resets SYNC and RPOL.	Display only	NTRG	Useful for debugging
10	SPHS	System Phase	Switches LO phase in a pseudo-random sequence to suppress multi-trip echoes.	not used		Possible future
11	DTRG	Digitizer Trigger	Precedes first sampling gate	Digital Receiver	DLAY (same as in SMGT)	
12	DCLK	Digitizer Clock	not used	not used	none	20 MHz clock

5. SOFTWARE

A C++ class called DigRcvr was designed to handle setup and operation of the Digital Receiver card. The objective was to give the user of the class an interface that was radar oriented and that hid the complexity of the Digital Receiver. A radar-oriented interface means that radar parameters such as range gate spacing, number of range gates and radar trigger length are used rather than parameters such as bandwidth and decimation. Because not all combinations of parameters are possible, a method called tryParams( ) was written that takes input parameters and adjusts them to something that the hardware can actually do. Once the digital receiver is started, it runs continuously. A method called readData( ) is used to read the I and Q data, which is double-buffered within the class. Data that is not read in time is discarded so as not to disrupt the data flow within the class.

5.1 Description of class DigRcvr

Class DigRcvr runs the ICS-554B digital receiver card in a way suitable for radar. The card is operated in the wideband downconvert mode and produces 24-bit I and Q data, each left justified in a 32-bit word. It is assumed that two IF channels (main and cross) will be used. Gaussian bandpass filters are implemented using the digital filtering capability on the Graychips. Data is digitized by the A/D's at the sampleRate (typ. 80 MHz for a 60 MHz IF). The data is mixed against ncoFreq (Numerically Controlled Oscillator) in the Graychip to bring it down to baseband. Decimation in the first filter (CIC) is kept to the minimum value of 4 so as to allow as many taps as possible in subsequent filters. The next filter (CFIR) implements the Gaussian-shaped bandpass response. The filtering capability of the PFIR is not used and so the data merely passes through it. The Resampler is used to perform decimations, but its digital filtering capability is also not used.

Because of limitations in the memory (FIFO) of the card, beams may be needed to be divided into sub-beams and collected together to reach the length required so that this class can return a complete beam of data. For a 50% FIFO utilization, which seems to perform well, the maximum product of gates*triggers must be <= 32768 for one acquisition cycle (sub-beam). When this product is exceeded, sub-beams must be used.

tryParams( ) calculates the size of the sub-beams and so the calling program may not get the exact number of gates and triggers that it requests, but the actual values used are returned by tryParams. Then setParams( ) is used to set these parameters into the digital receiver. Once startData( ) is called, data collection begins. Incoming data is double-buffered but readData( ) must be called at a sufficient rate or else data will be lost. It can be determined if data has been lost by looking at beamCntr in the packet header.

5.1.1 Data Types

Units used for numeric values are always in base units unless otherwise indicated. For instance, range gate spacing (spac) is in seconds so $1*10^{-6}$ is a typical value.

```
/* PCKT_HDR is at the beginning of each beam. DigRcvr fills in beamCntr,
 *  pcktCntr (= beamCntr), secs and nsec. Other information is filled in by
 *  other programs. pcktCntr becomes useful downstream if beam averaging is
```

```
 *  performed.
 */

struct PCKT_HDR     // PCKT_HDR appears at the beginning of data
{
   uint   pcktCntr;    // DR's packet counter
   uint   beamCntr;    // DR's beam counter
   uint   secs;        // Unix time in seconds
   uint   nsec;        // ..and nanoseconds
   float  azim;        // azimuth of beam in degrees
   float  elev;        // elevation of beam in degrees
};


/* DigRcvrInit contains parameters to initialize the Dig Rcvr card. These are
 * parameters that are usually fixed for a given hardware configuration. The
 * default set may be accessed by declaring 'extern DigRcvrInit initStruct'
 * in the user program.
 */

struct DigRcvrInit
{
   float  ncoFreq;        // frequency of local oscillator in tuner in Hz
   float  sampleRate;     // sampling rate of A/D's in MHz
   float  fifoUtil;       // desired FIFO utilization in percent
};

/* TmParams is used by tryParams() and setParams(). tryParams() takes the
 * first seven parameters and calculates the last two. Some of the first seven
 * may be altered to achievable values. setParams() uses all parameters as input
 * only and returns an error code if the parameters are unachievable.
 */

struct TmParams
{
   float  rtln;     // radar trigger length; used to set bandwidth of rcvr
   float  prpl;     // pair repetition period (used for checks only)
   float  prps;     // inter-pair period (used for checks only)
   float  dlay;     // delay from radar trigger to first range gate (checks only)
   float  spac;     // range gate spacing
   uint   ngat;     // number of range gates (must be multiple of 4)
   uint   ntrg;     // number of triggers in beam
   uint   nsbeams;  // number of sub-beams
   uint   ntrgsb;   // number of triggers in sub-beam
};

// This struct contains derived parameters and is returned from setParams().
struct DRparams
{
   int    error;       // error code. 0 if no error.
   uint   buffSize;    // size of ICS554 beam buffer in bytes
                           // size = (8*ngat*nsbeams*ntrgsb) + sizeof(PCKT_HDR)
   float  fifoUtil;    // actual FIFO utilization in percent
   uint   dec;         // total decimation of Graychip. Multiple of 8
};

// Format of a single complex sample returned from DigRcvr
// Order of real & imag picked to match order from ICS-554
struct DRsample
{
   int    imag;        // imaginary part
   int    real;        // real part. 24-bit left justified in 32-bit word
};
```

5.1.2 Public Methods

```
// DigRcvr class
// User must call setParams() before calling startData(). It is recommended that
```

```
//  tryParams() be called before setParams() because it will adjust the
//  timing parameters to achievable values.

class DigRcvr
{
public:
   DigRcvr(DigRcvrInit init);                 // basic DR init for fixed parameters
   TmParams tryParams(const TmParams* pIndy); // adjusts parameters
   DRparams setParams(TmParams);              // initializes the DR
   int    startData( );                       // starts DSP and data collection
   int    readData(void* pBuff);              // get data from DSP
   bool   isDataRunning( );                   // determine if dataThread is active
   void   stopData( );                        // stop DR and cancel thread
   void   prntDDCconfig( );                   // prints the GC configuration (debug)
   ~DigRcvr( );                               // close & unmap
};
```

Methods are listed in the order that they are normally called.

DigRcvr(DigRcvrInit init);

Constructor. Opens the drive and gets a file descriptor for it. Sets defaults for basic digital receiver parameters when called in this form. Other parameters that depend on TmParams are set later by setParams( ).

TmParams tryParams(const TmParams* pIndy);

Takes the first seven TmParams parameters and adjusts some of them to achiveable values. The last two parameters (the sub-beam parameters) are calculated by tryParams. This method should be called before setParams( ) so that the parameters are correct.

DRparams setParams(TmParams);

Completes the initialization of the digital receiver with the timing parameters. At this point, the receiver is primed to acquire data.

int startData( );

Starts the digital receiver. startData( ) returns quickly but spins off a thread that continues to run and acquire data until stopData( ) is called. This thread uses a double buffer to continuously acquire data that may be accessed by calling readData( ). If readData( ) is not called soon enough, entire beams will be lost. Data is acquired continuously with no gaps until stopData( ) is called.

bool isDataRunning( );

Checks whether the digital receiver is running.

int readData(DRsample* pBuff);

Data is taken from the last buffer acquired and placed in the buffer pointed to by pBuff. A PCKT_HDR packet will be at the beginning of the data. The data is in time order and consists of a series of type DRsample. The number of triggers and range gates must be used to demultiplex the data. This call will normally block while waiting for data. If readData( ) is called often enough, no data will be lost. If it is not called in a timely manner, entire beams will be missed. This can be detected by looking at the beam counter in the packet header.

void stopData( );

Stops the digital receiver.

~DigRcvr( );

Destructor. Stops the digital receiver if necessary and deallocates memory.

5.1.3 Decimation Algorithm

This algorithm calculates the decimation to use to achieve, as nearly as possible, a desired gate spacing. A derivation is given for the algorithm followed by the algorithm itself.

Independent variables:

spac -- desired gate spacing
rate -- A/D sampling rate (typ. 80 MHz)

Dependent variables:

dec -- total decimation in Graychip
spac2 -- achievable gate spacing

Decimation in Graychip

CIC ---->	CFIR ---->	PFIR ---->	ReSamp ---->	out
4	2	1	n	

dec = 8n decimations in chip are fixed, except for resampler decimation which is n
1 <= n <= 31 hardware limitation in Graychip

rate/dec = 1/spac this expresses the desired result
dec = rate*spac
8n = rate*spac
n = rate*spac/8
1 <= rate*spac/8 <= 31 apply the hardware limitation

Algorithm:
1) n = *floor*(rate*spac/8 + 0.5) *floor* function truncates fractional part of a number
2) Check that 1 <= n <= 31; if not pick 1 or 31 for n, whichever is appropriate
3) dec = 8n
4) spac2 = dec/rate

Example:
If rate = 80 MHz and spac = 1.55 μs, then n = 16, dec = 128 and spac2 = 1.6 μs.

6. STATUS

At the termination of the project, the DigRcvr class was working although not extensively tested. Also the issue of the gain through the Graychip had not been addressed. Gain can be set through the Coarse Gain block and with a fine gain setting in the PFIR.

DigRcvr was tested using a program called drex for Digital Receiver EXerciser. The drex program exercises DigRcvr by allowing an operator to input various parameters and observe the results as a listing of the output from the digital receiver.

7. FUTURE PLANS

Several tasks remain to finish the digital receiver system. On the hardware side, the Radar Timing Generator design needs to be ported to the PCI-based card. This is not expected to be a long task since the design has been implemented in three chips on a VME card and will be ported to a single chip on a PCI card with much more capability than the three chips put together. The chips are all from the same manufacturer. A diagnostic program was also written under Solaris that should port easily to Linux.

On the software side, gain in the DigRcvr class needs to be addressed. Then a class to control the RTG needs to be written. There is code for a VME RTG class (RtgCntrl) that was written that can be leveraged to help create this. Also a class that drives the digital synthesizer board needs to be written.

Then a class needs to be written that ties together the digital receiver, the RTG and the frequency synthesizer so that there is one interface to all the digital receiver hardware. This would then be used in drex to test the complete digital receiver system.

Finally, the main DIFRS program needs to be written. This program will take instructions and parameters over a socket from the RC+ computer, calculate covariances from the digital receiver data, and transfer the results to the RC+ computer. This program will not have any console control since X-windows operation increases interrupt latency significantly and interferes with the proper operation of the digital receiver.

Appendix I
GRIDS Covariance Algorithms

1. INTRODUCTION

This document specifies the covariance-based algorithm that will be performed in real-time in GRIDS. This algorithm is commonly called the pulse-pair algorithm because it measures the phase difference between the received signal from a pair of radar pulses. With a very high signal-to-noise ratio, this phase difference and the time between the pulses is all that is required to calculate the Doppler shift and consequently the radial velocity of the target. In practice, the signals from many pairs of pulses are summed together to reduce the uncertainty of the estimate to an acceptable level.

Included is a brief introduction to covariances in the following section to give some context to the algorithm definitions.

2. COMPLEX COVARIANCES AND SINE WAVES

Some of the signal processing used in GRADS is based on "pulse-pair" or covariance algorithms. The radar transmits pairs of pulses in the manner shown in Figure 1.

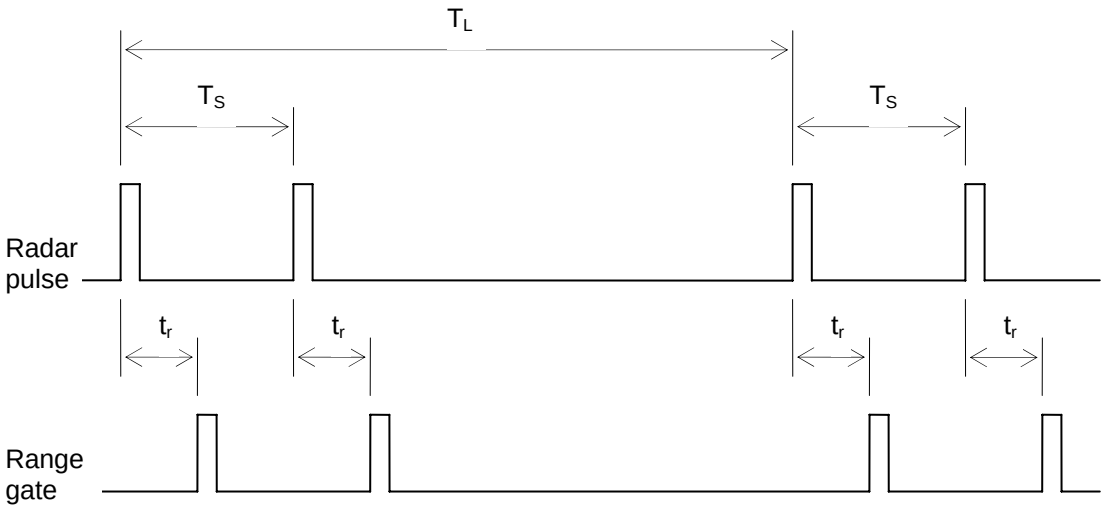

Figure 1. Transmitter pulses and a single range gate are shown for a double-pulse modulation scheme.

A single range gate is illustrated at a delay t_r from the transmitted pulses. Samples at the short pulse spacing, T_S, are used to give an estimate of the Doppler velocity. Results at the long pulse spacing, T_L, are summed together and used to reduce the uncertainty of the estimate. The advantage of this type of "double-pulse" modulation over equally spaced pulses is that by reducing T_S, the unambiguous velocity limit of the radar can be increased without increasing the transmitted power, which is limited by the characteristics of the transmitter tube. This is particularly useful for short-wavelength radars. The disadvantage is that the unambiguous range is limited by how close the pulses in the pair are. However, T_S can always be changed to half of T_L, if desired, to give equally spaced pulses.

In the following discussion, whenever a covariance product is calculated, it is done from pulses in the pair, while the sums of these products are performed over the pairs. The time T_L is not significant in the calculations, except indirectly in that increasing it reduces the number of samples taken in a given time and reduces the beneficial effects of averaging.

The complex covariance function is used for many purposes in statistics, but here it is used only to calculate the phase change between two points in complex sine waves, and the power present in a complex sine wave. Complex quantities are in **bold** in the following equations and in Table 3.

Consider two complex sequences, $\mathbf{X}_i$ and $\mathbf{Y}_i$. Then the general definition of complex covariance is given by

$$\mathbf{R}_{XY}(n) = \left\langle \left(\mathbf{X}_i^* - \left\langle \mathbf{X}_i^* \right\rangle \right) \cdot \left(\mathbf{Y}_{i+n} - \left\langle \mathbf{Y}_{i+n} \right\rangle \right) \right\rangle, \qquad \textbf{(Equation E-1)}$$

where $\mathbf{X}_i$ and $\mathbf{Y}_i$ represent complex sequences and n represents the number of lags to use in calculating the covariance. The "< >" notation represents the average and "*" denotes the complex conjugate.

This equation may be rewritten to give

$$\mathbf{R}_{XY}(n) = \left\langle \mathbf{X}_i^* \mathbf{Y}_{i+n} \right\rangle - \left\langle \mathbf{X}_i^* \right\rangle \left\langle \mathbf{Y}_{i+n} \right\rangle. \qquad \textbf{(Equation E-2)}$$

In GRIDS, $\mathbf{X}_i$ and $\mathbf{Y}_i$ are usually the same channel, which is the digitized representation of a voltage. This signal will be denoted $\mathbf{E}_i$. Since we are now using an auto-covariance, we can simplify our nomenclature to

$$\mathbf{R}(n) = \left\langle \mathbf{E}_i^* \mathbf{E}_{i+n} \right\rangle - \left\langle \mathbf{E}_i^* \right\rangle \left\langle \mathbf{E}_{i+n} \right\rangle. \qquad \textbf{(Equation E-3)}$$

For the zero-lag covariance, where i ranges over every pulse

$$\mathbf{R}(0) = \left\langle \mathbf{E}_i^* \mathbf{E}_i \right\rangle - \left\langle \mathbf{E}_i^* \right\rangle \left\langle \mathbf{E}_i \right\rangle = \left\langle \left| \mathbf{E}_i \right|^2 \right\rangle - \left\langle \mathbf{E}_i \right\rangle^* \left\langle \mathbf{E}_i \right\rangle,$$

or

$$R(0) = \left\langle \left| \mathbf{E}_i \right|^2 \right\rangle - \left| \left\langle \mathbf{E}_i \right\rangle \right|^2. \qquad \textbf{(Equation E-4)}$$

Note that R(0) is real-valued. This represents the average of the "power" (voltage squared) minus the average DC value squared. In other words, R(0) is the DC-corrected "power."

R(1) may be written as follows, where i increments by two (for pairs):

$$\mathbf{R}(1) = \left\langle \mathbf{E}_i^* \mathbf{E}_{i+1} \right\rangle - \left\langle \mathbf{E}_i^* \right\rangle \left\langle \mathbf{E}_{i+1} \right\rangle, \qquad \textbf{(Equation E-5)}$$

where $\mathbf{E}_{i+1}$ is the signal from the second pulse in the pair.

Now calculate $\mathbf{R}(1)$ for a complex sine wave as defined by

$$\mathbf{E}_i = Ae^{j\omega i T_S},$$

so

$$\mathbf{E}_{i+1} = Ae^{j\omega(i+1)T_S}.$$

Then

$$\mathbf{R}(1) = \left\langle Ae^{-j\omega i T_S} Ae^{j\omega(i+1)T_S} \right\rangle - \left\langle Ae^{-j\omega i T_S} \right\rangle \left\langle Ae^{j\omega(i+1)T_S} \right\rangle = \left\langle A^2 e^{j\omega T_S} \right\rangle - \left\langle Ae^{-j\omega i T_S} \right\rangle \left\langle Ae^{j\omega i T_S} e^{j\omega T_S} \right\rangle$$

$$\mathbf{R}(1) = A^2 e^{j\omega T_S} - A^2 e^{j\omega T_S} \left\langle e^{-j\omega i T_S} \right\rangle \left\langle e^{j\omega i T_S} \right\rangle = A^2 e^{j\omega T_S} \left(1 - \left\langle e^{-j\omega i T_S} \right\rangle \left\langle e^{j\omega i T_S} \right\rangle \right) \qquad \textbf{(Equation E-6)}$$

$$\mathbf{R}(1) = A^2 e^{j\omega T_S}\left(1 - \langle cos\ \omega i T_S - j\ sin\ \omega i T_S\rangle\langle cos\ \omega i T_S + j\ sin\ \omega i T\rangle\right)$$

$$\mathbf{R}(1) = A^2 e^{j\omega T_S}\left(1 - \langle cos\ \omega i T_S\rangle^2 - \langle sin\ \omega i T_S\rangle^2\right).$$

Therefore,

$$arg(\mathbf{R}(1)) = \omega T_S . \qquad \textbf{(Equation E-7)}$$

Since the angular frequency, ω, is related to the Doppler shift, this demonstrates how the Doppler velocity may be obtained, at least for the case of a sine wave. More elaborate derivations for signals plus noise may be found in the literature, but this illustrates the basic idea.

In GRIDS, the covariance sums are calculated on the Radar Data Acquisition Computer. We take the equation

$$\mathbf{R}(n) = \langle \mathbf{E}_i^* \mathbf{E}_{i+n} \rangle - \langle \mathbf{E}_i^* \rangle \langle \mathbf{E}_{i+n} \rangle$$

and partition it as follows. Let

$\mathbf{B}(n) = \langle \mathbf{E}_i^* \mathbf{E}_{i+n} \rangle$ and

$\mathbf{A}(n) = \langle \mathbf{E}_{i+n} \rangle$.

Then

$$\mathbf{R}(n) = \mathbf{B}(n) - \mathbf{A}(0)^* \cdot \mathbf{A}(n),$$

so

$R(0) = B(0) - \mathbf{A}(0)^* \cdot \mathbf{A}(0) = B(0) - |\mathbf{A}(0)|^2$ and

$$\mathbf{R}(1) = \mathbf{B}(1) - \mathbf{A}(0)^* \cdot \mathbf{A}(1).$$

Currently, n can be either 0 or 1, so we calculate the quantities **A0**, **A1**, B0 and **B1**, where **A0** is the complex sum from the first pulse in the pair, and **A1** is the complex sum from the second pulse in the pair. B0 is defined to be the sum over both the first and second pulse in the pair, and **B1** is just **B(1)**, which leads to the following equations:

$$R(0) = B0 - \frac{1}{2}\left(|\mathbf{A0}|^2 + |\mathbf{A1}|^2\right) \qquad \textbf{(Equation E-8)}$$

$$\mathbf{R}(1) = \mathbf{B1} - \mathbf{A0}^* \cdot \mathbf{A1} . \qquad \textbf{(Equation E-9)}$$

Note that **A0** and **A1** are both zero if there is no DC component in the time series. A DC component is caused by ground clutter in the echo and inclusion of the terms in the above equations removes the effects of ground clutter. Calculating the A's and B's separately and passing them on to the next step allows calculation of both DC-corrected and non-DC-corrected fields. Non-DC-corrected fields are useful for producing ground clutter maps, since normally ground targets would be suppressed by the DC correction.

3. APPLICATION OF COVARIANCE FUNCTIONS TO THE GRIDS RADAR

The GRIDS radar will transmit a single circular polarization and receive simultaneously a co-polarized signal and a cross-polarized signal. We will adopt the convention of using a "c" to represent the signal received on the co-polarized channel, and an "x" to represent the signal received on the cross-polarized channel.

Covariances of the form **R**(0), signifying zero lags, are formed from summing over every co- or cross-polarized *sample* in the beam, that is, both the first and second pulses of the pair. Covariances of the form **R**(1), signifying one lag, are formed from summing over every co- or cross-polarized *pair* in the beam, where the two factors in the covariance are taken from the first and second pulse of the pair.

The covariances we will use are shown in the table below. Complex quantities are in **bold**.

Table 1. Covariance products calculated

Symbol	Description	Used to calculate:
$R_{cc}(0)$	co-polarized "power"	co-polarized power
$R_{xx}(0)$	cross-polarized "power"	cross-polarized power
$\mathbf{R}_{cc}(1)$	co-polarized covariance, one lag	pulse-pair velocity from the co-polarized channel
$\mathbf{R}_{xx}(1)$	cross-polarized covariance, one lag	pulse-pair velocity from the cross-polarized channel

By calculating **B**'s and **A**'s separately, we make it possible to produce "non-DC-corrected" values of various quantities, such as received power, which may be useful for calibration. The table below shows "data products", which are quantities that are recorded. Total memory required is 56 bytes for each range gate.

Table 2. Recorded data products

Calculated variable name	Mathematical symbol	Description	Required for
Ac0	$\mathbf{A}_c(0)$	average of co-polarized samples from first pulse of pair	DC correction
Ax0	$\mathbf{A}_x(0)$	average of cross-polarized samples from first pulse of pair	DC correction
Ac1	$\mathbf{A}_c(1)$	average of co-polarized samples from second pulse of pair	DC correction
Ax1	$\mathbf{A}_x(1)$	average of cross-polarized samples from second pulse of pair	DC correction
Bcc0	$B_{cc}(0)$	uncorrected co-polarized covariance, zero lag	power & pulse-pair width
Bxx0	$B_{xx}(0)$	uncorrected cross-polarized covariance, zero lag	power & pulse-pair width
Bcc1	$\mathbf{B}_{cc}(1)$	uncorrected co-polarized covariance, one lag	pulse-pair velocity & width
Bxx1	$\mathbf{B}_{xx}(1)$	uncorrected cross-polarized covariance, one lag	pulse-pair velocity & width

The following table shows the display (discarded) products. A "U" at the end of a name means that the value has been calculated from non-DC-corrected covariances. All of these quantities are calculated for each range gate and are available for display.

Table 3. Display products (not recorded)

Description	**Derived from co-polarized channel**	**Derived from cross-polarized channel**	**Derived from both channels**	**Units**
velocity	Vc	Vx		m/s
velocity spread	Wc	Wx		m^2/s^2
correlation	Cc	Cx		none
intensity (power at receiver output)	Ic, IcU	Ix, IxU		dBm
power (power at antenna terminals)	Pc, PcU	Px, PxU		dBm
Reflectivity factor	Zc, ZcU	Zx, ZxU		dBZ
circular depolarization ratio			CDR	dB

The following equations will be used to calculate DC-corrected covariances from the uncorrected covariances:

$$R_{cc}(0) = B_{cc}(0) - \frac{1}{2}\left[\left|\mathbf{A}_c(0)\right|^2 + \left|\mathbf{A}_c(1)\right|^2\right]$$

$$R_{xx}(0) = B_{xx}(0) - \frac{1}{2}\left[\left|\mathbf{A}_x(0)\right|^2 + \left|\mathbf{A}_x(1)\right|^2\right]$$

$$\mathbf{R}_{cc}(1) = \mathbf{B}_{cc}(1) - \mathbf{A}_c^*(0) \bullet \mathbf{A}_c(1)$$

$$\mathbf{R}_{xx}(1) = \mathbf{B}_{xx}(1) - \mathbf{A}_x^*(0) \bullet \mathbf{A}_x(1)$$

The following equations are shown with R's for the covariances, but will also be used with B's to calculate uncorrected quantities where required. In the following equations z_0 is the receiver impedance (50 ohms), rnh and rnv are the co-polarized and cross-polarized receiver gains, c_0 is the speed of light, k_{hRC} and k_{vRC} are the co- and cross-polarized radar constants, f_T is the transmit frequency, T_S is the time between the first and second pulses in the pair, R'(0) is covariance with receiver noise, and r is the range in meters.

$Vc = \frac{-c_0}{4\pi f_T T_S}\arg\left(\mathbf{R}_{cc}(1)\right)$	$Vx = \frac{-c_0}{4\pi f_T T_S}\arg\left(\mathbf{R}_{xx}(1)\right)$	m/s
$Wc = \frac{c_0^2}{8\pi^2 f_T^2 T_S^2}\left(1 - \frac{\left\|\mathbf{R}_{cc}(1)\right\|}{R_{cc}(0) - R'_{cc}(0)}\right)$	$Wx = \frac{c_0^2}{8\pi^2 f_T^2 T_S^2}\left(1 - \frac{\left\|\mathbf{R}_{xx}(1)\right\|}{R_{xx}(0) - R'_{xx}(0)}\right)$	m^2/s^2
$Cc = \frac{\left\|\mathbf{R}_{cc}(1)\right\|}{R_{cc}(0)}$	$Cx = \frac{\left\|\mathbf{R}_{xx}(1)\right\|}{R_{xx}(0)}$	none
$Ic = 10 \bullet \log\left(\frac{R_{cc}(0)}{z_0}\right) + 30$	$Ix = 10 \bullet \log\left(\frac{R_{xx}(0)}{z_0}\right) + 30$	dBm at rcvr output
$Pc = Ic - rnh$	$Px = Ix - rnv$	dBm at antenna
$Zc = Pc + k_{hRC} + 20 \bullet \log(r) - 60$	$Zx = Px + k_{vRC} + 20 \bullet \log(r) - 60$	dBZ
$CDR = Pc - Px$		dB